

AN EFFICIENT BEAM AND CHANNEL ACQUISITION VIA SPARSITY MAP
AND JOINT ANGLE-DELAY POWER PROFILE ESTIMATION FOR
WIDEBAND MASSIVE MIMO SYSTEMS

A THESIS SUBMITTED TO
THE GRADUATE SCHOOL OF NATURAL AND APPLIED SCIENCES
OF
MIDDLE EAST TECHNICAL UNIVERSITY

BY

ALI OSMAN KALAYCI

IN PARTIAL FULFILLMENT OF THE REQUIREMENTS
FOR
THE DEGREE OF MASTER OF SCIENCE
IN
ELECTRICAL AND ELECTRONICS ENGINEERING

SEPTEMBER 2019

Approval of the thesis:

**AN EFFICIENT BEAM AND CHANNEL ACQUISITION VIA SPARSITY
MAP AND JOINT ANGLE-DELAY POWER PROFILE ESTIMATION FOR
WIDEBAND MASSIVE MIMO SYSTEMS**

submitted by **ALI OSMAN KALAYCI** in partial fulfillment of the requirements for
the degree of **Master of Science in Electrical and Electronics Engineering De-
partment, Middle East Technical University** by,

Prof. Dr. Halil Kalipçılar
Dean, Graduate School of **Natural and Applied Sciences** _____

Prof. Dr. İlkey Ulusoy
Head of Department, **Electrical and Electronics Engineering** _____

Assist. Prof. Dr. Gökhan Muzaffer Güvensen
Supervisor, **Electrical and Electronics Engineering, METU** _____

Examining Committee Members:

Prof. Dr. Yalçın Tanık
Electrical and Electronics Engineering, METU _____

Assist. Prof. Dr. Gökhan Muzaffer Güvensen
Electrical and Electronics Engineering, METU _____

Prof. Dr. Ali Özgür Yılmaz
Electrical and Electronics Engineering, METU _____

Prof. Dr. Tolga Duman
Electrical and Electronics Engineering, Bilkent University _____

Prof. Dr. Emre Aktaş
Electrical and Electronics Engineering, Hacettepe University _____

Date:

I hereby declare that all information in this document has been obtained and presented in accordance with academic rules and ethical conduct. I also declare that, as required by these rules and conduct, I have fully cited and referenced all material and results that are not original to this work.

Name, Surname: Ali Osman Kalaycı

Signature :

ABSTRACT

AN EFFICIENT BEAM AND CHANNEL ACQUISITION VIA SPARSITY MAP AND JOINT ANGLE-DELAY POWER PROFILE ESTIMATION FOR WIDEBAND MASSIVE MIMO SYSTEMS

Kalaycı, Ali Osman

M.S., Department of Electrical and Electronics Engineering

Supervisor: Assist. Prof. Dr. Gökhan Muzaffer Güvensen

September 2019, 114 pages

In this thesis, an efficient beam and instantaneous channel acquisition scheme together with joint angle-delay power profile (JADPP), *scatter map*, construction are proposed for single-carrier (SC) mm-wave wideband sparse massive multiple-input multiple-output (MIMO) channels when hybrid beamforming architecture is utilized. We consider two different modes of operation, namely *slow-time beam acquisition* and *fast-time instantaneous channel estimation*, in training stage of time division duplex (TDD) based systems. In the first mode, where pre-structured hybrid beams are formed to scan intended angular sectors, the joint angle-delay sparsity map together with power intensities of each user channels are obtained by using a novel *two-stage constant false alarm rate (CFAR) thresholding* algorithm inspired from *adaptive radar detection* theory. The proposed thresholding algorithm employs a spatio-temporal adaptive matched filter (AMF) type estimator, taking the strong interference due to simultaneously active multipath components (MPCs) of different user channels into account, in order to estimate JADPP of each user. After applying the proposed thresholding algorithm on the estimated power profile, the angle-

delay sparsity map of the massive MIMO channel is constructed, based on which the channel covariance matrices (CCMs) are formed with significantly reduced amount of training snapshots. Then, by using the estimated CCMs, the analog beamformer is reconstructed by means of a virtual sectorization (user-grouping via second-order channel statistics) while taking the inter-group and inter-symbol interference (ISI) into account. Finally, for the second mode of the training stage, two novel reduced-rank instantaneous channel estimators, operating in a proper beamspace formed by the hybrid structure, are proposed. The proposed techniques attains the channel estimation accuracy of minimum mean square error (MMSE) filter with true knowledge of CCMs while reducing the training overhead considerably (compared to the conventional least-square (LS) type estimators).

Keywords: Massive MIMO, multipath channel, single-carrier, wideband channel, millimeter wave, angle-delay channel sparsity, CFAR thresholding, adaptive matched filter, user-grouping, hybrid beamforming, channel estimation, reduced rank MMSE estimator, beamspace aware estimator, least square estimator

ÖZ

GENİŞ BANTLI MASİF MIMO SİSTEMLER İÇİN SEYREKLİK HARİTASI VE UZAY-ZAMAN GÜÇ PROFİLİ KESTİRİMİNE DAYALI ETKİLİ HÜZME VE KANAL ÖĞRENME ALGORİTMALARI

Kalaycı, Ali Osman

Yüksek Lisans, Elektrik ve Elektronik Mühendisliği Bölümü

Tez Yöneticisi: Dr. Öğr. Üyesi. Gökhan Muzaffer Güvensen

Eylül 2019 , 114 sayfa

Bu tez çalışmasında, hibrit hüzmeye oluşturma mimarisi altında tek-taşıyıcılı (SC) ve geniş bantlı milimetrik dalga masif çok-girdili çok-çıkıtlı (MIMO) seyrek kanallar için ortak uzay-zaman güç profili (JADPP), dağılım haritası, oluşturulması ile birlikte etkili hüzmeye ve anlık kanal edinim teknikleri önerilmiştir. Zaman bölmeli çoklama (TDD) tabanlı masif MIMO sistemler için *yavaş-zamanlı hüzmeye edinimi* ve *hızlı-zamanlı anlık kanal kestirimi* adı altında iki operasyon modundan oluşan bir eğitim aşaması üzerinde durulmuştur. İlgilenilen açıl sektörlere taramak için önceden oluşturulmuş hibrit hüzmelerin kullanıldığı ilk modda, *adaptif radar tespit* teorisinden ilham alarak yeni bir *iki-aşamalı sabit yanlış alarm oranlı (CFAR) eşikleme* algoritması önerilmiş ve bu algoritma kullanılarak her bir kullanıcı kanalının güç yoğunlukları ile birlikte ortak uzay-zaman seyreklik haritası elde edilmiştir. Önerilen eşikleme algoritması, aynı anda aktif olan farklı kullanıcılara ait çok-yollu bileşenlerden (MPCs) kaynaklı güçlü girişimleri dikkate alarak güç profili kestirebilen uzay-zamansal adaptif uyumlu bir süzgeç (AMF) kullanmaktadır. Önerilen eşikleme algoritması sonrası

elde edilen çok-kullanıcı kanala ait seyreklik haritası baz alınarak önemli miktarda azaltılmış eğitim verisi ile birlikte kanal kovaryans matrisleri (CCM) oluşturulmuştur. Daha sonra, kullanıcılar ve semboller arası girişim (ISI) dikkate alınarak ve oluşturulan kanal kovaryans matrisleri kullanılarak sanal sektörleştirme (ikinci derece kanal istatistiklerine dayalı kullanıcı gruplama) ile birlikte analog hüzmeleyici yeniden inşa edilmiştir. Son olarak, eğitim aşamasının ikinci modu için, hibrit yapı tarafından oluşturulmuş uygun bir hüzme uzayında çalışan iki yeni azaltılmış ranklı anlık kanal kestiricisi önerilmiştir. Önerilen teknikler eğitim yükünü dikkate değer miktarda azaltırken (geleneksel en küçük kareler (LS) tabanlı kestiricilere oranla), gerçek CCM bilgisine sahip minimum ortalama karesel hata (MMSE) filtresinin kanal kestirim doğruluğuna erişmektedir.

Anahtar Kelimeler: Masif MIMO, çok-yollu kanal, tek taşıyıcı, geniş bant kanal, milimetrik dalga, uzay-zaman kanal seyrekliği, CFAR eşikleme, adaptif uyumlu süzgeç, kullanıcı gruplama, hibrit hüzmeleyici, kanal kestirimi, azaltılmış ranklı MMSE kestirici, hüzme uzayı farkındalı kestirici, en küçük kareler kestirici

to my beloved family,

ACKNOWLEDGMENTS

I would like to first express my sincere gratitude to my advisor Assist. Prof. Dr. Gökhan Muzaffer Güvensen for the continuous support of my MSc study and research, for his patience, motivation, enthusiasm, and immense knowledge. His guidance helped me in all the time of research and writing of this thesis. Without our frequent technical discussions and his supervision during my research, I would never have been able to complete the work presented in this thesis.

I would like to thank The Scientific and Technological Research Council of Turkey (TÜBİTAK) for its financial support during my Msc study.

I am grateful to ASELSAN Inc. for facilitating my studies via flexible working hours, high performance computers and powerful simulation environment. My sincere thanks also goes to my colleagues Dr. Eren Akdemir, Dr. Özgür Oruç and Fehmi Emre Kadan for their encouragement, suggestions and for their having such friendly environment at ASELSAN Inc. during my studies.

Last but not the least, I must express my very profound gratitude to my parents for providing me with endless support throughout my whole life. This accomplishment would not have been possible without them.

TABLE OF CONTENTS

ABSTRACT	v
ÖZ	vii
ACKNOWLEDGMENTS	x
TABLE OF CONTENTS	xi
LIST OF TABLES	xv
LIST OF FIGURES	xvi
LIST OF ABBREVIATIONS	xxiii
NOMENCLATURE	xxv
CHAPTERS	
1 INTRODUCTION	1
1.1 Motivation	1
1.2 Outline and Contribution of the Thesis	4
1.3 Notations	6
2 SYSTEM MODEL	9
2.1 Introduction	9
2.2 Discrete Time Received Signal Model	9
2.3 Statistical Models for MPCs	10

2.4	Equivalent Multi-Ray Channel Model for MPCs	13
3	HYBRID BEAMFORMING BASED JADPP ESTIMATION FOR WIDE- BAND MASSIVE MIMO SYSTEMS	15
3.1	Introduction	15
3.2	Discrete Time Spatio-Temporal Domain Signal Model for JADPP Estimation	17
3.3	Initial Beam Acquisition Mode	18
3.4	Proposed JADPP Estimation Techniques	19
3.4.1	Spatio-Temporal Adaptive Matched Filter (AMF)	20
3.4.2	Spatio-Temporal Matched Filter (MF)	21
4	SPARSE CCM CONSTRUCTION FOR WIDEBAND MASSIVE MIMO CHANNELS	23
4.1	Introduction	23
4.2	User Activity Detection and Sparsity Map Construction via Constant False Alarm Rate (CFAR) Algorithm	23
4.2.1	Two-Stage CFAR Algorithm	24
4.2.1.1	Temporal thresholding for selected resolution cell	25
4.2.1.2	Spatial thresholding for selected resolution cell	25
4.2.2	Joint Angle-Delay Domain Sparsity Map Construction of User Power Profiles	26
4.2.3	Performance Metrics for User Activity Detection	27
4.3	CCM Construction Based on Estimated Sparsity Map	29
5	NEARLY OPTIMAL COVARIANCE-BASED REDUCED RANK ANA- LOG BEAMFORMER DESIGN	31
5.1	Introduction	31
5.2	User Grouping Stage	32

5.3	Post-User Grouping Stage	33
5.3.1	MPC Grouping for Efficient Analog Beamformer Design	34
5.3.2	Nearly Optimal Analog Beamformer Construction	37
5.3.3	Optimal RF Chain Distribution Among MPCs	37
6	INSTANTANEOUS CHANNEL ESTIMATION WITH HYBRID BEAM-FORMING	39
6.1	Introduction	39
6.2	Joint Angle-Delay Domain Reduced Rank Minimum Mean Square Error (RR-MMSE) Estimator	41
6.3	Joint Angle-Delay Domain Beam-space Aware Least Square (BA-LS) Estimator	41
6.4	Conventional LS Estimator	43
6.5	Performance Evaluation for Instantaneous Channel Estimation	43
7	NUMERICAL RESULTS	47
7.1	Introduction	47
7.2	Performance vs. SNR	51
7.3	Performance vs. Number of Slow-Time Training Snapshots	69
7.4	Performance vs. Fast-Time Training Length	76
7.5	Performance vs. Slow-Time Training Length	78
7.6	Performance vs. Number of RF Chains	84
7.7	Performance vs. Look Spread	86
7.8	Performance vs. Search Dimension	88
7.9	Performance vs. Number of Angular Resolution Cells	100
7.10	Performance vs. Angular Spread of MPCs	102

8 CONCLUSIONS	105
REFERENCES	107
APPENDICES	
A DERIVATION OF AMF TYPE JADPP ESTIMATOR	113

LIST OF TABLES

TABLES

Table 7.1 True Angle-Delay profile of all users	50
---	----

LIST OF FIGURES

FIGURES

Figure 2.1	Angle-delay power profile of active users in massive MIMO system	11
Figure 3.1	Beam acquisition scheme	16
Figure 4.1	JADPP for user 1 and user 2 ($K = 2, T = 16, \beta^{(1)} = 40$ dB, $\beta^{(2)} = 50$ dB)	27
Figure 4.2	Sparsity map for user 1 and user 2 ($K = 2, T = 16, \beta^{(1)} = 40$ dB, $\beta^{(2)} = 50$ dB)	28
Figure 6.1	Overall System Architecture	44
Figure 7.1	Joint angle-delay map of all users	49
Figure 7.2	Average P_D vs SNR curves for equal averaged received power levels ($T = 32, D_{search} = 5$)	51
Figure 7.3	Performance of different channel estimators for equal averaged received power levels ($K = 8, T = T_{fast} = 32, D_{search} = 5$)	53
Figure 7.4	Performance of different channel estimators for equal averaged received power levels ($K = 16, T = T_{fast} = 32, D_{search} = 5$)	53
Figure 7.5	Average P_D vs SNR curves for different averaged received power levels ($K = 8, T = 32, D_{search} = 5, 10 \log (\bar{\beta}^{(4)} / \bar{\beta}^{(1)}) = 15$ dB)	54
Figure 7.6	Performance of different channel estimators for weakest user group ($K = 8, T = T_{fast} = 32, D_{search} = 5, 10 \log (\bar{\beta}^{(4)} / \bar{\beta}^{(1)}) = 15$ dB)	56

Figure 7.7	Performance of different channel estimators for strongest user group ($K = 8, T = T_{fast} = 32, D_{search} = 5, 10 \log (\bar{\beta}^{(4)} / \bar{\beta}^{(1)}) = 15$ dB)	56
Figure 7.8	Average P_D vs SNR curves for different averaged received power levels ($K = 16, T = 32, D_{search} = 5, 10 \log (\bar{\beta}^{(4)} / \bar{\beta}^{(1)}) = 15$ dB)	57
Figure 7.9	Performance of different channel estimators for weakest user group ($K = 16, T = T_{fast} = 32, D_{search} = 5, 10 \log (\bar{\beta}^{(4)} / \bar{\beta}^{(1)}) = 15$ dB)	59
Figure 7.10	Performance of different channel estimators for strongest user group ($K = 16, T = T_{fast} = 32, D_{search} = 5, 10 \log (\bar{\beta}^{(4)} / \bar{\beta}^{(1)}) = 15$ dB)	59
Figure 7.11	Average P_D vs SNR curves for different averaged received power levels ($K = 16, T = 32, D_{search} = 5, 10 \log (\bar{\beta}^{(4)} / \bar{\beta}^{(1)}) = 30$ dB)	60
Figure 7.12	Performance of different channel estimators for weakest user group ($K = 16, T = T_{fast} = 32, D_{search} = 5, 10 \log (\bar{\beta}^{(4)} / \bar{\beta}^{(1)}) = 30$ dB)	62
Figure 7.13	Performance of different channel estimators for strongest user group ($K = 16, T = T_{fast} = 32, D_{search} = 5, 10 \log (\bar{\beta}^{(4)} / \bar{\beta}^{(1)}) = 30$ dB)	62
Figure 7.14	Average P_D vs SNR curve for different averaged received power levels ($K = 16, T = 128, D_{search} = 5, 10 \log (\bar{\beta}^{(4)} / \bar{\beta}^{(1)}) = 30$ dB)	63
Figure 7.15	Performance of different channel estimators for weakest user group ($K = 16, T = 128, D_{search} = 5, T_{fast} = 32, 10 \log (\bar{\beta}^{(4)} / \bar{\beta}^{(1)}) = 30$ dB)	65
Figure 7.16	Performance of different channel estimators for strongest user group ($K = 16, T = 128, D_{search} = 5, T_{fast} = 32, 10 \log (\bar{\beta}^{(4)} / \bar{\beta}^{(1)}) = 30$ dB)	65
Figure 7.17	Average P_D vs SNR curves for different averaged received power levels ($K = 16, T = 32, D_{search} = 10, 10 \log (\bar{\beta}^{(4)} / \bar{\beta}^{(1)}) = 30$ dB)	66

Figure 7.18	Performance of different channel estimators for weakest user group ($K = 16, T = 32, D_{search} = 10, T_{fast} = 32, 10 \log (\bar{\beta}^{(4)} / \bar{\beta}^{(1)}) = 30$ dB)	68
Figure 7.19	Performance of different channel estimators for strongest user group ($K = 16, T = 32, D_{search} = 10, T_{fast} = 32, 10 \log (\bar{\beta}^{(4)} / \bar{\beta}^{(1)}) = 30$ dB)	68
Figure 7.20	Average P_D vs J curves for equal averaged received power levels ($K = 8, D_{search} = 5, T = 32, \text{SNR}^{(g)} = 30$ dB for $g = 1, \dots, G$)	70
Figure 7.21	Average P_D vs J curves for equal averaged received power levels ($K = 16, D_{search} = 5, T = 32, \text{SNR}^{(g)} = 30$ dB for $g = 1, \dots, G$)	70
Figure 7.22	Performance of different channel estimators averaged over all groups for different J ($K = 8, D_{search} = 5, T = T_{fast} = 32, \text{SNR}^{(g)} = 30$ dB for $g = 1, \dots, G$)	71
Figure 7.23	Performance of different channel estimators averaged over all groups for different J ($K = 16, D_{search} = 5, T = T_{fast} = 32, \text{SNR}^{(g)} = 30$ dB for $g = 1, \dots, G$)	71
Figure 7.24	Average P_D vs J curves for different averaged received power levels ($K = 8, D_{search} = 5, T = 32, 10 \log (\bar{\beta}^{(4)} / \bar{\beta}^{(1)}) = 15$ dB)	73
Figure 7.25	Average P_D vs J curves for different averaged received power levels ($K = 16, D_{search} = 5, T = 32, 10 \log (\bar{\beta}^{(4)} / \bar{\beta}^{(1)}) = 15$ dB)	73
Figure 7.26	Performance of different channel estimators in terms of nMSE vs J for weakest user group ($K = 8, D_{search} = 5, T = T_{fast} = 32, 10 \log (\bar{\beta}^{(4)} / \bar{\beta}^{(1)}) = 15$ dB)	74
Figure 7.27	Performance of different channel estimators in terms of nMSE vs J for strongest user group ($K = 8, D_{search} = 5, T = T_{fast} = 32, 10 \log (\bar{\beta}^{(4)} / \bar{\beta}^{(1)}) = 15$ dB)	74

Figure 7.28	Performance of different channel estimators in terms of nMSE vs J for weakest user group ($K = 16, D_{search} = 5, T = T_{fast} = 32, 10 \log (\bar{\beta}^{(4)} / \bar{\beta}^{(1)}) = 15$ dB)	75
Figure 7.29	Performance of different channel estimators in terms of nMSE vs J for strongest user group ($K = 16, D_{search} = 5, T = T_{fast} = 32, 10 \log (\bar{\beta}^{(4)} / \bar{\beta}^{(1)}) = 15$ dB)	75
Figure 7.30	Performance of different channel estimators averaged over all groups for different T_{fast} ($K = 8, D_{search} = 5, T = 32, \text{SNR}^{(g)} = 30$ dB for $g = 1, \dots, G$)	77
Figure 7.31	Performance of different channel estimators averaged over all groups for different T_{fast} ($K = 16, D_{search} = 5, T = 32, \text{SNR}^{(g)} = 30$ dB for $g = 1, \dots, G$)	77
Figure 7.32	Average P_D vs T curves for equal averaged received power levels ($K = 16, D_{search} = 5$)	79
Figure 7.33	Performance of different channel estimators averaged over all groups for different T ($K = 16, D_{search} = 5, T_{fast} = 32, \text{SNR}^{(g)} = 20$ dB for $g = 1, \dots, G$)	79
Figure 7.34	Average P_D vs T curves for different averaged received power levels ($K = 16, D_{search} = 5, 10 \log (\bar{\beta}^{(4)} / \bar{\beta}^{(1)}) = 15$ dB)	80
Figure 7.35	Performance of different channel estimators in terms of nMSE vs T for weakest user group ($K = 16, D_{search} = 5, T_{fast} = 32, 10 \log (\bar{\beta}^{(4)} / \bar{\beta}^{(1)}) = 15$ dB)	81
Figure 7.36	Performance of different channel estimators in terms of nMSE vs T for strongest user group ($K = 16, D_{search} = 5, T_{fast} = 32, 10 \log (\bar{\beta}^{(4)} / \bar{\beta}^{(1)}) = 15$ dB)	81
Figure 7.37	Average P_D vs T curves for different averaged received power levels ($K = 16, D_{search} = 5, 10 \log (\bar{\beta}^{(4)} / \bar{\beta}^{(1)}) = 30$ dB)	82

Figure 7.38	Performance of different channel estimators in terms of nMSE vs T for weakest user group ($K = 16, D_{search} = 5, T_{fast} = 32, 10 \log(\bar{\beta}^{(4)}/\bar{\beta}^{(1)}) = 30$ dB)	83
Figure 7.39	Performance of different channel estimators in terms of nMSE vs T for strongest user group ($K = 16, D_{search} = 5, T_{fast} = 32, 10 \log(\bar{\beta}^{(4)}/\bar{\beta}^{(1)}) = 30$ dB)	83
Figure 7.40	Performance of different channel estimators averaged over all groups for different D ($K = 8, D_{search} = 5, T = T_{fast} = 32, \text{SNR}^{(g)} = 30$ dB for $g = 1, \dots, G$)	85
Figure 7.41	Performance of different channel estimators averaged over all groups for different D ($K = 16, D_{search} = 5, T = T_{fast} = 32, \text{SNR}^{(g)} = 30$ dB for $g = 1, \dots, G$)	85
Figure 7.42	Average P_D vs σ curves for equal averaged received power levels ($K = 8, D_{search} = 5, T = 32$)	86
Figure 7.43	Performance of different channel estimators averaged over all groups for different values of σ ($K = 8, D_{search} = 5, T = T_{fast} = 32, \text{SNR}^{(g)} = 10$ dB for $g = 1, \dots, G$)	87
Figure 7.44	Performance of different channel estimators averaged over all groups for different values of σ ($K = 8, D_{search} = 5, T = T_{fast} = 32, \text{SNR}^{(g)} = 30$ dB for $g = 1, \dots, G$)	87
Figure 7.45	Average P_D vs D_{search} curves for equal averaged received power levels ($K = 8, T = 32$)	89
Figure 7.46	Average P_D vs D_{search} curves for equal averaged received power levels ($K = 16, T = 32$)	89
Figure 7.47	Performance of different channel estimators averaged over all groups for different values of D_{search} ($K = 8, T = T_{fast} = 32, \text{SNR}^{(g)} = 10$ dB for $g = 1, \dots, G$)	90

Figure 7.48	Performance of different channel estimators averaged over all groups for different values of D_{search} ($K = 8, T = T_{fast} = 32, \text{SNR}^{(g)} = 30$ dB for $g = 1, \dots, G$)	90
Figure 7.49	Performance of different channel estimators averaged over all groups for different values of D_{search} ($K = 16, T = T_{fast} = 32, \text{SNR}^{(g)} = 10$ dB for $g = 1, \dots, G$)	91
Figure 7.50	Performance of different channel estimators averaged over all groups for different values of D_{search} ($K = 16, T = T_{fast} = 32, \text{SNR}^{(g)} = 30$ dB for $g = 1, \dots, G$)	91
Figure 7.51	Average P_D vs D_{search} curves for different averaged received power levels ($K = 8, T = 32, 10 \log (\bar{\beta}^{(4)} / \bar{\beta}^{(1)}) = 15$ dB)	93
Figure 7.52	Average P_D vs D_{search} curves for different averaged received power levels ($K = 16, T = 32, 10 \log (\bar{\beta}^{(4)} / \bar{\beta}^{(1)}) = 15$ dB)	93
Figure 7.53	Performance of different channel estimators in terms of nMSE vs D_{search} for weakest user group ($10 \log (\bar{\beta}^{(4)} / \bar{\beta}^{(1)}) = 15$ dB, $K = 8, T = T_{fast} = 32$)	94
Figure 7.54	Performance of different channel estimators in terms of nMSE vs D_{search} for strongest user group ($10 \log (\bar{\beta}^{(4)} / \bar{\beta}^{(1)}) = 15$ dB, $K = 8, T = T_{fast} = 32$)	94
Figure 7.55	Performance of different channel estimators in terms of nMSE vs D_{search} for weakest user group ($10 \log (\bar{\beta}^{(4)} / \bar{\beta}^{(1)}) = 15$ dB, $K = 16, T = T_{fast} = 32$)	95
Figure 7.56	Performance of different channel estimators in terms of nMSE vs D_{search} for strongest user group ($10 \log (\bar{\beta}^{(4)} / \bar{\beta}^{(1)}) = 15$ dB, $K = 16, T = T_{fast} = 32$)	95
Figure 7.57	Average P_D vs D_{search} curves for different averaged received power levels ($K = 16, T = 32, 10 \log (\bar{\beta}^{(4)} / \bar{\beta}^{(1)}) = 30$ dB)	97

Figure 7.58	Average P_D vs D_{search} curves for different averaged received power levels ($K = 16, T = 128, 10 \log (\bar{\beta}^{(4)} / \bar{\beta}^{(1)}) = 30$ dB)	97
Figure 7.59	Performance of different channel estimators in terms of nMSE vs D_{search} for weakest user group ($10 \log (\bar{\beta}^{(4)} / \bar{\beta}^{(1)}) = 30$ dB, $K = 16, T = T_{fast} = 32$)	98
Figure 7.60	Performance of different channel estimators in terms of nMSE vs D_{search} for strongest user group ($10 \log (\bar{\beta}^{(4)} / \bar{\beta}^{(1)}) = 30$ dB, $K = 16, T = T_{fast} = 32$)	98
Figure 7.61	Performance of different channel estimators in terms of nMSE vs D_{search} for weakest user group ($K = 16, T = 128, T_{fast} = 32, 10 \log (\bar{\beta}^{(4)} / \bar{\beta}^{(1)}) = 30$ dB)	99
Figure 7.62	Performance of different channel estimators in terms of nMSE vs D_{search} for strongest user group ($K = 16, T = 128, T_{fast} = 32, 10 \log (\bar{\beta}^{(4)} / \bar{\beta}^{(1)}) = 30$ dB)	99
Figure 7.63	Average P_D vs M curve for equal averaged received power levels ($K = 8, D_{search} = 5, T = T_{fast} = 32, \text{SNR}^{(g)} = 30$ dB for $g = 1, \dots, G$)	101
Figure 7.64	Performance of different channel estimators averaged over all groups for different values of M ($K = 8, D_{search} = 5, T = T_{fast} = 32, \text{SNR}^{(g)} = 30$ dB for $g = 1, \dots, G$)	101
Figure 7.65	Average P_D curves of AMF for equal averaged received power levels ($K = 8, D_{search} = 5, T = 32$)	103
Figure 7.66	Average P_D curves of MF for equal averaged received power levels ($K = 8, D_{search} = 5, T = 32$)	103

LIST OF ABBREVIATIONS

ABBREVIATIONS

AMF	Adaptive Matched Filter
AML	Approximate Maximum Likelihood
AoA	Angle of Arrival
AS	Angular Spread
AWGN	Additive White Gaussian Noise
BA-LS	Beamspace Aware Least Square
BS	Base Station
CFAR	Constant False Alarm Rate
CCM	Channel Covariance Matrix
CSI	Channel State Information
CUT	Cell-Under-Test
5G	Fifth Generation
JADPP	Joint Angle-Delay Power Profile
JSDM	Joint Spatial Division Duplexing
KLT	Karhunen-Loeve Transform
LS	Least Square
MC	Monte Carlo
MF	Matched Filter
MIMO	Multiple-Input and Multiple-Output
ML	Maximum Likelihood
MMSE	Minimum Mean Square Error
MPC	Multipath Component

MRC	Maximal Ratio Combining
MSE	Mean Square Error
nMSE	Normalized Mean Square Error
OMP	Orthogonal Matching Pursuit
PAPR	Peak-to-Average Power Ratio
PSK	Phase-Shift Keying
QAM	Quadrature Amplitude Modulation
RF	Radio Frequency
RR-MMSE	Reduced Rank Minimum Mean Square Error
SC	Single Carrier
SMI	Sample Matrix Inversion
SNR	Signal-to-Noise Ratio
3D	Three-Dimensional
TDD	Time Division Duplex
UE	User Equipment
ULA	Uniform Linear Array
UPA	Uniform Planar Array
WSSUS	Wide Sense Stationary Uncorrelated Scattering

NOMENCLATURE

SCALARS

γ_2	Angular CFAR threshold
$\psi_l^{(k)}$	Angular index pointing the mean AoA of l^{th} MPC of k^{th} user
$\rho_l^{(k)}$	Angular power density of l^{th} MPC of k^{th} user
$\Delta_l^{(k)}$	Angular spread of l^{th} MPC of k^{th} user
d	Antenna spacing
$\phi_{l,p}^{(k)}$	AoA of p^{th} ray from l^{th} MPC of k^{th} user
P_{FA}	Average false alarm probability
P_D	Average probability of detection
$\beta^{(k)}$	Average received power for k^{th} user
$\beta_l^{(k)}$	Average received power for l^{th} MPC of k^{th} user
$\text{SNR}_l^{(k)}$	Average received SNR for the l^{th} MPC of k^{th} user
E_s	Average transmitted symbol power
γ	CFAR threshold
L	Channel memory of multipath channels
$\alpha_{l,p}^{(k)}$	Complex gain of the p^{th} ray of the l^{th} MPC of k^{th} user having AoA $\phi_{l,p}^{(k)}$
\bar{P}_{FA}	Desired average false alarm probability of the test
$\alpha_l^{(k)}$	Effective complex channel gain for l^{th} MPC of k^{th} user
$\hat{\beta}_l^{(k)}$	Estimate of average received power for the l^{th} MPC of k^{th} user
$\hat{\beta}_{l,j}^{(k)}(\phi_i)$	Estimated received power obtained from j^{th} slow-time training snapshot
$\hat{\alpha}_l^{(k)}$	Estimate of effective complex channel gain of l^{th} MPC for k^{th} user

T_{fast}	Fast-time training sequence length
g	Group index
Π_{ϕ_i}	Guard interval, an angular window with mean angle of ϕ_i
g_k	Index for the k^{th} user in group g
$\Omega_\phi(i)$	i^{th} element of ordered set Ω_ϕ
σ	Look spread, angular width of the selected patch in sector- p
$\mu_l^{(k)}$	Mean look angle
N_0	Noise power
$nMSE^{(g)}$	Normalized mean square estimation error of user channels in group g
$\lambda_{\ell,n}^{(g)}$	n^{th} dominant generalized eigenvalue of $\hat{\mathbf{R}}_\ell^{(g)}$ and $\hat{\mathbf{R}}_\eta^{(g)}$
D_g	Number of RF chains assigned to group g
$d_\ell^{(g)}$	Number of RF chains assigned to the ℓ^{th} MPC of group g
K_g	Number of users in group g , cardinality of Ω_g
$\varphi_{ll'}^{(g)}$	Overlapping ratio between l^{th} and l'^{th} active MPCs of group g
ζ	Overlapping threshold
$\Omega_\phi^{(p)}$	p^{th} angular sub-sector
D_{search}	Search dimension (Number of digital beams)
ϕ_i	Selected i^{th} look angle of ordered set Ω_ϕ
λ	Signal carrier wavelength
T	Slow-time training sequence length
W	Symbol rate
γ_1	Temporal CFAR threshold
N	Total number of antenna elements at base station
P	Total number of rays
M	Total number of resolution cells in angular domain
$c_l^{(k)}$	Total number of resolution cells where l^{th} MPC of k^{th} user exists

$MPC^{(g)}$	Total number of resolvable MPCs of group g in angular domain after MPC grouping
D	Total number of RF chains
J	Total number of slow-time training snapshots
\mathcal{P}	Total number of sub-sectors
K	Total number of users that the BS serves
G	Total number of user groups
$x_n^{(k)}$	Training symbol for the k^{th} user at n^{th} instant
k	User index
Ω_ϕ	Whole angular search sector of interest

SETS

$S_l^{(k)}$	Angular support set of l^{th} MPC of k^{th} user
Ω_g	Set of all UEs in group g
$\mathfrak{D}_\ell^{(g)}$	Set of column indices of the analog beamformer matrix $\mathbf{S}^{(g)}$
\mathbb{C}	Set of complex numbers
$\Gamma_l^{(g)}$	Set of angular indices i such that the look angle $\phi_i \in \Omega_\phi$ is inside the angular region which is determined to have non-zero power level for l^{th} MPC of group g
$\Gamma_l^{(k)}$	Set of angular indices i such that the look angle $\phi_i \in \Omega_\phi$ is inside the angular support set $S_l^{(k)}$
\mathbb{Z}^+	Set of positive integers
$\mathcal{L}^{(k)}$	Set of temporal indices of active MPCs having positive $\beta_l^{(k)}$
$\mathfrak{L}_\ell^{(g)}$	Set of temporal indices of spatially overlapping active MPCs in user group g
S	Signal Constellation

VECTORS

$\mathbf{u}(\phi)$	Array manifold (steering) vector
\mathbf{n}_n	AWGN vectors during uplink pilot segment at n^{th} instant
$\bar{\mathbf{h}}_{eff}^{(g)}$	Concatenated effective channel vector of group g
$\bar{\mathbf{h}}_{eff}^{(gk)}$	Concatenated effective channel vector of k^{th} user in group g
$\mathbf{y}^{(g)}$	$D_g T$ -dimensional space-time received signal vector
$\mathbf{h}_{eff,l}^{(gk)}$	Effective channel vector of the l^{th} MPC of k^{th} user in group g
$\hat{\mathbf{h}}_{eff}^{(g)}$	Estimate of effective channel vector of group g
$\hat{\mathbf{h}}_{eff,l}^{(gk)}$	Estimate of effective channel vector of l^{th} MPC of k^{th} user in group g
$\mathbf{h}_l^{(gk)}$	Full dimensional channel vector for the l^{th} MPC of the k^{th} user in group g
$\boldsymbol{\eta}_n$	Inter-group interference to group g with AWGN at n^{th} instant
$\boldsymbol{\eta}_{l,i}^{(k)}$	i^{th} column of $\tilde{\mathbf{N}}_l^{(k)}$
$\mathbf{e}^{(g)}$	MMSE vector
$\mathbf{h}_l^{(k)}$	Multipath channel vector of l^{th} MPC of k^{th} user
$\mathbf{x}_l^{(k)}$	Pilot (training) sequence vector for l^{th} MPC of k^{th} user
\mathbf{y}_n	Received signal vector taken at n^{th} instant
$\tilde{\mathbf{y}}_n$	Received signal vector at n^{th} instant after hybrid beamforming
$\tilde{\mathbf{u}}(\phi)$	Reduced dimensional array manifold (steering) vector

MATRICES

$\mathbf{S}^{(g)}$	Analog beamformer matrix
$\mathbf{W}^{(g)}$	Arbitrary estimator matrix for the intended group g
$\mathbf{R}_l^{(g)}$	Common spatial covariance matrix of UEs belonging to group g at l^{th} delay

$\mathbf{R}_{eff}^{(g)}$	Covariance matrix of the effective extended multipath channel vector of group g
$\mathbf{R}_{\tilde{y}}$	Covariance matrix of the received signal of all users after hybrid beamforming
$\mathbf{R}_y^{(g)}$	Covariance matrix of the received signal vector of group g after analog beamforming
$\mathbf{R}_{code}^{(g)}(l)$	Covariance matrix of training sequences belonging to the active MPCs of group g
$\mathbf{E}_{L,l}$	Elementary diagonal matrix where all the entries except the $(l + 1)^{th}$ diagonal one are zero
$\mathbf{W}_{ba-ls}^{(g)}$	Estimated beamspace aware estimator matrix of group g
$\hat{\mathbf{R}}_l^{(gk)}$	Estimated channel covariance matrix for l^{th} MPC of k^{th} user in group g
$\hat{\mathbf{R}}_{\eta'}^{(g)}$	Estimated covariance matrix of interfering components to ℓ^{th} MPC of group g
$\hat{\mathbf{R}}_{\eta}^{(g)}$	Estimated covariance matrix of inter-group interference to g^{th} group
$\hat{\mathbf{R}}_l^{(k)}$	Estimated channel covariance matrix of l^{th} MPC of k^{th} user
$\hat{\mathbf{R}}_{\ell}^{(g)}$	Estimated covariance matrix of $\mathcal{L}_{\ell}^{(g)}$
$\mathbf{W}_{ls}^{(g)}$	Estimated least-square estimator matrix of group g
$\hat{\mathbf{W}}_{mmse}^{(g)}$	Estimated MMSE estimator (filter) matrix of group g
$\hat{\mathbf{R}}_y$	Estimated spatial covariance matrix of received signal
Ψ	Estimated total interfering signal component
$\Psi_l^{(k)}$	Estimated total interfering signal component l^{th} MPC of k^{th} user
\mathbf{U}	Hybrid beamformer matrix
\mathbf{I}	Identity matrix with appropriate size
\mathbf{U}_{RF}	Initial analog beamformer matrix

\mathbf{U}_{ϕ_i}	Intra-sector digital fine search beam matrix for the look angle ϕ_i
$\mathbf{R}_{mmse}^{(g)}$	MMSE covariance matrix for the case when optimal MMSE estimator with perfect knowledge of CCMs is used
$\mathbf{W}_{mmse}^{(g)}$	MMSE estimator (filter) matrix of group g when true CCMs are used
\mathbf{Y}	Received signal matrix
$\tilde{\mathbf{Y}}$	Reduced dimensional received signal matrix
\mathbf{R}_{ϕ_i}	Reduced dimensional spatial autocorrelation matrix of the user channels of selected angular patch in $\Omega_{\phi}^{(p)}$ whose center is ϕ_i
$\tilde{\mathbf{N}}_l^{(k)}$	Reduced dimensional total interfering component to l^{th} MPC of k^{th} user
$\text{SNR}_{mimo}^{(g)}(l)$	SINR matrix obtained at the output of the beamformer when passing the l^{th} MPC of group g signals and rejecting the inter-group interference
$\mathbf{I}^{(k)}$	Sparsity map (matrix) of k^{th} user
$\mathbf{R}_{\eta,l}^{(k)}$	Spatial autocorrelation matrix of interfering MPCs other than the one located in CUT
$\mathbf{R}^{(sector-p)}$	Spatial autocorrelation matrix of user channels in sector p
$\mathbf{S}_{\ell}^{(g)}$	Sub-analog-beamformer matrix that allows ℓ^{th} resolvable MPC of group g to pass while suppressing the inter-group interference in the spatial domain, and also the rejecting each MPC of group g other than the one at delay ℓ
$\mathbf{N}_l^{(k)}$	Total interfering component to l^{th} MPC of k^{th} user
$\mathbf{X}_k^{(g)}$	Training matrix (convolution matrix)
$\mathbf{R}_l^{(k)}$	True channel auto-covariance matrix of l^{th} MPC of k^{th} user
$\mathbf{R}_{\eta}^{(g)}$	True covariance matrix of the inter-group interference to group g with AWGN

CHAPTER 1

INTRODUCTION

1.1 Motivation

Multi-user massive multiple-input multiple-output (MIMO) cellular systems, where a base station (BS) is equipped with hundreds or even thousands of antennas [1] to simultaneously serve single-antenna user equipments (UEs) is one of the key technologies for next-generation cellular systems such as the upcoming fifth generation (5G) wireless standard [2], [3]. Massive MIMO systems has been widely investigated because it provides large gains in spectral and energy efficiency, high spatial resolution, and simple transceiver design [1], [3], [4]. Massive MIMO systems, operating at mm-wave frequency band with large bandwidths [5], [6], are going to be able to meet the throughput necessities for future standards [2].

To embrace aforementioned gains, instantaneous channel state information (CSI) is requisite for multi-user precoding at downlink or multi-user decoding at uplink in a massive MIMO system. However, the CSI acquisition is recognized as a very challenging task for massive MIMO systems, due to the high dimensionality of channel matrices, uplink pilot contamination, downlink training overhead, computational complexity and so on [1]. Hence, the acquisition of CSI in massive MIMO transmission has attracted many researchers in this field. Various channel estimation algorithms are proposed, from which channel covariance matrix (CCM) based channel estimation methods offer additional statistical knowledge about the channel variants and therefore achieve much better channel estimation accuracy when compared to the compressive sensing approaches which try to recover CSI from fewer sub-Nyquist sampling points [7], [8] or the angle-space methods which exploit the intrinsic an-

gle parameters [9], [10]. Moreover, space-time preprocessing at BS, like hybrid beamforming [11], can benefit from the knowledge of CCMs as well. To benefit from CCMs, however, they must be estimated first. There are different approaches to obtain CCMs such as using temporal averaging of received signal snapshots in full dimension [12], [13], employing compressive sensing algorithms [14], [15], and applying approximate maximum likelihood (AML) technique formulated as a semi-definite program in low dimensional subspace [16]. In [17], CCMs are constructed by exploiting power angular spectrum and angle parameters of channels by neglecting angular spreads (AS), though, it is shown by [18] that there exist non-negligible angular spreads along the dominant propagation directions in practical mm-wave channel. Also, the authors in [17] take only the angular sparsity of the wideband channel into account while overlooking the joint angle-delay sparsity of the mm-wave channels as did by the many researchers in this field so far. In contrast, next generation wireless systems will inevitably be broadband due to the much higher throughput requirements thus leading wideband massive MIMO channel to be sparse both in angle and time (delay) domain.

Most of the existing researches for massive MIMO systems adopt flat-fading channel models assuming that OFDM will be used for wideband frequency-selective channels since OFDM decomposes the wideband channel into a set of narrow-band flat fading sub-channels [19]. However, due to the drawbacks of OFDM signals (e.g., high peak-to-average-power ratio (PAPR)), the use of single-carrier (SC) in massive MIMO systems is studied in the literature, and its optimality was demonstrated in [20]. Especially, for mm-wave channels exhibiting sparsity both in angle and delay domain, the mitigation of ISI via reduced complexity beamspace processing rather than temporal processing motivates the use of SC in spatially correlated wideband massive MIMO channels [21], [22], [23]. Furthermore, SC receivers necessitates no equalization in mm-wave band unlike OFDM receivers which requires FFT processing for equalization. Time division duplex (TDD) and frequency division duplex (FDD) modes are also extensively studied in the literature [24], [25]. In FDD mode, CSI is typically obtained through explicit downlink training and uplink (limited feedback). However, as the number of BS antennas increases, the traditional downlink channel estimation strategy for FDD systems becomes infeasible [19]. Therefore, al-

ternatively, CSI at the BS can be acquired by means of uplink training in TDD mode, where the uplink pilots provide the BS with downlink and uplink channel estimates simultaneously thanks to the channel reciprocity [19], [26]. Although, the need of feedback can be eliminated and pilot overhead can be reduced in TDD mode when compared to the FDD mode, computational burden of processing large-dimensional signals still constitutes a bottleneck for the performance of massive MIMO transmission. Therefore, some effective channel dimensionality reduction techniques, considering the long-term channel parameters (such as angles of arrivals (AoAs), temporal delays, and average power of the arriving signals) into account, are required to benefit from the advantages of massive MIMO architecture.

In order to reduce the effective channel dimensions, hence, to relieve computational burden of massive MIMO system operations, two-stage beamforming concept under the name of Joint Spatial Division and Multiplexing (JSDM) has been proposed [27], [28]. In JSDM framework, users are partitioned into multiple groups where the users in the same group have approximately same channel covariance eigenspaces. Then, an analog beamformer, distinguishing intra-group signals while suppressing inter-group interference, can be constructed from the long-term parameters (not from instantaneous CSI) in order to reduce the signaling dimension. Subsequently, operations like downlink multi-user precoding and uplink detection/decoding can be carried out based on the CSI of the effective channel with significantly reduced dimensions after analog beamforming. Furthermore, the training dimension necessary to learn the effective channels of each user is reduced considerably. Also, the JSDM framework motivates the use of hybrid beamforming architectures [29], [30] instead of using fully digital precoding/decoding in mm wave, where efficient reconfigurable radio frequency (RF) architectures can be implemented at competitive cost, size, and energy. In the hybrid beamforming architecture, the statistical analog beamformer can be implemented in the analog RF domain, while the multi-user MIMO precoding/decoding stage can be implemented by standard baseband processing (in digital domain).

1.2 Outline and Contribution of the Thesis

In this thesis, efficient algorithms are proposed to estimate the joint angle-delay sparsity map and power profile of SC wideband massive MIMO channel to construct CCMs, based on which an adaptive beam and instantaneous channel acquisition is carried out for JSMD architecture in mm-wave bands. Throughout the thesis, we conceive two modes of operation for beam and channel acquisition, namely *slow-time beam acquisition* and *fast-time instantaneous channel estimation* in training stage of TDD based massive MIMO system utilizing hybrid beamforming structure. In the first mode, initially, pre-structured hybrid search beams are utilized to scan the intended angular sector of interest. Then, by using significantly reduced amount of slow-time training data, an adaptive spatio-temporal matched filter (AMF), taking the simultaneously active interferers into account, is designed to estimate power intensities of active multipath components (MPCs) for each user channel (scatter map) on joint angle-delay plane. Following the joint angle-delay power profile (JADPP) estimator, a novel constant false alarm rate (CFAR) algorithm, inspired from *adaptive radar detection* theory, is applied onto the estimated JADPPs in order to extract joint angle-delay sparsity map, showing the spatio-temporal locations (cells) where the power of each MPC is concentrated. After obtaining the sparsity map and power profiles, the parametric construction of CCMs for each active MPC is realized in full dimension and reduced complexity on the contrary to compressive sensing algorithms such as orthogonal matching pursuit (OMP) in [7]. Subsequently, as in the case of JSMD framework, all active users can be partitioned into groups to be served simultaneously via using their estimated spatial signatures/CCMs, and based on user-grouping, an efficient reconstruction of analog beamformer is fulfilled by exploiting the estimated CCMs and sparsity map such that the inter-group and inter-symbol interference in SC transmission are mitigated. Finally, in second mode of operation, the instantaneous CSI is acquired in reduced dimensional beamspace formed by the proposed hybrid architecture. It is shown that the proposed CCM construction and hybrid beamforming technique are so effective that the accuracy of minimum mean square error (MMSE) type channel estimator with true channel covariance is attained without necessitating the use of orthogonal pilot sequences while diminishing the training overhead significantly.

The contribution of this thesis is two-fold. First, for hybrid beamforming based wideband massive MIMO systems, a novel two-stage CFAR thresholding algorithm, which employs adaptive spatio-temporal preprocessing to suppress simultaneously active interfering MPCs, is designed to extract the joint angle-delay sparsity map and power profiles for each active user in SC transmission. The novelty lies behind the integration of efficient adaptive detection/estimation algorithms in radar literature with massive MIMO hybrid beamforming in order to extract the scatter map of frequency-selective multi-user channel where the MPCs are resolvable both in angular and temporal domain. To the author's knowledge, there is no such prior work, that obtains the sparsity map both in angle and delay domain for SC transmission when hybrid massive MIMO architecture is utilized. Here, with the help of proposed methodology based on CFAR thresholding, the sparsity map and CCMs are acquired with lowered dimensional observation after hybrid beamforming for SC transmission. The construction of CCMs is completely different than the aforementioned studies in the literature. Second, based on the estimated CCMs, a novel statistical analog beamformer, suppressing both inter-group interference and ISI, and taking the doubly sparse structure of wideband channel into account, is designed for JSDM framework. In this thesis, a novel design methodology is proposed by inspiring from the work in [21] where a nearly optimal Capon like beamformer for general rank signal model is constructed. Here, the distribution of RF chains among different MPCs, by considering the amount of interference they are subject to, is optimized for SC transmission by using the estimated sparsity map and CCMs of all users. After reducing the dimension via the proposed statistical beamformer, efficient beamspace aware instantaneous CSI estimators are provided. It is shown that the proposed CCM construction and reduced rank channel acquisition techniques necessitate considerably lowered slow and fast time training overhead. Furthermore, the performance benchmark for doubly sparse SC wideband massive MIMO channel is achieved via the proposed algorithms which can be regarded as promising beam and channel acquisition techniques in this regard for next generation wireless networks.

In Chapter 2, a discrete time received signal model for the BS and statistical models for the MPCs in the region of interest are given. Also, an equivalent multi-ray channel model is provided.

In Chapter 3, an equivalent discrete time spatio-temporal domain signal model for JADPP estimation is derived. Also, how to efficiently receive signals at BS by constructing proper analog and digital beamspace in the hybrid beamforming structure adopted is explained. Finally, two different JADPP estimation algorithms are derived and provided.

In Chapter 4, sparsity map of each user on angle-delay plane is obtained by applying proposed two-stage CFAR thresholding algorithm onto the JADPPs constructed in the previous chapter. Then, the CCMs of each MPCs are constructed by means of JADPPs and sparsity map.

In Chapter 5, the analog beamformer design is tackled for frequency-selective massive MIMO systems employing SC modulation in TDD mode where the JADPP and sparsity map of the user channel is taken into account in general. Our goal is to find a good subspace (spanned by the columns of matrix \mathbf{U}_{RF}) on which the reduced dimensional instantaneous channel estimation can be realized as accurately as possible, so that a minimal performance compromise in the subsequent statistical signal processing operations after beamforming is provided.

In Chapter 6, after slow-time beam acquisition mode and user grouping based on JSDFM framework, fine instantaneous channel estimates are obtained in reduced dimension for each user.

In Chapter 7, probability of detection (P_D) curves are provided to evaluate the performance of AMF and MF based JADPP estimators. Also, performance of the channel estimators with respect to various parameters (e.g., signal-to-noise ratio (SNR), fast-time training sequence length (T_{fast}), and number of slow-time training snapshots (J), etc.) are demonstrated for different number of active users via normalized mean square error (nMSE) curves.

1.3 Notations

Throughout this thesis, vectors and matrices are denoted by boldface small and capital letters; the transpose, Hermitian and inverse of the matrix \mathbf{A} are denoted by \mathbf{A}^T , \mathbf{A}^H

and \mathbf{A}^{-1} ; $[\mathbf{A}]_{(i,j)}$ is the $(i,j)^{th}$ entry of \mathbf{A} ; the entry index of the vector and the matrix starts from 0; $\text{Tr}\{\mathbf{A}\}$ is the trace of \mathbf{A} ; $\det[\mathbf{A}]$ is the determinant of \mathbf{A} ; \mathbf{I} is the identity matrix with appropriate size; $\mathbb{E}\{\cdot\}$ is the statistical expectation; $|\mathcal{S}|$ denotes the cardinality of the set \mathcal{S} ; “\” stands for the set subtraction operation; $\|\mathbf{a}\|$ denotes the Euclidean norm of vector \mathbf{a} ; “ \rightarrow ” denotes that the variable on the left hand side of this operator *goes to* (approaches) the one on the right hand of side, and $\delta_{nn'}$ is the Kronecker-Delta function which is equal to 1 if $n = n'$ otherwise 0.

CHAPTER 2

SYSTEM MODEL

2.1 Introduction

In this chapter, a discrete time received signal model for the BS and statistical models for the MPCs in the region of interest are given. Also, an equivalent multi-ray channel model is provided.

Throughout this thesis, we consider a multi-user massive MIMO system operating at mm-wave frequency bands in TDD mode. We assume a SC (and linear) modulation (e.g., phase shift keying (PSK) or quadrature amplitude modulation (QAM)) and a transmission over frequency-selective channel, where the transmitted signal reaches the BS through multiple propagation paths (reflections from buildings, etc.), each having a different relative delay and amplitude, for all UEs with a slow evolution in time relative to the signaling interval (symbol duration). In addition, block fading channel model where the channel is locally time-invariant over a time slot but changes over time slots is assumed consistent with the many existing cellular network standards which implicitly assumes block fading [31].

2.2 Discrete Time Received Signal Model

It is assumed that the BS is equipped with N antennas and serves K single-antenna users. At the beginning of every coherence interval, time duration over which the channel impulse response is assumed to be not varying, all users transmit training sequences with length T . Then, the baseband equivalent received signal samples,

taken at symbol rate (W) after pulse matched filtering, are expressed as

$$\mathbf{y}_n = \sum_{k=1}^K \sum_{l=0}^{L-1} \mathbf{h}_l^{(k)} x_{n-l}^{(k)} + \mathbf{n}_n \quad (2.1)$$

for $n = 0, \dots, T - 1$, where $\mathbf{h}_l^{(k)}$ is $N \times 1$ multipath channel vector, namely, the array impulse response of the serving BS stemming from the l^{th} MPC of k^{th} user. Here, $\{x_n^{(k)}; -L + 1 \leq n \leq T - 1\}$ are the training symbols for the k^{th} user, L is the channel memory of k^{th} user multipath channels, and frequency-selective properties of the channel are specified in terms of quantized-normalized delays (i.e. delay indices, l , measured in unit of the symbol rate) owing to the wideband property of the channel. The $L - 1$ symbols at the start of the preamble, prior to the first observation at $n = 0$, are the precursors. Training symbols are selected from a signal constellation $S \in \mathbb{C}$ and $\mathbb{E} \left\{ |x_n^{(k)}|^2 \right\} = E_s$ is set to 1 for all k . In (2.1), \mathbf{n}_n are the additive complex white Gaussian noise (AWGN) vectors during uplink pilot segment with spatially and temporarily independent and identically distributed (*i.i.d.*) as $\mathcal{CN}(\mathbf{0}, N_0 \mathbf{I}_N)$, and N_0 is the noise power.

2.3 Statistical Models for MPCs

Measurement results [32], [33] have shown that there are fewer dominant scatterers in mm-wave due to the significance of blockage and the reduced effects of diffraction unlike UHF band environment [18]. Due to the short wavelength in mm-wave, a transmitted signal does not reflect well with surrounding environment. As the signal disperses due to roughness of the reflecting surface, it loses power. Therefore, the high path loss leads fewer propagation paths to be primary, such that the number of incoming signal path is limited [34] as demonstrated in Fig. 2.1. Due to these facts, in the JSDM framework adopted in this thesis, local scattering model is assumed. MPCs tend to occur in clusters on the angle-delay plane as a result of the interaction with physical clusters of the scatterers in the real environment. Then, AS seen by the BS becomes very narrow. This leads to the phenomenon called channel sparsity where the channel power of the MPCs is concentrated in a finite region of angles or delays. This sparsity can be resolved in the angle domain with the use of massive antenna arrays. Therefore, in this study, each resolvable MPC of the users is assumed to span some

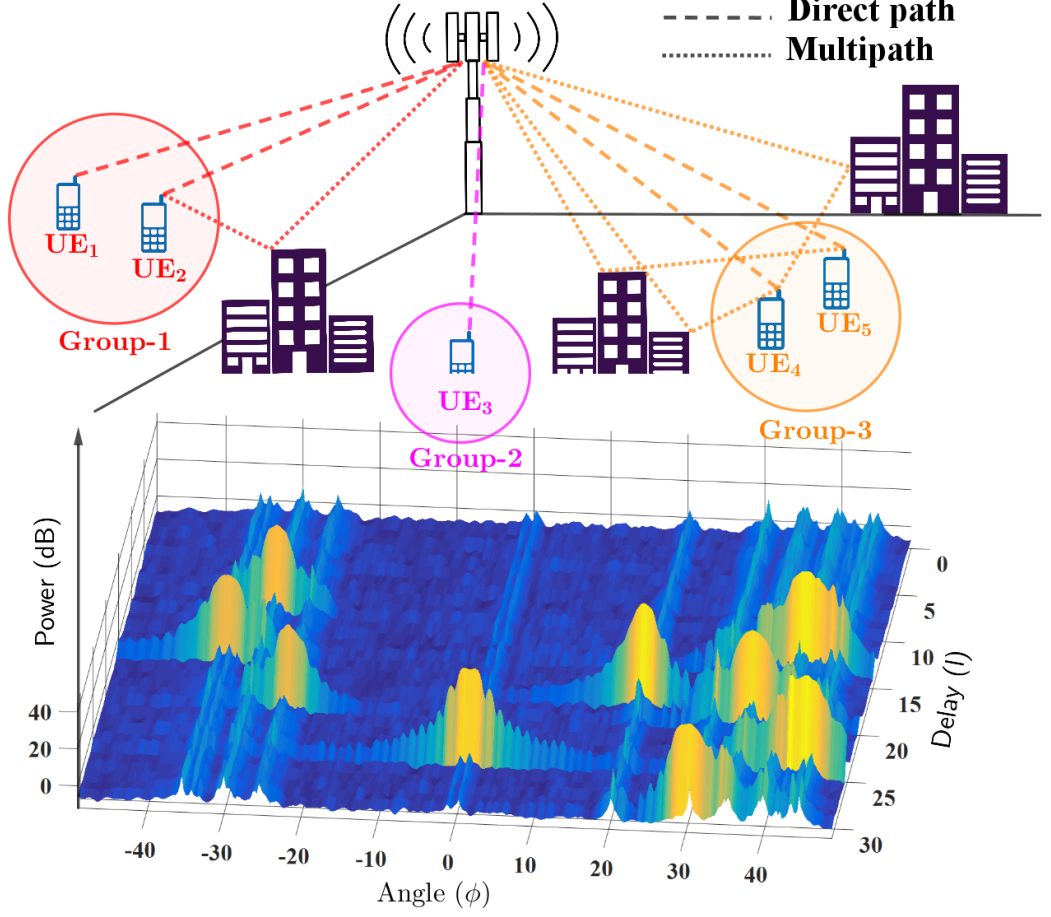


Figure 2.1: Angle-delay power profile of active users in massive MIMO system

particular angular sector, capturing local scattering around the corresponding UE's angle of arrival (AoA). In this study, we assume Rayleigh-correlated MPCs where each user has channel $\mathbf{h}_l^{(k)} \sim \mathcal{CN}(\mathbf{0}, \mathbf{R}_l^{(k)})$. It is important to note that Rayleigh channel model is only chosen for simulating the worst case scenario and subsequent algorithms are applicable to any channel distribution. Then, the cross-covariance matrix of l^{th} MPC of k^{th} user can be expressed in the form of

$$\mathbb{E} \left\{ \mathbf{h}_l^{(k)} \left(\mathbf{h}_{l'}^{(k')} \right)^H \right\} = \mathbf{R}_l^{(k)} \delta_{kk'} \delta_{ll'} \quad (2.2)$$

by using the uncorrelated local scattering model where all MPCs are assumed to be mutually independent according to the well-known wide sense stationary uncorrelated scattering (WSSUS) model [35], [36]; the multipath channel vectors are uncorrelated with respect to l , and also mutually uncorrelated with that of the different users. The average received SNR for the l^{th} MPC of k^{th} user can be defined as $\text{SNR}_l^{(k)} \triangleq \frac{E_s}{N_0} \beta_l^{(k)}$

where $\beta_l^{(k)} \triangleq \text{Tr}\{\mathbf{R}_l^{(k)}\}$ ¹. Then, the total received SNR of k^{th} user is $\frac{E_s}{N_0}\beta^{(k)}$ where $\beta^{(k)} \triangleq \sum_{l=0}^{L-1} \text{Tr}\{\mathbf{R}_l^{(k)}\} = \sum_{l=0}^{L-1} \beta_l^{(k)}$.

In mm-wave bands, an important phenomena is *channel sparsity* observed both in angular and temporal domain. That is to say, most of the channel power is concentrated in a finite region on *angle-delay* plane, corresponding to the interaction with physical clusters of scatterers in the real world [35]. Thus the number of significant MPCs is reduced to a much lower value than that for a microwave system, and these dominant MPCs are seen by the BS under a very constrained angular range (AoA support). Then, the CCM of a particular MPC is given by [27], [37]

$$\mathbf{R}_l^{(k)} \triangleq \int_{\mu_l^{(k)} - \frac{\Delta_l^{(k)}}{2}}^{\mu_l^{(k)} + \frac{\Delta_l^{(k)}}{2}} \rho_l^{(k)}(\phi) \mathbf{u}(\phi) \mathbf{u}^H(\phi) d\phi \quad (2.3)$$

where $\mathbf{u}(\phi) \in \mathbb{C}^{N \times 1}$ with $\|\mathbf{u}(\phi)\|^2 = 1$ is the array manifold (steering) vector whose expression is dependent on the array geometry. In this thesis, uniform linear array (ULA) structure is adopted and the corresponding manifold vector² is expressed

$$\mathbf{u}(\phi) = \frac{1}{\sqrt{N}} [1, e^{j\pi \sin(\phi)}, \dots, e^{j\pi(N-1)\sin(\phi)}]^T \quad (2.4)$$

where the antenna spacing d is the half of the signal carrier wavelength λ for $-\pi \leq \phi < \pi$. Note that, in this study, ULA structure is used for the ease of simulations, yet one can use uniform planar array (UPA) or more generally 3D (three-dimensional) MIMO antenna arrays instead. In (2.3), $\Delta_l^{(k)}$ is the AS of l^{th} MPC of k^{th} user with mean look angle $\mu_l^{(k)}$ and $\rho_l^{(k)}(\phi)$ is the angular power density of l^{th} MPC of k^{th} user at angle ϕ . The angular power density $\rho_l^{(k)}(\phi)$ is non-zero if $\phi \in S_l^{(k)}$ where $S_l^{(k)}$ is the angular support set of l^{th} MPC of k^{th} user and defined as

$$S_l^{(k)} \triangleq \left[\mu_l^{(k)} - \frac{\Delta_l^{(k)}}{2}, \mu_l^{(k)} + \frac{\Delta_l^{(k)}}{2} \right]. \quad (2.5)$$

Based on (2.3), it is simple to note that $\beta_l^{(k)}$ can be expressed in terms of $\rho_l^{(k)}(\phi)$ as

$$\beta_l^{(k)} = \text{Tr}\{\mathbf{R}_l^{(k)}\} = \int_{-\pi}^{\pi} \rho_l^{(k)}(\phi) d\phi. \quad (2.6)$$

¹ It shows the average SNR after maximal ratio combining (MRC) when the beam is steered toward the angular position of l^{th} MPC of k^{th} user. Then, $\frac{1}{N} \frac{E_s}{N_0} \beta_l^{(k)}$ can be seen as the average received SNR at each antenna element before beamforming.

² This is the typical expression for far-field narrow-band signals, while the the proposed idea can be easily extended to the near-field or wideband cases.

$\mathbf{R}_l^{(k)}$ in (2.2) is formed based on the small-scale fading given by the WSSUS model adopted [35], [38], [39]. Moreover, $\mathbf{R}_l^{(k)}$ is normalized so that the large-scale fading parameters such as path loss and shadowing are incorporated into the average received SNR. These parameters are assumed to be locally static, and the average channel strength can be easily learned over a long period of time. Therefore, $\mathbf{R}_l^{(k)}$ in (2.2), varying at a much lower rate compared to the instantaneous CSI, can be estimated with guaranteed accuracy for all intended users in practice, since there are enough time-frequency resources to be exploited for this purpose.

As can be seen from (2.3), the CCM of a particular MPC is a function of the power intensity $\rho_l^{(k)}(\phi)$ which is non-zero only for particular values of l among $\{0, 1, \dots, L - 1\}$ and for a constrained angular range of ϕ . These particular values on joint angle-delay plane for which $\rho_l^{(k)}(\phi)$ is significantly above the noise level, can be used to construct *sparsity map*, a matrix composed of ones and zeros only. The non-zero entries of this matrix shows the temporal locations and angular supports of active MPCs for each user channel on joint angle-delay plane. The sparsity map together with power intensities are slowly varying in time as the AoA of each user signal evolves depending on the user mobility, variation rate of the scattering environment characteristics, etc. [35], [40], [41], [42]. The rate of change of these long term parameters is much smaller than that of the actual small-scale fading process. This fact helps us design channel estimators in hybrid architecture after effectively reducing the signaling dimension via these slowly-varying parameters.

2.4 Equivalent Multi-Ray Channel Model for MPCs

The objective in this thesis is to determine the regions on joint angle-delay power map where $\rho_l^{(k)}$ is non-zero, and thus to estimate $\mathbf{R}_l^{(k)}$ based on (2.3). In order to realize this, the following practical model for the MPC of each user channel, namely $\mathbf{h}_l^{(k)}$ in (2.1), is adopted

$$\mathbf{h}_l^{(k)} \approx \sqrt{\frac{\Delta_l^{(k)}}{P}} \sum_{p=0}^{P-1} \alpha_{l,p}^{(k)} \mathbf{u}(\phi_{l,p}^{(k)}) \quad (2.7)$$

where the propagation from l^{th} MPC of k^{th} user to BS is assumed to be composed of P rays, and $\alpha_{l,p}^{(k)}$ represents the complex gain of the p^{th} ray having AoA $\phi_{l,p}^{(k)} \triangleq$

$\mu_l^{(k)} + \Delta_l^{(k)} \left(\frac{p}{P} - \frac{1}{2} \right)$, $p = 0, \dots, P-1$ [10], [17]. Since the WSSUS model is adopted, $\alpha_{l,p}^{(k)}$ satisfies the following equation

$$\mathbb{E} \left\{ \alpha_{l,p}^{(k)} \left[\alpha_{l,p'}^{(k)} \right]^* \right\} = \rho_l^{(k)}(\phi_{l,p}^{(k)}) \delta_{pp'}, \quad \phi_{l,p}^{(k)} \in S_l^{(k)}. \quad (2.8)$$

Based on the given model in (2.7), one can validate that the covariance of $\mathbf{h}_l^{(k)}$ asymptotically satisfies (2.3) after Riemann integration

$$\begin{aligned} \mathbf{R}_l^{(k)} &= \mathbb{E} \left\{ \mathbf{h}_l^{(k)} \left(\mathbf{h}_l^{(k)} \right)^H \right\} = \lim_{P \rightarrow \infty} \frac{\Delta_l^{(k)}}{P} \sum_{p=0}^{P-1} \mathbb{E} \left\{ \left| \alpha_{l,p}^{(k)} \right|^2 \right\} \mathbf{u}(\phi_{l,p}^{(k)}) \mathbf{u}^H(\phi_{l,p}^{(k)}) \\ &= \int_{S_l^{(k)}} \rho_l^{(k)}(\phi) \mathbf{u}(\phi) \mathbf{u}^H(\phi) d\phi \end{aligned} \quad (2.9)$$

where $\frac{\Delta_l^{(k)}}{P} \rightarrow d\phi$, and $\phi_{l,p}^{(k)} \rightarrow \phi$ as $P \rightarrow \infty$.

CHAPTER 3

HYBRID BEAMFORMING BASED JADPP ESTIMATION FOR WIDEBAND MASSIVE MIMO SYSTEMS

3.1 Introduction

In the previous chapter, statistical signal and MPC models for the adopted massive MIMO system are provided. In this chapter, we derive an equivalent discrete time spatio-temporal domain signal model to facilitate JADPP estimation. Also, we explain how to efficiently receive signals at BS by constructing proper analog and digital beamspace in the hybrid beamforming structure adopted. Finally, two different JADPP estimation algorithms are derived and provided.

When systems operate at mm-wave frequency bands, especially in massive MIMO systems, equipping each antenna element with its own RF chain is impractical due to the high implementation cost and power consumption. For this reason, a combination of analog beamforming (operating in passband) [43] and digital beamforming (operating in baseband) [44] is one of the low-cost solutions, and this combination is called hybrid beamforming [45], [46]. Note that, while analog beamforming has a specific geometrical meaning in the sense of collecting (or directing) energy from (or towards) specific angles using the array pattern of an antenna array, digital beamforming has rather an algebraic meaning, that is, a coefficient matrix [47].

In order to estimate the CCMs and sparsity map of each users, we need to estimate their JADPPs, i.e., $\rho_l^{(k)}(\phi)$ in (2.3) together with their angular support $S_l^{(k)}$ first. Since hybrid beamforming structure is used, limited number of RF chains (D) is utilized ($D \ll N$). In hybrid structure, before estimating the power profile of each MPCs, initially, the sector of interest, in which the users are to be served, is divided into

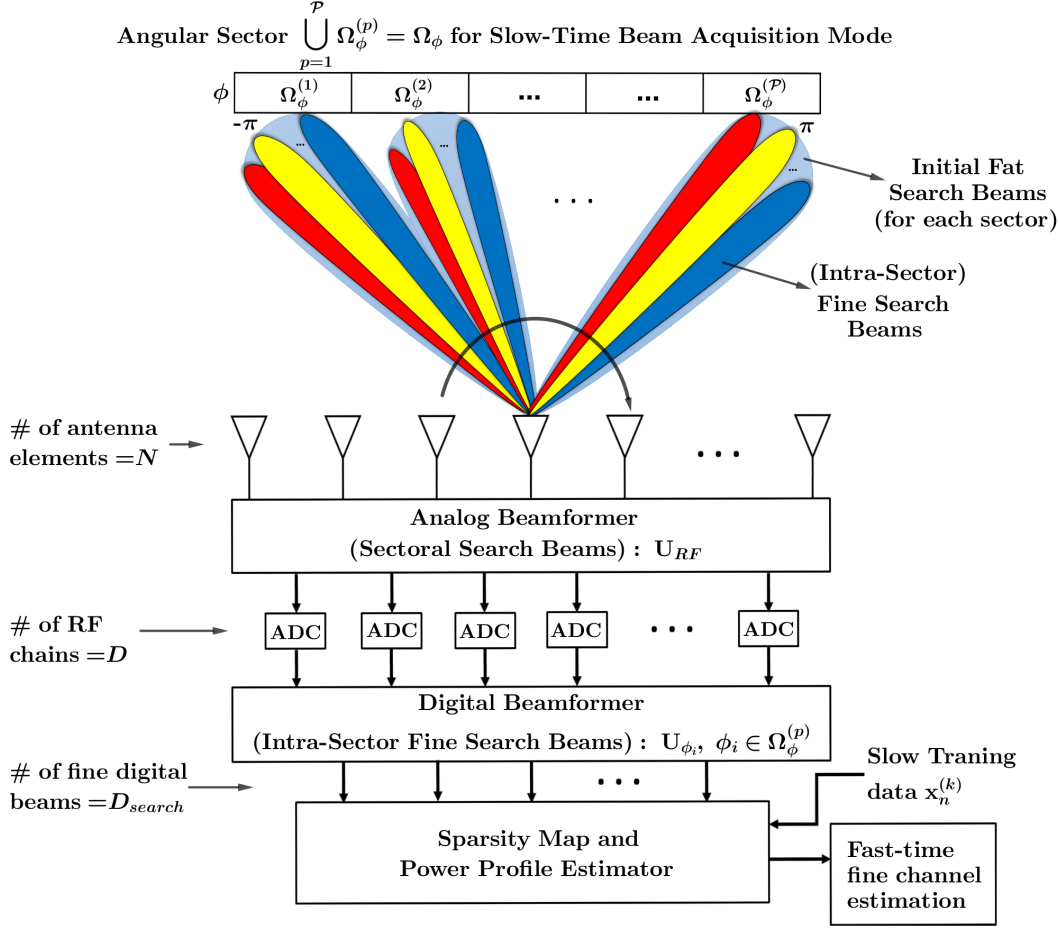


Figure 3.1: Beam acquisition scheme

non-overlapping sub-angular sectors (which are scanned by initial search beams constructed in analog domain). Then, JADPPs and sparsity map are extracted for each user in the sector of interest. This mode of operation is called as *slow-time beam acquisition mode* (or *slow-time training mode*) as illustrated in Fig. 3.1. In this mode, each user equipment (UE) transmits its *slow-time* training sequence so that the BS estimates the angular locations of each user MPCs in TDD mode. We define $T \times 1$ pilot (training) sequence vector for l^{th} MPC of k^{th} user as follows

$$\mathbf{x}_l^{(k)} \triangleq \left[x_{-l}^{(k)} \quad \dots \quad x_{T-1-l}^{(k)} \right]^H, \quad l = 0, \dots, L-1. \quad (3.1)$$

In addition, the angular search sector of interest, Ω_ϕ , which is defined as the ordered set of look angles ϕ (to which the beam is steered towards), is taken as

$$\Omega_\phi = \left\{ \phi \mid \phi = \phi_i; \phi_i = -\pi + i \frac{2\pi}{M}, i = 0, \dots, M-1 \right\}. \quad (3.2)$$

Then, the angular sub-sectors $\Omega_\phi^{(p)}$ in Fig. 3.1 are constructed such that $\bigcup_{p=1}^{\mathcal{P}} \Omega_\phi^{(p)} = \Omega_\phi$ where \mathcal{P} is the total number of angular sub-sectors. In slow-time training mode, where $\Omega_\phi^{(p)}$'s are scanned by initial search beams (constructed by the columns of analog beamformer matrix \mathbf{U}_{RF} peculiar to each sub-sector in Fig. 3.1) separately, each UE repeats its training sequence $\left\{x_n^{(k)}\right\}_{n=-L+1}^{T-1}$ in (2.1) at least \mathcal{P} times so that the power profiles of all users in Ω_ϕ are acquired by the BS.

3.2 Discrete Time Spatio-Temporal Domain Signal Model for JADPP Estimation

If the selected look angle $\phi_i \in \Omega_\phi$ is in the support set $S_l^{(k)}$, and the AS is narrow enough (which is the case for mm-wave channels [24]), we can approximate $\mathbf{h}_l^{(k)}$ by assuming $\phi_{l,p}^{(k)} \approx \phi_i$ in (2.7) as

$$\mathbf{h}_l^{(k)} \approx \sqrt{\frac{\Delta_l^{(k)}}{P}} \sum_{p=0}^{P-1} \alpha_{l,p}^{(k)} \mathbf{u}(\phi_{l,p}^{(k)}) \approx \alpha_l^{(k)} \mathbf{u}(\phi_i), \quad \phi_i \in \Omega_\phi \quad (3.3)$$

where $\alpha_l^{(k)} \triangleq \sum_{p=0}^{P-1} \sqrt{\frac{\Delta_l^{(k)}}{P}} \alpha_{l,p}^{(k)}$. Here, $\alpha_l^{(k)}$ can be regarded as the effective complex channel gain (reflection coefficient) of l^{th} MPC for k^{th} user at look angle ϕ_i . Asymptotically, one can calculate the corresponding average channel power as

$$\begin{aligned} \mathbb{E} \left\{ \left| \alpha_l^{(k)} \right|^2 \right\} &= \lim_{P \rightarrow \infty} \mathbb{E} \left\{ \left| \sum_{p=0}^{P-1} \sqrt{\frac{\Delta_l^{(k)}}{P}} \alpha_{l,p}^{(k)} \right|^2 \right\} \\ &= \lim_{P \rightarrow \infty} \sum_{p=0}^{P-1} \frac{\Delta_l^{(k)}}{P} \rho_l^{(k)}(\phi_{l,p}^{(k)}) \\ &= \int_{S_l^{(k)}} \rho_l^{(k)}(\phi) d\phi \\ &= \beta_l^{(k)} \end{aligned} \quad (3.4)$$

when $P \rightarrow \infty$ in (2.7), and it can be noted that if uniform power distribution is assumed, then $\beta_l^{(k)} = \rho_l^{(k)} \Delta_l^{(k)}$. During the slow-time training phase, if the BS intends to estimate the effective channel gain of the l^{th} MPC for the k^{th} user at look angle ϕ_i , namely $\alpha_l^{(k)}$, it is useful to construct the following discrete time equivalent signal

model in spatio-temporal domain by using (2.1), (3.1), and (3.3):

$$\begin{aligned} \mathbf{Y} \triangleq \begin{bmatrix} \mathbf{y}_0 & \mathbf{y}_1 & \cdots & \mathbf{y}_{T-1} \end{bmatrix}_{N \times T} &= \mathbf{h}_l^{(k)} \left(\mathbf{x}_l^{(k)} \right)^H + \mathbf{N}_l^{(k)} \\ &\triangleq \alpha_l^{(k)}(\phi_i) \mathbf{u}(\phi_i) \left(\mathbf{x}_l^{(k)} \right)^H + \mathbf{N}_l^{(k)} \end{aligned} \quad (3.5)$$

where $\mathbf{N}_l^{(k)}$, total interfering component to l^{th} MPC of the k^{th} user, is given as

$$\mathbf{N}_l^{(k)} \triangleq \sum_{l'=0, l' \neq l}^{L-1} \mathbf{h}_{l'}^{(k)} \left(\mathbf{x}_{l'}^{(k)} \right)^H + \sum_{k'=1, k' \neq k}^K \sum_{l'=0}^L \mathbf{h}_{l'}^{(k')} \left(\mathbf{x}_{l'}^{(k')} \right)^H + \begin{bmatrix} \mathbf{n}_0 & \cdots & \mathbf{n}_{T-1} \end{bmatrix}. \quad (3.6)$$

Note that in (3.6), $\mathbf{N}_l^{(k)}$ is composed of self interference signal stemming from the MPCs of k^{th} user other than the l^{th} MPC, inter-user interference signal and AWGN. Based on (3.5), $\mathbb{E} \left\{ \left| \alpha_l^{(k)} \right|^2 \right\}$ is to be estimated at preassumed spatio-temporal locations $\{\phi_i, l\}$ on joint angle-delay map for all active users. That is to say, average power of the MPCs, which are likely to exist, at each angular and temporal delay locations (for $l = 0, \dots, L-1$ and $\forall \phi_i \in \Omega_\phi$) is to be estimated for all active users.

3.3 Initial Beam Acquisition Mode

In hybrid beamforming architecture adopted, the initial analog beamformer matrix, \mathbf{U}_{RF} , is constructed to illuminate the intended sub-sector of interest $\Omega_\phi^{(p)}$ where $\phi_i \in \Omega_\phi^{(p)}$ as shown in Fig. 3.1¹. In order to maximize the coverage of the intended sector, the columns of \mathbf{U}_{RF} (where $\mathbf{U}_{RF}^H \mathbf{U}_{RF} = \mathbf{I}_D$) can be obtained as the most dominant D (number of RF chains) eigenvectors of the following matrix

$$\mathbf{R}^{(sector-p)} \triangleq \int_{\phi \in \Omega_\phi^{(p)}} \mathbf{u}(\phi) \mathbf{u}^H(\phi) d\phi. \quad (3.7)$$

Here, $\mathbf{R}^{(sector-p)}$ can be regarded as the spatial autocorrelation matrix of user channels in sector p , and the analog beamforming via \mathbf{U}_{RF} in this mode is nothing but the Karhunen-Loeve Transform (KLT) in angular domain [44]. Assuming that each user in sector- p having a mean AoA uniformly distributed over the sector of interest, $\mathbf{R}^{(sector-p)}$ can also be considered as the initial CCM estimate of each user MPCs in sector- p . Similarly, intra-sector digital fine search beams for the look angle $\phi_i \in \Omega_\phi^{(p)}$

¹ The initial analog beamformer \mathbf{U}_{RF} used to estimate power profile in slow-time training mode needs to satisfy $\mathbf{u}(\phi_i) \approx \mathbf{U}_{RF} \mathbf{U}_{RF}^H \mathbf{u}(\phi_i)$ in order for intended sector to be covered properly.

shown in Fig. 3.1, namely \mathbf{U}_{ϕ_i} 's are constructed after projection on the range space of \mathbf{U}_{RF} . After illuminating the intended sector $\Omega_{\phi}^{(p)}$ by \mathbf{U}_{RF} , the digital search beams in reduced dimension are steered towards ϕ_i at which $\mathbb{E}\left\{\left|\alpha_l^{(k)}\right|^2\right\}$ in (3.3) is to be estimated. In order to realize this, a particular angular region (patch) in $\Omega_{\phi}^{(p)}$ whose center is the look angle ϕ_i , which we are interested in, is to be selected and illuminated by \mathbf{U}_{ϕ_i} . Here, \mathbf{U}_{ϕ_i} can be contemplated as the $D \times D_{search}$ matrix of the eigenvectors corresponding to the largest D_{search} eigenvalues of \mathbf{R}_{ϕ_i} which is defined as the reduced dimensional spatial autocorrelation matrix of the user channels of selected angular patch in $\Omega_{\phi}^{(p)}$ whose center is ϕ_i , and D_{search} is the search dimension (number of digital beams to be constructed). Then, \mathbf{R}_{ϕ_i} can be constructed for the mean look angle $\phi_i \in \Omega_{\phi}^{(p)}$ as

$$\mathbf{R}_{\phi_i} = \mathbf{U}_{RF}^H \left(\int_{\phi_i - \sigma/2}^{\phi_i + \sigma/2} \mathbf{u}(\phi) \mathbf{u}^H(\phi) d\phi \right) \mathbf{U}_{RF} \quad (3.8)$$

where σ is the angular width of the selected patch in sector- p which is simply called as the look spread. While constructing these initial intra-sector digital beams, \mathbf{U}_{ϕ_i} 's can be normalized such that $\mathbf{U}_{\phi_i}^H \mathbf{U}_{\phi_i} = \mathbf{I}_{D_{search}}$ for proper operation. Then, we can define a hybrid beamformer matrix in slow-time training mode as $\mathbf{U} \triangleq \mathbf{U}_{RF} \mathbf{U}_{\phi_i}$ and express the signals of (3.5) in reduced dimensional digital beamspace as

$$\tilde{\mathbf{Y}} = \mathbf{U}^H \mathbf{Y}, \quad \tilde{\mathbf{N}}_l^{(k)} = \mathbf{U}^H \mathbf{N}_l^{(k)}, \quad \tilde{\mathbf{u}}(\phi_i) = \mathbf{U}^H \mathbf{u}(\phi_i). \quad (3.9)$$

Based on (3.9), firstly $\mathbb{E}\left\{\left|\alpha_l^{(k)}\right|^2\right\}$ is to be estimated in order to construct JADPP and the sparsity map of each active user for each look angle $\phi_i \in \Omega_{\phi}$. Later, \mathbf{U}_{RF} is to be updated for *fast-time instantaneous channel acquisition* (as explained in Section 5.3) by using the estimated CCMs (which are constructed via the JADPP and sparsity map of each user).

3.4 Proposed JADPP Estimation Techniques

By using the reduced dimensional observations obtained after hybrid beamforming in (3.9), we propose efficient algorithms to estimate the average channel power $\mathbb{E}\left\{\left|\alpha_l^{(k)}\right|^2\right\}$ in (3.3) for each look angle $\phi_i \in \Omega_{\phi}^{(p)}$ and temporal delays $l = 0, \dots, L-1$.

Here, we first conceive that $\alpha_l^{(k)}$ is to be estimated for each preassumed *spatio-temporal resolution cell* which is defined as the pair $\{\phi_i, l\}$ on joint angle-delay map by using each slow-time training snapshot \mathbf{Y} in (3.5). We denote this estimate as $\hat{\alpha}_l^{(k)}(\phi_i)$. Then, the estimate of $\mathbb{E}\left\{|\alpha_l^{(k)}|^2\right\}$ at look angle ϕ_i , which is denoted by $\hat{\beta}_l^{(k)}(\phi_i)$, is constructed as $\hat{\beta}_l^{(k)}(\phi_i) = |\hat{\alpha}_l^{(k)}(\phi_i)|^2$. Since $\mathbb{E}\left\{|\alpha_l^{(k)}|^2\right\}$ is proportional with $\rho_l^{(k)}(\phi_i)$ from (3.4) when $|\Omega_\phi| = M$ is large enough, $\hat{\beta}_l^{(k)}(\phi_i)$ gives us the estimate of the angular power density at look angle ϕ_i . We develop two different approaches in order to construct $\hat{\alpha}_l^{(k)}(\phi_i)$ for each spatio-temporal resolution cell $\{\phi_i, l\}$:

3.4.1 Spatio-Temporal Adaptive Matched Filter (AMF)

After reducing the dimension of spatio-temporal observation \mathbf{Y} via hybrid beamformer in (3.9), the maximum likelihood (ML) estimate of non-random parameter $\alpha_l^{(k)}$ at look angle $\phi_i \in \Omega_\phi$ can be obtained as

$$\hat{\alpha}_l^{(k)}(\phi_i) = \frac{1}{\|\mathbf{x}_l^{(k)}\|^2} \frac{\tilde{\mathbf{u}}^H(\phi_i) \left[\Psi_l^{(k)} \right]^{-1} \tilde{\mathbf{Y}} \mathbf{x}_l^{(k)}}{\tilde{\mathbf{u}}^H(\phi_i) \left[\Psi_l^{(k)} \right]^{-1} \tilde{\mathbf{u}}(\phi_i)}, \quad i = 0, \dots, M-1 \quad (3.10)$$

where

$$\Psi_l^{(k)} = \tilde{\mathbf{Y}} \left[\mathbf{I} - \frac{\mathbf{x}_l^{(k)} \left(\mathbf{x}_l^{(k)} \right)^H}{\|\mathbf{x}_l^{(k)}\|^2} \right] \tilde{\mathbf{Y}}^H \quad (3.11)$$

whose detailed derivation is given in Appendix I. While obtaining (3.10), the spatial covariance matrix of interfering MPCs are also assumed to be unknown non-random parameters to be estimated together with $\alpha_l^{(k)}(\phi_i)$. We call this estimator as adaptive matched filter (AMF), inspired from the adaptive detection algorithm in [48], since a sample matrix inversion (SMI) type adaptive filtering is utilized in (3.10) to construct $\left[\Psi_l^{(k)} \right]^{-1}$. The spatial autocorrelation matrix of interfering MPCs (given by $\mathbf{N}_l^{(k)}$ in (3.6)) is estimated by means of a simple temporal averaging of the columns of $\tilde{\mathbf{Y}}$. The most important difference of the proposed AMF from the conventional SMI based detectors in [12], [48], and [49] is that the temporal averaging to form $\Psi_l^{(k)}$ is obtained after projecting the observation signal $\tilde{\mathbf{Y}}$ on the desired signal nullspace (i.e., the null-space of $\left(\mathbf{x}_l^{(k)} \right)^H$ in (3.1)) in order to eliminate the signal contamination due to desired MPC at $\{\phi_i, l\}$ for k^{th} user.

3.4.2 Spatio-Temporal Matched Filter (MF)

As a special case, one can simplify (3.10) by taking $\Psi_l^{(k)}$ as $\mathbf{I}_{D_{search}}$, which corresponds to assuming spatially white interfering signal to desired MPC at $\{\phi_i, l\}$. In this case, the following estimator, which is a spatio-temporal matched filter (MF) without any adaptive cancellation of interference in (3.5), is given:

$$\hat{\alpha}_l^{(k)}(\phi_i) = \frac{\tilde{\mathbf{u}}^H(\phi_i) \tilde{\mathbf{Y}} \mathbf{x}_l^{(k)}}{\|\tilde{\mathbf{u}}(\phi_i)\|^2 \|\mathbf{x}_l^{(k)}\|^2}, \quad i = 0, \dots, M - 1 \quad (3.12)$$

Then, the outputs of AMF/MF type estimators will be provided to the subsequent thresholding algorithm to construct the joint angle-delay sparsity map of each user in the sector of interest.

CHAPTER 4

SPARSE CCM CONSTRUCTION FOR WIDEBAND MASSIVE MIMO CHANNELS

4.1 Introduction

In a massive MIMO system, the propagation between users and BS antennas occurs through relatively sparse MPCs in the angle-delay domain [32]. This allows to resolve channel MPCs in the joint angle-delay domain, where the signal subspace of other MPCs can be separated from that of the intended MPC based on their different multipath footprint in the angle-delay domain.

In the previous chapter, two different JADPP estimation algorithms (AMF in (3.10) and MF in (3.12)) are proposed. The JADPPs are constructed by assuming that an MPC is likely to exist at each spatio-temporal cell on angle-delay domain. Therefore, an efficient thresholding algorithm is required to acquire the narrow and sparse MPC regions from JADPP estimates on the whole angle-delay plane. In this chapter, sparsity map of each user on angle-delay plane is obtained by applying proposed two-stage CFAR thresholding algorithm onto the JADPPs constructed in the previous chapter. Then, the CCMs of each MPCs are formed by means of JADPPs and sparsity map.

4.2 User Activity Detection and Sparsity Map Construction via Constant False Alarm Rate (CFAR) Algorithm

Based on the estimated JADPPs, one can construct the sparsity map composed of the spatio-temporal resolution cells $\{\phi_i, l\}$ in joint angle-delay domain where $\rho_i^{(k)}(\phi_i)$ is

determined to be non-zero for $\phi_i \in \Omega_\phi$ and $l = 0, \dots, L - 1$. In order to construct the sparsity map, two-stage adaptive thresholding is applied onto $\hat{\beta}_l^{(k)}(\phi_i) = |\hat{\alpha}_l^{(k)}(\phi_i)|^2$ (obtained via AMF/MF type JADPP estimators in (3.10) and (3.12)) by inspiring from the well known cell-averaging CFAR technique in radar literature [50]. Thus, the regions where the power of MPCs concentrated on joint angle-delay map is determined for each user. The following adaptive thresholding can be applied to each resolution cell $\{\phi_i, l\}$, called as *cell-under-test (CUT)*, on joint angle-delay domain:

$$\hat{\beta}_l^{(k)}(\phi_i) \underset{H_0}{\overset{H_1}{\geq}} \gamma, \quad \phi_i \in \Omega_\phi \quad \text{and} \quad l = 0, \dots, L - 1 \quad (4.1)$$

where γ is a CFAR threshold which is to be adaptively determined. While constructing $\hat{\beta}_l^{(k)}(\phi_i)$, one can use multiple non-coherent snapshots, i.e., independent observations \mathbf{Y} in (3.5) of the same sector obtained via the slow-time training data. Then, the random fluctuations on $\hat{\beta}_l^{(k)}(\phi_i)$ can be smoothed out by taking simple averaging over multiple snapshots:

$$\hat{\beta}_l^{(k)}(\phi_i) = \frac{1}{J} \sum_{j=1}^J \hat{\beta}_{l,j}^{(k)}(\phi_i), \quad \phi_i \in \Omega_\phi \quad \text{and} \quad l = 0, \dots, L - 1 \quad (4.2)$$

where $\hat{\beta}_{l,j}^{(k)}(\phi_i) = |\hat{\alpha}_{l,j}^{(k)}(\phi_i)|^2$ is the estimated power profiles obtained from j^{th} slow-time training snapshot for $j = 1, \dots, J$ and J is the total number of slow-time training snapshots. In order to smooth out the fluctuations on the estimated power profiles and also capture the power profile of whole region of interest, we need to wait a duration which is equal to $\mathcal{P} \times J$ slow-time training snapshots. However, this slow-time long-term parameter learning process is repeated in a much slower rate when compared to the fast-time operations, thus, it does not heavily affect the training overhead.

4.2.1 Two-Stage CFAR Algorithm

The following *two-stage CFAR* algorithm, which can be realized via adaptive thresholding both in temporal and spatial domain for the CUT on joint angle-delay map, is proposed:

4.2.1.1 Temporal thresholding for selected resolution cell

For each user, firstly, temporal thresholding on $\hat{\beta}_l^{(k)}(\phi_i)$ at each look angle $\phi_i \in \Omega_\phi$ is applied:

$$\hat{\beta}_l^{(k)}(\phi_i) \underset{H_0}{\overset{H_1}{\geq}} \gamma_1, \quad (4.3)$$

$$\gamma_1 = \left(\bar{P}_{FA}^{-\frac{1}{L-1}} - 1 \right) \left(\sum_{l'=0, l' \neq l}^{L-1} \hat{\beta}_{l'}^{(k)}(\phi_i) \right), \quad i = 0, \dots, M-1. \quad (4.4)$$

where \bar{P}_{FA} is the desired average false alarm probability of the test. In (4.4), the adaptive threshold γ_1 is obtained by simple averaging over JADPPs of each user for different delay locations other than l at the selected look angle ϕ_i similar to the well-known cell-averaging CFAR tests in radar literature [50]. By assuming that $\hat{\beta}_l^{(k)}$'s $\forall l$ are exponential *i.i.d.* random variables, one can obtain the threshold level γ_1 which provides constant false alarm rate despite varying interference power levels¹. That is to say, the test in (4.3) yields average false alarm probability which does not depend on the actual value of interfering signal levels.

4.2.1.2 Spatial thresholding for selected resolution cell

Similarly, adaptive spatial thresholding on estimated JADPPs at each spatio-temporal location $\{\phi_i, l\}$ on angle-delay domain can be applied as

$$\hat{\beta}_l^{(k)}(\phi_i) \underset{H_0}{\overset{H_1}{\geq}} \gamma_2, \quad (4.5)$$

$$\gamma_2 = \left(\bar{P}_{FA}^{-\frac{1}{M-|\Pi_{\phi_i}|}} - 1 \right) \left(\sum_{\{\forall \phi' \in \Omega_\phi | \phi' \notin \Pi_{\phi_i}\}} \hat{\beta}_l^{(k)}(\phi') \right), \quad i = 0, \dots, M-1 \quad (4.6)$$

where $M = |\Omega_\phi|$, and Π_{ϕ_i} is the guard interval, which is an angular window with mean angle of ϕ_i . It is taken as

$$\Pi_{\phi_i} = \left\{ \phi \mid \phi = \phi_i + m \frac{2\pi}{M}, \quad m = -\kappa, \dots, \kappa \right\} \quad (4.7)$$

where $|\Pi_{\phi_i}| \triangleq 2\kappa + 1$ is the length of guard interval, i.e., the number of angular resolution cells around the CUT (which are taken as guard cells, not used in cell

¹ The false alarm rate is nothing but the probability of declaring an empty resolution cell, where $\rho_l^{(k)}(\phi_i) = 0$, as an active MPC having non-zero power level.

averaging). In (4.6), the adaptive threshold γ_2 is obtained by averaging over estimated JADPPs of each user for different look angles $\phi' \in \Omega_\phi \setminus \Pi_{\phi_i}$ at selected temporal delay l .

4.2.2 Joint Angle-Delay Domain Sparsity Map Construction of User Power Profiles

After thresholding, the sparsity map of k^{th} user, $\mathbf{I}^{(k)}$, which is $M \times L$ matrix, where M is the number of resolution cells in angular domain, is constructed. If there is a detection at a particular CUT, the corresponding entry is set to 1, otherwise 0. That is to say, $[\mathbf{I}^{(k)}]_{(i,l)}$ is obtained for $l = 0, \dots, L - 1$ and $\forall \phi_i \in \Omega_\phi$ as

$$[\mathbf{I}^{(k)}]_{(i,l)} = \begin{cases} 1, & \text{if } \hat{\beta}_l^{(k)}(\phi_i) > \gamma_1 \text{ and } \hat{\beta}_l^{(k)}(\phi_i) > \gamma_2 \\ 0, & \text{otherwise} \end{cases}. \quad (4.8)$$

Note that, when all elements of $\mathbf{I}^{(k)}$ is zero, it means that k^{th} user is not an active user.

An Exemplary Scenario: In Fig. 4.1, the estimated power levels of each MPCs of active users obtained via the proposed JADPP estimators, namely AMF and MF are demonstrated. A scenario where a BS with $N = 100$ antenna elements in the form of ULA is serving $K = 2$ single-antenna users is investigated. It is assumed that both users have two active MPCs where the resolution cells with non-zero power levels are $\{\phi, l\} = \{2.8, 2\}$ and $\{-7.1, 10\}$ for the first user, and $\{\phi, l\} = \{6.3, 5\}$ and $\{9.2, 8\}$ for the second one respectively. For all MPCs, the AS is taken as 2° and $T = 16$ is used in simulations. It is assumed that the received power levels are $\beta^{(1)} = 40$ dB and $\beta^{(2)} = 50$ dB. In Fig. 4.2, sparsity maps after applying two-stage thresholding on JADPP estimations are provided. Here, \bar{P}_{FA} is set to 10^{-3} and $|\Pi_{\phi_i}|$ is taken as 4° . It is seen from Fig. 4.1 that, AMF based JADPP estimator provides clearer power profiles for both users while MF based one yields polluted power profile for each user. In correspondence with the given JADPP estimations, it is seen from Fig. 4.2 that AMF based two-stage CFAR thresholding algorithm is able to detect each MPCs of both users while MF based one misses one of the MPCs belonging to the first user, whose SNR is low with respect to the second user, taking strong inter-user interference. Also, for the second user, MF based thresholding could not eliminate an MPC where there is no user activity in fact. Since MF based JADPP estimator does not

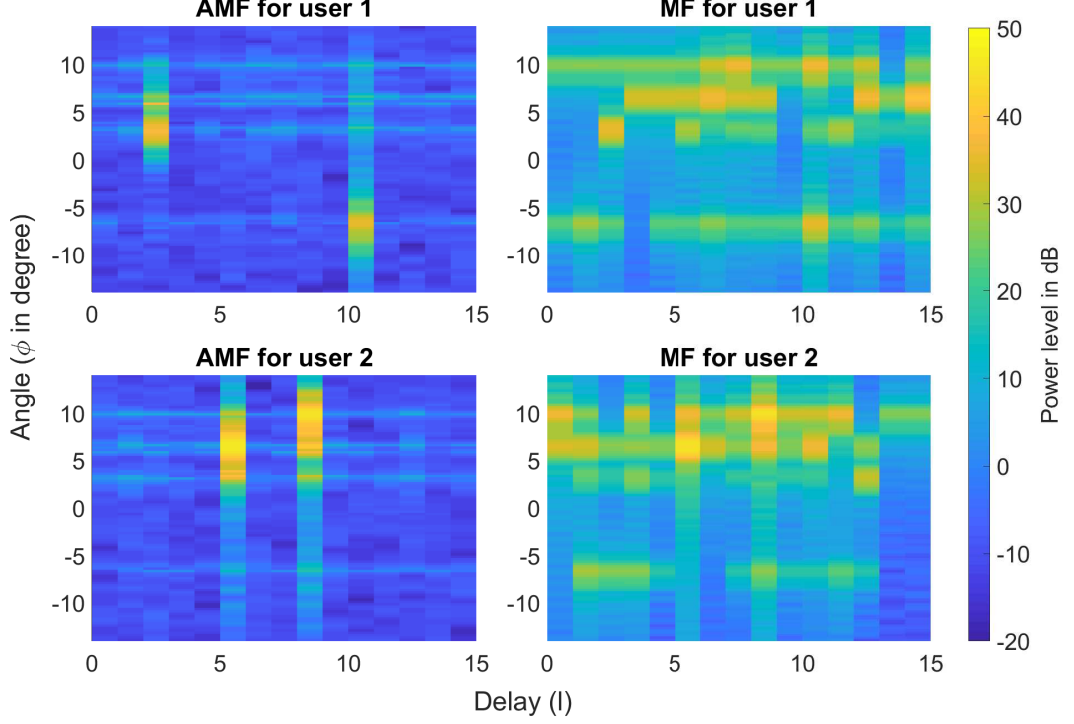


Figure 4.1: JADPP for user 1 and user 2 ($K = 2$, $T = 16$, $\beta^{(1)} = 40$ dB, $\beta^{(2)} = 50$ dB)

take the inter-user interference into account, it yields polluted and non-homogenous power profiles which deteriorates the performance of CFAR thresholding algorithm remarkably as demonstrated in the given figures.

4.2.3 Performance Metrics for User Activity Detection

Here, the aim is to find the probability of detecting the active MPCs, which have non-zero power at a given angle-delay resolution cell. We use two performance metrics to compare AMF in (3.10) and MF in (3.12), namely the probability of detection (P_D) and the probability of false alarm (P_{FA}). By using the constructed sparsity map in (4.8), the probability of detection for the active MPCs of k^{th} user can be expressed as

$$P_D^{(k)} \triangleq \frac{1}{|\mathcal{L}^{(k)}|} \sum_{l \in \mathcal{L}^{(k)}} \Pr \left\{ [\mathbf{I}^{(k)}]_{(\psi_l^{(k)}, l)} = 1 \right\} \quad (4.9)$$

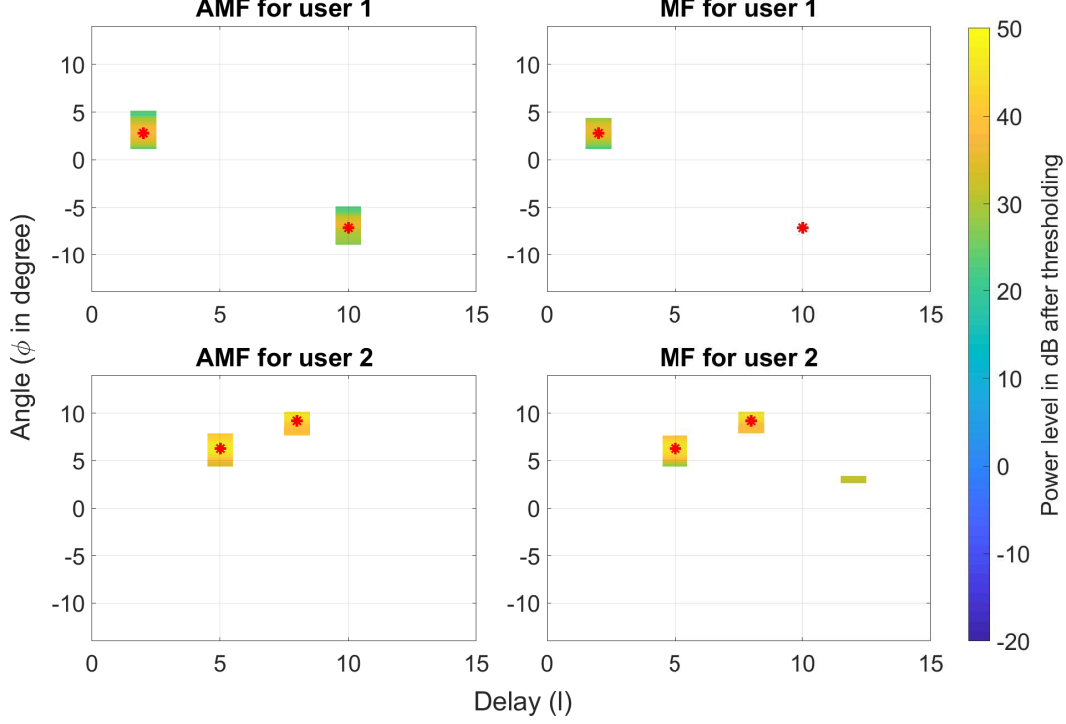


Figure 4.2: Sparsity map for user 1 and user 2 ($K = 2$, $T = 16$, $\beta^{(1)} = 40$ dB, $\beta^{(2)} = 50$ dB)

where $\mathcal{L}^{(k)}$ is the set of indices of active MPCs having positive $\beta_l^{(k)}$, and $\psi_l^{(k)}$ is the angular index pointing the mean AoA for l^{th} MPC of k^{th} user defined as

$$\psi_l^{(k)} \triangleq \arg \min_{i=0, \dots, M-1} |\mu_l^{(k)} - \Omega_\phi(i)| \quad (4.10)$$

where $\Omega_\phi(i)$ is i^{th} element of Ω_ϕ . Similarly, the probability of false alarm, showing the probability that inactive MPCs (having zero $\beta_l^{(k)}$) are declared as active for k^{th} user, can be expressed as

$$P_{FA}^{(k)} \triangleq \frac{1}{ML} \sum_{l=0}^{L-1} \sum_{i=0, i \notin \Gamma_l^{(k)}}^{M-1} \Pr \left\{ [\mathbf{I}^{(k)}]_{(i,l)} = 1 \right\} \quad (4.11)$$

where $\Gamma_l^{(k)}$ is the set of indices i such that the look angle $\phi_i \in \Omega_\phi$ is inside the angular support set $S_l^{(k)}$. In other words, $\Gamma_l^{(k)}$ can be expressed as

$$\Gamma_l^{(k)} = \left\{ i \mid i = 0, \dots, M-1 \text{ and } \Omega_\phi(i) \in S_l^{(k)} \right\}. \quad (4.12)$$

4.3 CCM Construction Based on Estimated Sparsity Map

CCMs can be constructed purely based on the estimated power levels and sparsity map of each user. It is important to note that the observation signal \mathbf{Y} in (3.5) is not available in full dimension in our hybrid structure, however each CCM needs to be estimated in full dimension. Also, we need to obtain accurate enough CCM estimates with significantly reduced amount of training snapshots. That is why we need parametric construction of CCM by exploiting its reduced rank property due to sparse nature of the channel. Hence, we can construct CCMs for each user by using sparsity matrix $\mathbf{I}^{(k)}$ and power estimates $\hat{\beta}_l^{(k)}$ as follows

$$\hat{\mathbf{R}}_l^{(k)} = \begin{cases} \mathbf{0}_{N \times N}, & \text{if } c_l^{(k)} = 0 \\ \sum_{i=0}^{M-1} \frac{\hat{\beta}_l^{(k)}(\phi_i)}{c_l^{(k)}} [\mathbf{I}^{(k)}]_{(i,l)} \mathbf{u}(\phi_i) \mathbf{u}^H(\phi_i), & \text{otherwise} \end{cases} \quad (4.13)$$

where $c_l^{(k)} \triangleq \sum_{i=0}^{M-1} [\mathbf{I}^{(k)}]_{(i,l)}$ for $l = 0, \dots, L-1$ and $\phi_i \in \Omega_\phi$. The proposed construction technique in (4.13) is completely different from the conventional ones, which are based on SMI type temporal averaging in full dimension necessitating large amount of training snapshots for proper operation [12].

Asymptotic Convergence of the Proposed CCM Estimation:

It is interesting to see that $\hat{\mathbf{R}}_l^{(k)}$ in (4.13) converges to true CCM values, $\mathbf{R}_l^{(k)}$ in (2.3) when the sparsity map in (4.8) is perfectly acquired, i.e.,

$$[\mathbf{I}^{(k)}]_{(i,l)} = \begin{cases} 1, & \text{if } \phi_i \in S_l^{(k)} \\ 0, & \text{if } \phi_i \notin S_l^{(k)} \end{cases} \quad (4.14)$$

When $\hat{\beta}_l^{(k)}(\phi_i) = \rho_l^{(k)}(\phi_i) \Delta_l^{(k)}$ (if AS is narrow enough), we can obtain the asymptotic

value of $\hat{\mathbf{R}}_l^{(k)}$ by letting $c_l^{(k)} = P$ in (4.13), and both $M, P \rightarrow \infty$, as follows

$$\begin{aligned}
\hat{\mathbf{R}}_l^{(k)} &= \lim_{M \rightarrow \infty} \sum_{\left\{ \substack{\forall \phi_i \in S_l^{(k)} \\ i=0, \dots, M-1} \right\}} \frac{\rho_l^{(k)}(\phi_i)}{P} \Delta_l^{(k)} \mathbf{u}(\phi_i) \mathbf{u}^H(\phi_i) \\
&= \lim_{P \rightarrow \infty} \frac{\Delta_l^{(k)}}{P} \sum_{p=0, \phi_{l,p}^{(k)} \in S_l^{(k)}}^{P-1} \rho_l^{(k)}(\phi_{l,p}^{(k)}) \mathbf{u}(\phi_{l,p}^{(k)}) \mathbf{u}^H(\phi_{l,p}^{(k)}) \quad \left(\frac{\Delta_l^{(k)}}{P} \rightarrow d\phi, \phi_{l,p}^{(k)} \rightarrow \phi \right) \\
&= \int_{S_l^{(k)}} \rho_l^{(k)}(\phi) \mathbf{u}(\phi) \mathbf{u}^H(\phi) d\phi \\
&= \mathbf{R}_l^{(k)}.
\end{aligned} \tag{4.15}$$

This shows that when the number of angular resolution cells is high enough, and accurate JADPP estimates are available, parametric construction of $\mathbf{R}_l^{(k)}$ by (4.13) in full dimension can be realized efficiently after hybrid beamforming.

CHAPTER 5

NEARLY OPTIMAL COVARIANCE-BASED REDUCED RANK ANALOG BEAMFORMER DESIGN

5.1 Introduction

In the previous chapter, sparsity map and CCMs of each users are obtained via the estimated JADPPs. In this chapter, based on the estimated CCMs in (4.13), the analog beamformer, \mathbf{U}_{RF} in Fig. 3.1 is updated by using the statistical properties of each user channels. In *slow-time beam acquisition* mode, the long term parameters of each user channels, i.e., JADPPs $\rho_l^{(k)}(\phi)$, the sparsity map $\mathbf{I}^{(k)}$, and CCMs $\mathbf{R}_l^{(k)}$ are acquired by using slow-time training snapshots as explained in previous chapters. Then, here, the analog beamformer \mathbf{U}_{RF} can be optimized by exploiting these slowly-varying long term parameters. It is important to note that slow-time training data is transmitted much slower compared to the rate of change of instantaneous CSI.

In this chapter, the analog beamformer is designed for frequency-selective massive MIMO systems employing SC modulation in TDD mode where the JADPP of each users is taken into account. Our goal is to find a proper beamspace (spanned by the columns of matrix \mathbf{U}_{RF}) on which the reduced dimensional CSI estimation can be realized as accurately as possible, so that a minimal performance trade-off in the subsequent statistical signal processing operations after beamforming is ensured. Using CSI estimation accuracy after beamforming as a performance measure with the use of more general joint angle-delay channel profile, is completely different than the previous works in the massive MIMO literature.

5.2 User Grouping Stage

In slow-time beam acquisition mode, since no a priori information is assumed related with these slowly varying parameters initially, predetermined search sector beams together with slow-time training data are utilized to extract the spatial signatures of each user (based on AMF in (3.10) and MF in (3.12)). This initial step can be regarded as *pre-grouping stage*. After this initial stage, an efficient reconstruction of analog beamformer \mathbf{U}_{RF} in Fig. 3.1 can be carried out by using the estimated CCMs and sparsity map. This can be realized by means of a virtual sectorization (via second-order channel statistics based *user-grouping*) inspired from JSDM framework [27], [28]. In this framework, all active K users can be divided into G groups based on their spatial information, i.e., the estimated sparsity map and CCMs, by using proper user grouping algorithms known in the literature¹ (as in the case of JSDM). We define Ω_g as the set of all UEs in group g with cardinality $|\Omega_g| = K_g$, and $\{g_k\}_{k=1}^{K_g}$ are UE indices forming Ω_g , where the K_g users in group g are assumed to have statistically *i.i.d.* channels.

In user grouping stage, one need to construct the common covariance matrix of each MPCs in group g , denoted by $\mathbf{R}_l^{(g)}$ which can be considered as the common spatial covariance matrix of UEs belonging to group g at l^{th} delay. Instead of using the true covariance matrices of each MPCs, which can not be known accurately, we can construct estimated $\hat{\mathbf{R}}_l^{(g)}$ by using the acquired CCMs in (4.13) as follows

$$\hat{\mathbf{R}}_l^{(g)} \triangleq \sum_{k=1}^{K_g} \hat{\mathbf{R}}_l^{(g_k)}, \quad g = 1, \dots, G \quad (5.1)$$

where $\hat{\mathbf{R}}_l^{(g_k)}$ is the estimated covariance matrix for the l^{th} MPC of the k^{th} user in group g . Similarly, the estimated spatial covariance matrix of received signal in (2.1) (assuming that the transmitted symbols are *i.i.d.* with unity power) can be obtained as

$$\hat{\mathbf{R}}_y \triangleq \sum_{g=1}^G \sum_{l=0}^{L-1} \hat{\mathbf{R}}_l^{(g)} + N_0 \mathbf{I} \quad (5.2)$$

and the estimated covariance matrix of the inter-group interference to group g , consisting of the statistical information for all inter-group users interfering with group g ,

¹ The design of user grouping algorithm is out of scope of this thesis. An efficient procedure can be found in [28], [51].

can be constructed as

$$\hat{\mathbf{R}}_\eta^{(g)} \triangleq \hat{\mathbf{R}}_y - \sum_{l=0}^{L-1} \hat{\mathbf{R}}_l^{(g)}, \quad g = 1, \dots, G. \quad (5.3)$$

5.3 Post-User Grouping Stage

Since massive MIMO systems are equipped with a large number of antenna elements, the received signal for uplink decoding or downlink precoding at BS becomes large dimensional, and thus instantaneous CSI acquisition like basic operations becomes infeasible. To cope with this problem, a pre-processing stage that captures the essence of the input at a reduced dimension is adopted. As in JSDM framework [27], [52], an analog beamformer, which is to be designed based only on statistical CSI, not on instantaneous CSI, is exploited to reduce the dimension of the signaling space. After analog beamforming projection, the multi-user precoding at downlink or multi-user decoding at uplink, necessitating instantaneous CSI for proper operation, can be fulfilled at reduced dimension with significantly reduced complexity.

After user grouping stage, an efficient analog beamformer for each user group can be designed via the estimated group covariance matrices given in (5.1), (5.2), (5.3). This stage can be regarded as *post-grouping stage*. Here, we load \mathbf{U}_{RF} in Fig. 3.1 with the optimized statistical analog beamformer, which is applied in order to distinguish *intra-group* signal of users in group g from other groups by suppressing the *inter-group interference* while reducing the signaling dimension of \mathbf{Y} in (3.5). In this stage, a $D_g T$ -dimensional space-time vector $\mathbf{y}^{(g)}$, where D_g is the number of RF chains assigned to group g , can be formed by using \mathbf{Y} for all groups after the following linear transformation:

$$\mathbf{y}^{(g)} \triangleq \left(\mathbf{I}_T \otimes [\mathbf{S}^{(g)}]^H \right) \text{vec} \{ \mathbf{Y} \}, \quad g = 1, \dots, G \quad (5.4)$$

where $\mathbf{S}^{(g)}$ is an $N \times D_g$ statistical analog beamformer matrix that projects the N -dimensional received signal samples $\{\mathbf{y}_n\}_{n=0}^{T-1}$ in (2.1) on a suitable D_g -dimensional subspace in spatial domain. Here, since a limited number of RF chains, D , are used in hybrid architecture, we have the following constraint: $\sum_{g=1}^G D_g = D$. After constructing the optimal analog beamformer matrix $\mathbf{S}^{(g)}$, \mathbf{U}_{RF} in Fig. 3.1 is replaced with $\left[\begin{array}{cccc} \mathbf{S}^{(1)} & \mathbf{S}^{(2)} & \dots & \mathbf{S}^{(G)} \end{array} \right]_{N \times D}$.

5.3.1 MPC Grouping for Efficient Analog Beamformer Design

If there exists a significant overlap among some of the MPCs of group g in the angular domain, one can simply form groups of nonresolvable MPCs, and process them jointly. One can group l^{th} and l'^{th} active MPCs of group g into one MPC group if the following criteria holds

$$\varphi_{ll'}^{(g)} \triangleq \frac{|\Gamma_l^{(g)} \cap \Gamma_{l'}^{(g)}|}{\min \{|\Gamma_l^{(g)}|, |\Gamma_{l'}^{(g)}|\}} \geq \zeta \quad (5.5)$$

where ζ is the overlapping threshold, and $\Gamma_l^{(g)}, \Gamma_{l'}^{(g)}$ are the set of indices i such that $\phi_i \in \Omega_\phi$ is inside the angular region which is determined to have non-zero power level for l^{th} and l'^{th} MPCs of group g respectively:

$$\Gamma_l^{(g)} \triangleq \left\{ i \mid \sum_{k=1}^{K_g} [\mathbf{I}^{(g_k)}]_{(i,l)} \neq 0, g_k \in \Omega_g, i = 0, \dots, M-1 \right\}. \quad (5.6)$$

If (5.5) is not satisfied, the corresponding MPCs are assumed to be *resolvable* in angular domain. After computing $\varphi_{ll'}^{(g)}$ for all $(l, l')^{th}$ active pair, one can group non-resolvable active MPCs to form spatially resolvable MPC groups in angular domain which is denoted by $\mathcal{L}_\ell^{(g)}$:

$$\mathcal{L}_\ell^{(g)} = \{l \mid \text{a set of temporal (delay) indices of spatially overlapping active MPCs in user group } g\}. \quad (5.7)$$

Here, ℓ shows the indices of MPC groups consisting of non-resolvable components². Note that it is enough for an active MPC to be put into an MPC group if it has significant overlap with at least one of the MPCs in that group. In other words, l^{th}, l'^{th} , and l''^{th} MPCs are put into the same MPC group even if $\varphi_{ll''}^{(g)} < \zeta$ but $\varphi_{ll'}^{(g)} \geq \zeta, \varphi_{l'l''}^{(g)} \geq \zeta$. The detailed MPC grouping algorithm is provided in Algorithm 1. Then, the CCM of an MPC group, $\mathcal{L}_\ell^{(g)}$, can be constructed as

$$\hat{\mathbf{R}}_\ell^{(g)} \triangleq \sum_{l \in \mathcal{L}_\ell^{(g)}} \hat{\mathbf{R}}_l^{(g)}. \quad (5.8)$$

² One can denote the set of temporal indices of all (resolvable and nonresolvable) active MPCs of group g as $\mathcal{L}^{(g)}$, and the total number of resolvable MPCs of group g in angular domain as $\mathcal{MPC}^{(g)}$ after MPC grouping. Then, it can be seen that $\mathcal{MPC}^{(g)} \leq |\mathcal{L}^{(g)}| \leq L$, and $\sum_{\ell=0}^{\mathcal{MPC}^{(g)}-1} |\mathcal{L}_\ell^{(g)}| = |\mathcal{L}^{(g)}|$.

Algorithm 1 Nonresolvable MPC Grouping

Input:

$\varphi_{ll'}$ ^(g): Overlapping ratio, ζ : Overlapping threshold, c_l ^(g): Activity indicator of l^{th} MPC for user group g

Output:

\mathcal{L}_ℓ ^(g): The set of non-zero (temporal) delays belonging to the ℓ^{th} resolvable MPC group in user group g

- 1: **Initialize:** $pair \leftarrow []$, $flag \leftarrow L \times \text{ones}(1,L)$, $i \leftarrow 0$, $m \leftarrow 0$, $\ell \leftarrow 0$
▷ Find the indices of active overlapping MPC pairs and store them in the $pair$ matrix
 - 2: **for** $l \leftarrow 0$ to $L - 2$ **do**
 - 3: **for** $l' \leftarrow l + 1$ to $L - 1$ **do**
 - 4: **if** $c_l^{(g)} > 0$ & $c_{l'}^{(g)} > 0$ **then**
 - 5: **if** $\varphi_{ll'} \geq \zeta$ **then**
 - 6: $pair(i, 0) = l$; $pair(i, 1) = l'$; $i \leftarrow i + 1$;
 - 7: **end if**
 - 8: **end if**
 - 9: **end for**
 - 10: **end for**
 - 11: **if** $pair \neq []$ **then**
 - 12: **for** $l \leftarrow 0$ to $L - 1$, $c_l^{(g)} > 0$ **do**
▷ Find the row and column indices of l^{th} MPC if it is going to be grouped with any active MPC. If l^{th} MPC is not going to be grouped with any active MPC then row and col will be empty vectors.
 - 13: $[row, col] = \text{find}\{abs(pair - l) == 0\}$
 - 14: **Initialize:** $ind \leftarrow \mathbf{0}_{1 \times (\text{length}\{row\} + 1)}$
 - 15: $ind(end) = l$
▷ Find the indices of the MPCs which are going to be grouped with l^{th} MPC if row and col are not empty vectors.
 - 16: **if** $row \neq []$ & $col \neq []$ **then**
 - 17: **for** $j \leftarrow 0$ to $\text{length}\{row\} - 1$ **do**
 - 18: $ind(j) = pair(row(j), abs(col(j) - 1))$
 - 19: **end for**
 - 20: **end if**
-

▷ Assign a common index m to the active MPCs that are to be grouped if none of them have been assigned to an index before. If any of the MPCs that are to be grouped have been assigned to a group before, then assign all these MPCs to this group as well.

```

21:     if  $m \leq \min\{flag(ind)\}$  then
22:          $flag(ind) = m; m \leftarrow m + 1$ 
23:     else
24:          $flag(ind) = \min\{flag(ind)\}$ 
25:     end if
26: end for
27: for  $\ell \leftarrow 0$  to  $m - 1$  do
28:      $\mathcal{L}_\ell^{(g)} = \{l | flag(l) = \ell, l = 0, \dots, L - 1\}$ 
29: end for
30: else
31:     for  $l \leftarrow 0$  to  $L - 1, c_l^{(g)} > 0$  do
32:          $\mathcal{L}_\ell^{(g)} = \{l\}; \ell \leftarrow \ell + 1$ 
33:     end for
34: end if

```

5.3.2 Nearly Optimal Analog Beamformer Construction

By assuming that eigenspaces of each MPCs are nearly orthogonal, which is indeed the case in mm-wave massive MIMO systems due to sparse nature of the channel, we can construct the analog beamformer of group g as

$$\mathbf{S}^{(g)} \triangleq \begin{bmatrix} \mathbf{S}_0^{(g)} & \mathbf{S}_1^{(g)} & \dots & \mathbf{S}_{\mathcal{MPC}^{(g)}-1}^{(g)} \end{bmatrix}_{N \times D_g} \quad (5.9)$$

where the $N \times d_\ell^{(g)}$ sub-matrix $\mathbf{S}_\ell^{(g)}$ can be seen as the sub-beamformer that allows ℓ^{th} resolvable MPC of group g to pass while suppressing the *inter-group interference* in the spatial domain, and also the rejecting each MPC of group g other than the one at delay ℓ . Here, $d_\ell^{(g)}$ is the number of RF chains assigned to the ℓ^{th} MPC of group g where $\sum_{\ell=0}^{\mathcal{MPC}^{(g)}-1} d_\ell^{(g)} = D_g$. For a given $d_\ell^{(g)}$, nearly optimal analog beamformer matrix, $\mathbf{S}_\ell^{(g)}$, can be obtained as

$$\mathbf{S}_\ell^{(g)} \triangleq \text{eigs}(\hat{\mathbf{R}}_\ell^{(g)}, \hat{\mathbf{R}}_y - \hat{\mathbf{R}}_\ell^{(g)}, d_\ell^{(g)}) = \text{eigs}(\hat{\mathbf{R}}_\ell^{(g)}, \hat{\mathbf{R}}_y, d_\ell^{(g)}) \quad (5.10)$$

where eigs operation yields $d_\ell^{(g)}$ dominant generalized eigenvectors of $\hat{\mathbf{R}}_\ell^{(g)}$ and $\hat{\mathbf{R}}_y$ corresponding to largest generalized eigenvalues. The procedure, here, is adopted from [21] by replacing the true group CCMs with the estimated ones.

5.3.3 Optimal RF Chain Distribution Among MPCs

Here, firstly, we assume that RF chains are distributed to groups proportional with the number of users they have. Then, the optimal values of $\{d_\ell^{(g)}, \ell = 0, \dots, \mathcal{MPC}^{(g)} - 1\}$, in terms of channel estimation accuracy, can be found by using the generalized eigenvalues [21] as

$$\{d_\ell^{(g)}\}_{opt} = \arg \min_{\{d_\ell^{(g)}\}} \sum_{\ell=0}^{\mathcal{MPC}^{(g)}-1} \sum_{n=1}^{d_\ell^{(g)}} \frac{1}{\lambda_{\ell,n}^{(g)} + 1} \quad (5.11)$$

with the constraint of $\sum_{\ell=0}^{\mathcal{MPC}^{(g)}-1} d_\ell^{(g)} = D_g$, and $\sum_{g=1}^G D_g = D$. Here, $\lambda_{\ell,n}^{(g)}$ is the n^{th} dominant generalized eigenvalue of $\hat{\mathbf{R}}_\ell^{(g)}$ and $\hat{\mathbf{R}}_{\eta'}^{(g)}$ which is defined as

$$\hat{\mathbf{R}}_{\eta'}^{(g)} \triangleq \hat{\mathbf{R}}_y - \hat{\mathbf{R}}_\ell^{(g)} \text{ for } \ell = 1, \dots, \mathcal{MPC}^{(g)} - 1. \quad (5.12)$$

It can be shown from (5.10) that

$$\lambda_{\ell,n}^{(g)} = \left[\left(\left[\mathbf{S}_{\ell}^{(g)} \right]^H \hat{\mathbf{R}}_{\eta'}^{(g)} \mathbf{S}_{\ell}^{(g)} \right)^{-1} \left(\left[\mathbf{S}_{\ell}^{(g)} \right]^H \hat{\mathbf{R}}_{\ell}^{(g)} \mathbf{S}_{\ell}^{(g)} \right) \right]_{(n,n)}, \quad n = 1, \dots, d_{\ell}^{(g)}. \quad (5.13)$$

Various other criteria different than (5.11) can also be used to distribute RF chains among different active MPCs as stated in [21], which head to same optimal distribution.

CHAPTER 6

INSTANTANEOUS CHANNEL ESTIMATION WITH HYBRID BEAMFORMING

6.1 Introduction

In the previous chapter, nearly optimal covariance-based reduced rank analog beamformer design is provided. Thanks to the analog beamformer constructed in the previous chapter, high-dimensional channels are projected onto low-dimensional subspaces so that the computational complexity is reduced. In this chapter, after slow-time beam acquisition mode and user grouping based on JSDM framework, fine instantaneous channel estimates in reduced dimension can be obtained for each group users. We name this acquisition stage as *fast-time instantaneous channel estimation mode* where reduced rank instantaneous CSI estimation can be carried out accurately and efficiently in a proper beamspace (formed by $\mathbf{S}^{(g)}$) via small amount of fast-time training data in front of each data transmission. In this mode, with the help of updated analog beamformer, the training overhead is shown to be reduced considerably.

After analog beamforming, downlink and uplink processes can only be fulfilled at reduced dimension by utilizing the *effective* multipath channel vector of each group user. The effective channels of each user, appearing at the output of analog beamformer, (which is utilized by digital beamformer for intra-group processing) can be defined as $\mathbf{h}_{eff,l}^{(gk)} \triangleq [\mathbf{S}^{(g)}]^H \mathbf{h}_l^{(gk)}$ where $\mathbf{h}_l^{(gk)}$ is the full dimensional channel vector for the l^{th} MPC of the k^{th} user in group g . Then, it will be beneficial to express the variables in a single concatenated vector, namely, the *effective* extended multipath channel vector of group g , as

$$\bar{\mathbf{h}}_{eff}^{(g)} \triangleq \left[\left[\bar{\mathbf{h}}_{eff}^{(g1)} \right]^H \left[\bar{\mathbf{h}}_{eff}^{(g2)} \right]^H \cdots \left[\bar{\mathbf{h}}_{eff}^{(gK_g)} \right]^H \right]^H, \quad (6.1)$$

$$\bar{\mathbf{h}}_{eff}^{(g_k)} \triangleq \left[\left[\mathbf{h}_{eff,0}^{(g_k)} \right]^H \left[\mathbf{h}_{eff,1}^{(g_k)} \right]^H \cdots \left[\mathbf{h}_{eff,L-1}^{(g_k)} \right]^H \right]^H. \quad (6.2)$$

In this mode, a $T_{fast} \times L$ training matrix (or convolution matrix) is defined as $\mathbf{X}_k^{(g)} \triangleq \text{conj} \left\{ \left[\mathbf{x}_0^{(g_k)} \quad \mathbf{x}_1^{(g_k)} \quad \cdots \quad \mathbf{x}_{L-1}^{(g_k)} \right] \right\}$ where it contains the transmitted pilots with the precursors for k^{th} user in group g , and $\mathbf{x}_l^{(g_k)}$ is defined in (3.1). The length of fast-time training data is taken as T_{fast} which is supposed to be much smaller than that of the slow-time training data T . Then, the complete fast-time training matrix of all users in group g during the signaling interval T_{fast} is given by¹

$$\mathbf{X}^{(g)} \triangleq \left[\mathbf{X}_1^{(g)} \quad \mathbf{X}_2^{(g)} \quad \cdots \quad \mathbf{X}_{K_g}^{(g)} \right]_{T \times K_g L}. \quad (6.3)$$

By using the definitions in (6.1), (6.2), and (6.3) together with (2.1) and (3.5), one can express the analog beamformer output in (5.4) as

$$\mathbf{y}^{(g)} = \left[\mathbf{X}^{(g)} \otimes \mathbf{I}_D \right] \bar{\mathbf{h}}_{eff}^{(g)} + \text{vec} \left\{ \left[\mathbf{S}^{(g)} \right]^H \left[\boldsymbol{\eta}_0^{(g)} \quad \cdots \quad \boldsymbol{\eta}_{T-1}^{(g)} \right] \right\}, \quad g = 1, \dots, G \quad (6.4)$$

where $\boldsymbol{\eta}_n^{(g)} = \sum_{g'=1, g' \neq g}^G \left(\sum_{k=1}^{K_{g'}} \sum_{l=0}^{L-1} \mathbf{h}_l^{(g'_k)} x_{n-l}^{(g'_k)} \right) + \mathbf{n}_n$, which is the inter-group interference to group g with AWGN, and $\left\{ x_n^{(g'_k)} \right\}$ for $g' \neq g$ are assumed to be composed of *i.i.d.* data symbols. The true covariance matrix of $\boldsymbol{\eta}_n^{(g)}$, denoted by $\mathbf{R}_{\eta}^{(g)}$, can be calculated as $\mathbf{R}_{\eta}^{(g)} \triangleq \sum_{g'=1, g' \neq g}^G \sum_{l=0}^{L-1} \mathbf{R}_l^{(g)}$. By using the reduced dimensional observations in digital domain in (6.4), the effective channel estimates for each group can be obtained as $\hat{\mathbf{h}}_{eff}^{(g)} = \left(\mathbf{W}^{(g)} \right)^H \mathbf{y}^{(g)}$ where $\mathbf{W}^{(g)}$ is the estimator matrix for the intended group g and of size $TD_g \times K_g LD_g$. Then, the concatenated vector $\hat{\mathbf{h}}_{eff}^{(g)}$ can be partitioned to get effective channel estimates $\hat{\mathbf{h}}_{eff,l}^{(g_k)}$ according to the structure given in (6.1) and (6.2). In this stage, we utilize three different estimators in reduced dimension, described in the following subsections.

¹ Here, asynchronous transmission is possible. We consider a fast-time training phase in which only the intended group g trains and other groups are in the data mode where their transmitted symbols are assumed to be *i.i.d.* Alternatively, same fast-time training matrix can be assigned to different groups since different groups are discriminated by their spatial signatures via the proposed analog beamformer.

6.2 Joint Angle-Delay Domain Reduced Rank Minimum Mean Square Error (RR-MMSE) Estimator

By using the analog beamformer output $\mathbf{y}^{(g)}$ in (6.4), a RR-MMSE type estimator, adopted from [21], can be constructed as $\hat{\mathbf{h}}_{eff}^{(g)} \triangleq \left(\hat{\mathbf{W}}_{mmse}^{(g)} \right)^H \mathbf{y}^{(g)}$ where

$$\hat{\mathbf{h}}_{eff}^{(g)} \triangleq \left(\hat{\mathbf{W}}_{mmse}^{(g)} \right)^H \mathbf{y}^{(g)}, \quad (6.5)$$

where

$$\hat{\mathbf{W}}_{mmse}^{(g)} = \left(\sum_{l=0}^{L-1} \mathbf{R}_{code}^{(g)}(l) \otimes \left[\text{SNR}_{mimo}^{(g)}(l) \right] + \mathbf{I}_{TD_g} \right)^{-1} \left(\sum_{l=0}^{L-1} \left(\mathbf{X}^{(g)} \left[\mathbf{I}_{K_g} \otimes \mathbf{E}_{L,l} \right] \right) \otimes \text{SNR}_{mimo}^{(g)}(l) \right), \quad (6.6)$$

$$\text{SNR}_{mimo}^{(g)}(l) \triangleq \left([\mathbf{S}^{(g)}]^H \hat{\mathbf{R}}_{\eta}^{(g)} \mathbf{S}^{(g)} \right)^{-1} \left([\mathbf{S}^{(g)}]^H \hat{\mathbf{R}}_l^{(g)} \mathbf{S}^{(g)} \right), \quad (6.7)$$

$$\mathbf{R}_{code}^{(g)}(l) \triangleq \left(\mathbf{X}^{(g)} \left[\mathbf{I}_{K_g} \otimes \mathbf{E}_{L,l} \right] \left[\mathbf{X}^{(g)} \right]^H \right). \quad (6.8)$$

Note that $\hat{\mathbf{W}}_{mmse}^{(g)}$ is an approximated MMSE estimator where the sparsity map in (4.8) and estimated CCMs in (4.13) are utilized instead of their true values in the formulation². In (6.6), $\mathbf{E}_{L,l}$ is an $L \times L$ elementary diagonal matrix where all the entries except the $(l+1)^{th}$ diagonal one are zero. In (6.7), $\hat{\mathbf{R}}_{\eta}^{(g)}$ is the estimated correlation matrix of inter-group interference to group g given in (5.3). If $\hat{\mathbf{R}}_l^{(g)}$ is a perfect estimate, the estimator in (6.6) becomes the optimal reduced rank linear estimator (Wiener filter) in mean square error (MSE) sense [24], whose performance is to be used as benchmark.

6.3 Joint Angle-Delay Domain Beamspace Aware Least Square (BA-LS) Estimator

One can simplify the RR-MMSE estimator in (6.6) by assuming that the eigenspaces of each MPCs after analog beamforming are almost orthogonal, an effect which is

² While deriving (6.6), it is assumed that each user in the same group has *i.i.d.* channels with $\mathcal{CN}(\mathbf{0}, \mathbf{R}_l^{(g)})$ where $\mathbf{R}_l^{(g)} \triangleq \sum_{k=1}^{K_g} \mathbf{R}_l^{(gk)}$ for $g = 1, \dots, G$. This is a common assumption for JSDM framework [21], [28], [35].

more strongly observed in mm-wave channels especially for the case of large number of antenna elements [24]. Based on this orthogonality assumption, we can construct an estimator, called as BA-LS, which exploits only the joint angle-delay sparsity of the channels, as

$$\hat{\mathbf{h}}_{eff}^{(g)} \triangleq \left(\mathbf{W}_{ba-ls}^{(g)} \right)^H \mathbf{y}^{(g)}, \quad (6.9)$$

where

$$\mathbf{W}_{ba-ls}^{(g)} = \sum_{\ell=0}^{\mathcal{MPC}^{(g)}-1} \left(\text{pinv} \left\{ \left[\mathbf{I}_{K_g} \otimes \sum_{m \in \mathcal{L}_\ell^{(g)}} \mathbf{E}_{L,m} \right] [\mathbf{X}^{(g)}]^H \right\} \otimes \left[\sum_{n \in \mathcal{D}_\ell^{(g)}} \mathbf{E}_{D_g,n} \right] \right). \quad (6.10)$$

In (6.10), $\mathcal{MPC}^{(g)}$ is the total number of MPC clusters, resolvable in angular domain, in group g having nearly non-overlapping AoA support. The set $\mathcal{L}_\ell^{(g)}$ in (5.7), which is obtained via the estimated sparsity map $\mathbf{I}^{(k)}$'s, is composed of estimated active (temporal) delays belonging to the ℓ^{th} resolvable multipath group having MPCs with significantly overlapping AoA support in the angular domain for $\ell = 1, \dots, \mathcal{MPC}^{(g)} - 1$. In (6.10), the set $\mathcal{D}_\ell^{(g)}$ is defined as

$$\mathcal{D}_\ell^{(g)} \triangleq \left\{ n \in \mathbb{Z}^+ \mid \sum_{m=0}^{\ell-1} d_m^{(g)} < n \leq \sum_{m=0}^{\ell} d_m^{(g)} \right\} \quad (6.11)$$

for $\ell = 1, \dots, \mathcal{MPC}^{(g)} - 1$, and $\mathcal{D}_\ell^{(g)} \triangleq \{ n \in \mathbb{Z}^+ \mid 0 < n \leq d_0^{(g)} \}$ for $\ell = 0$ where $|\mathcal{D}_\ell^{(g)}| = d_\ell^{(g)}$. Here, $\mathcal{D}_\ell^{(g)}$ shows the column indices of the analog beamformer matrix $\mathbf{S}^{(g)}$ in Section 5.3.2 allowing to pass the ℓ^{th} resolvable MPC cluster of group g . For BA-LS estimator, only the estimated sparsity map $\mathbf{I}^{(k)}$ in (4.8) is necessary to construct $\mathcal{L}_\ell^{(g)}$. Here, $\text{pinv} \{ \}$, denoting the pseudo-inverse operation, can be seen as the temporal correlator preceded by the analog beamformer. It performs the task of LS type estimation of reduced dimensional channels corresponding to the ℓ^{th} MPC cluster in group g . Furthermore, with the help of $\mathbf{S}^{(g)}$, which orthogonalize the MPCs in reduced dimensional beamspace (eigenspace), the estimation of channel response for each MPCs can be fulfilled separately in their individual beamspace. This reduces T_{fast} significantly compared to conventional LS type estimators.

6.4 Conventional LS Estimator

Different from (6.10), LS type estimator can be constructed in a conventional way [26], after analog beamforming, as

$$\hat{\mathbf{h}}_{eff}^{(g)} \triangleq \left(\mathbf{W}_{ls}^{(g)} \right)^H \mathbf{y}^{(g)}, \quad (6.12)$$

where

$$\mathbf{W}_{ls}^{(g)} = \begin{cases} [\mathbf{X}^{(g)}] \left([\mathbf{X}^{(g)}]^H \mathbf{X}^{(g)} \right)^{-1} \otimes [\mathbf{I}_{D_g}] & \text{if } T \geq K_g L, \\ \left(\mathbf{X}^{(g)} [\mathbf{X}^{(g)}]^H \right)^{-1} [\mathbf{X}^{(g)}] \otimes [\mathbf{I}_{D_g}] & \text{if } T < K_g L \end{cases} \quad (6.13)$$

and $\mathbf{X}^{(g)}$ in (6.3) is assumed to be full column or row rank. In (6.13), a conventional LS estimator in reduced dimensional beamspace (formed by $\mathbf{S}^{(g)}$) is constructed without taking the joint angle-delay sparsity of the channels into account.

Finally, the overall hybrid beamforming based system architecture consisting of initial slow-time beam acquisition mode (JADPP, two-stage CFAR thresholding, CCM and sparsity map construction together with analog beamformer update), and fast-time instantaneous channel estimation mode (RR-MMSE, BA-LS, LS in reduced beamspace) are summarized in Fig. 6.1.

6.5 Performance Evaluation for Instantaneous Channel Estimation

In order to compare the performances of proposed JADPP estimators, namely AMF in (3.10) and MF in (3.12) and, different channel estimators, namely MMSE, BA-LS and conventional LS in (6.6), (6.10) and (6.13), we define the following performance metric below

$$nMSE^{(g)} = \frac{\mathbb{E}_{\mathbf{W}^{(g)}, \mathbf{S}^{(g)}} \left\{ \mathbb{E} \left\{ \|\bar{\mathbf{h}}_{eff}^{(g)} - \hat{\mathbf{h}}_{eff}^{(g)}\|^2 \mid \mathbf{W}^{(g)} \right\} \right\}}{\mathbb{E}_{\mathbf{S}^{(g)}} \left\{ \mathbb{E} \left\{ \|\bar{\mathbf{h}}_{eff}^{(g)}\|^2 \mid \mathbf{S}^{(g)} \right\} \right\}} \quad (6.14)$$

which shows the nMSE of the channel estimates for group g users. In (6.14), $\hat{\mathbf{h}}_{eff}^{(g)} = \left(\mathbf{W}^{(g)} \right)^H \mathbf{y}^{(g)}$, where $\mathbf{W}^{(g)}$ can be seen as an arbitrary linear estimator. For performance evaluation, $\hat{\mathbf{W}}_{mmse}^{(g)}$, $\mathbf{W}_{ba-ls}^{(g)}$, $\mathbf{W}_{ls}^{(g)}$ are to be used in place of $\mathbf{W}^{(g)}$ while CCMs are constructed by AMF or MF type preprocessing (in pre-grouping stage).

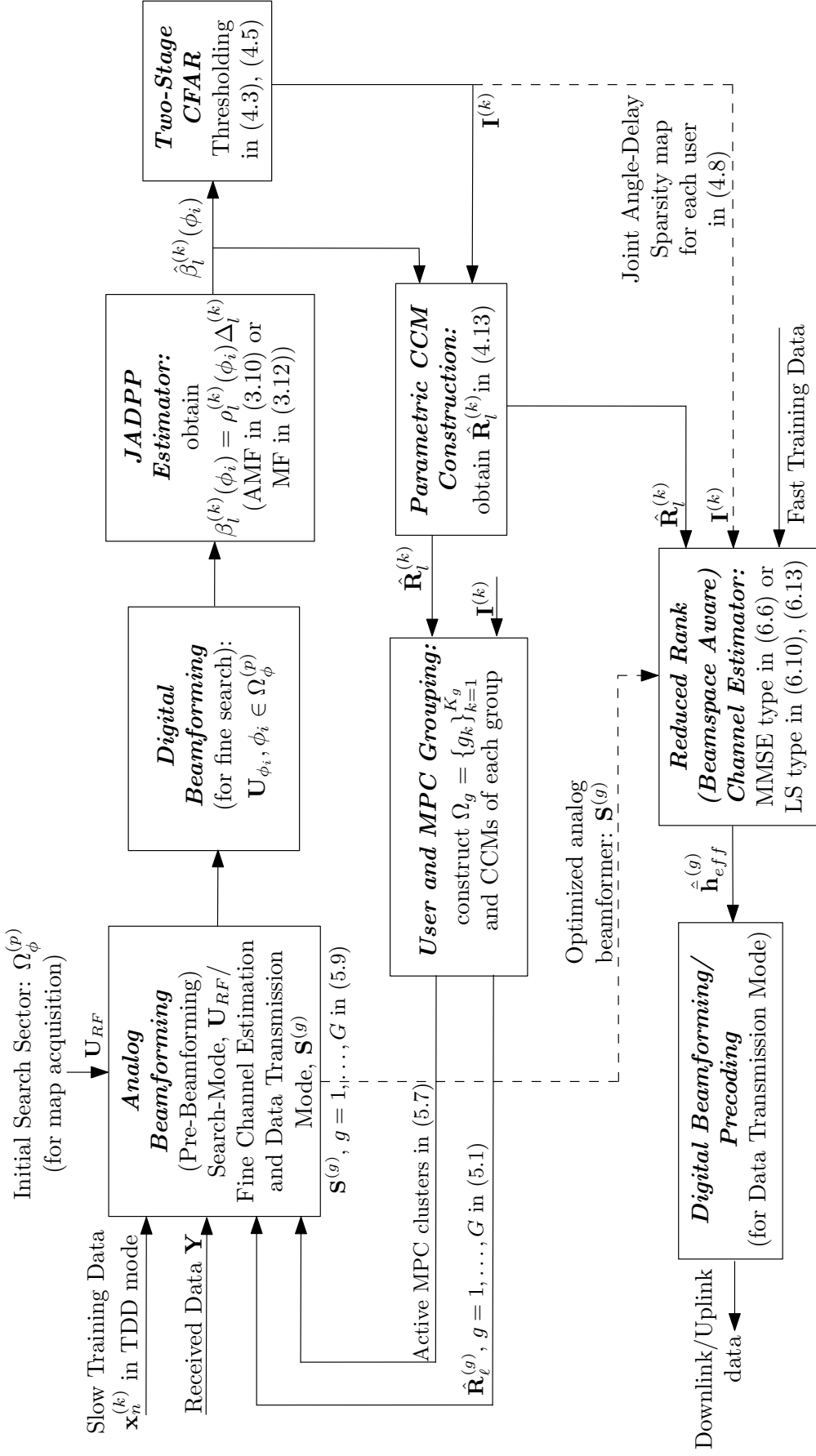


Figure 6.1: Overall System Architecture

Given the analog beamformer $\mathbf{S}^{(g)}$ and channel estimator matrix $\mathbf{W}^{(g)}$, the numerator and denominator of the conditional expectations in (6.14) can be found analytically as³

$$\begin{aligned} & \mathbb{E} \left\{ \|\bar{\mathbf{h}}_{eff}^{(g)} - \hat{\mathbf{h}}_{eff}^{(g)}\|^2 \mid \mathbf{W}^{(g)} \right\} \\ &= \mathbb{E} \left\{ \text{Tr} \left\{ \left(\bar{\mathbf{h}}_{eff}^{(g)} - (\mathbf{W}^{(g)})^H \mathbf{y}^{(g)} \right) \left(\bar{\mathbf{h}}_{eff}^{(g)} - (\mathbf{W}^{(g)})^H \mathbf{y}^{(g)} \right)^H \right\} \right\} \\ &= \text{Tr} \left\{ \mathbf{R}_{mmse}^{(g)} \right\} + \text{Tr} \left\{ (\mathbf{W}^{(g)} - \mathbf{W}_{mmse}^{(g)})^H \mathbf{R}_y^{(g)} (\mathbf{W}^{(g)} - \mathbf{W}_{mmse}^{(g)}) \right\} \end{aligned} \quad (6.15)$$

$$\mathbb{E} \left\{ \|\bar{\mathbf{h}}_{eff}^{(g)}\|^2 \mid \mathbf{S}^{(g)} \right\} = \text{Tr} \left\{ \mathbf{R}_{eff}^{(g)} \right\} \quad (6.16)$$

where

$$\begin{aligned} \mathbf{R}_{eff}^{(g)} &\triangleq \mathbb{E} \left\{ \bar{\mathbf{h}}_{eff}^{(g)} \left[\bar{\mathbf{h}}_{eff}^{(g)} \right]^H \right\} = \sum_{l=0}^{L-1} \left[\mathbf{I}_{K_g} \otimes \mathbf{E}_{L,l} \right] \otimes \left(\left[\mathbf{S}^{(g)} \right]^H \mathbf{R}_l^{(g)} \left[\mathbf{S}^{(g)} \right] \right) \\ \mathbf{R}_{mmse}^{(g)} &\triangleq \mathbb{E} \left\{ \mathbf{e}^{(g)} \left(\mathbf{e}^{(g)} \right)^H \mid \mathbf{W}^{(g)} = \mathbf{W}_{mmse}^{(g)} \right\} = \mathbf{R}_{eff}^{(g)} - \mathbf{A} \left(\mathbf{R}_y^{(g)} \right)^{-1} \mathbf{A}^H \\ \mathbf{e}^{(g)} &\triangleq \bar{\mathbf{h}}_{eff}^{(g)} - \left[\mathbf{W}_{mmse}^{(g)} \right]^H \mathbf{y}^{(g)} \\ \mathbf{R}_y^{(g)} &\triangleq \mathbb{E} \left\{ \mathbf{y}^{(g)} \left(\mathbf{y}^{(g)} \right)^H \right\} \\ &= \sum_{l=0}^{L-1} \left(\mathbf{X}^{(g)} \left(\mathbf{I}_{K_g} \otimes \mathbf{E}_{L,l} \right) \left(\mathbf{X}^{(g)} \right)^H \right) \otimes \left(\left(\mathbf{S}^{(g)} \right)^H \mathbf{R}_l^{(g)} \left(\mathbf{S}^{(g)} \right) \right) \\ &\quad + \mathbf{I}_T \otimes \left(\left(\mathbf{S}^{(g)} \right)^H \mathbf{R}_\eta^{(g)} \left(\mathbf{S}^{(g)} \right) \right) \\ \mathbf{A} &= \sum_{l=0}^{L-1} \left(\mathbf{I}_{K_g} \otimes \mathbf{E}_{L,l} \right) \left(\mathbf{X}^{(g)} \right)^H \otimes \left(\left[\mathbf{S}^{(g)} \right]^H \mathbf{R}_l^{(g)} \left[\mathbf{S}^{(g)} \right] \right). \end{aligned} \quad (6.17)$$

In (6.15), $\mathbf{R}_{mmse}^{(g)}$ is the MMSE covariance matrix for the case when optimal MMSE estimator called as $\mathbf{W}_{mmse}^{(g)}$, with perfect knowledge of CCMs are used in place of $\mathbf{W}^{(g)}$.

³ Here, Block Fading channel model is assumed where each user channel changes independently from block to block. Therefore, the expectations in (6.14) can be found by using Monte Carlo (MC) based averaging over independent training snapshots where independent JADPP estimates and CCMs are obtained to construct $\mathbf{S}^{(g)}$ and $\mathbf{W}^{(g)}$.

CHAPTER 7

NUMERICAL RESULTS

7.1 Introduction

In the previous chapters, two different JADPP estimation algorithms and a two-stage CFAR thresholding algorithm are proposed to obtain sparse power profile of each UE. Then, parametric CCM construction is provided and a nearly optimal analog beamformer is designed. Finally, different channel estimators based on the estimated CCMs and constructed beamformers are proposed. In this chapter, here, some numerical results, which are obtained after MC based simulations, are presented to evaluate the performance of AMF and MF type JADPP estimators (given in Section 3.4) via probability of detection (P_D) curves. Also, performance of the channel estimators (given in Chapter 6) with respect to some parameters such as SNR, fast-time training sequence length (T_{fast}) and number of slow-time training snapshots (J) are demonstrated for different number of users (K) via nMSE curves. Throughout the demonstrations, we consider a massive MIMO system with uplink training in TDD mode where the BS is equipped with a ULA of $N = 100$ antenna elements, and each of K users has a single antenna. It is assumed that $K = 8$ or 16 users are clustered into four groups ($G = 4$) where the true angle-delay profile of all UEs for $K = 16$ case is shown in Fig. 7.1, while numerical values of mean AoA and AS of each MPCs are provided in Table 7.1. If K is taken as 8, two users to be active were selected randomly among others in each group¹. Due to hybrid beamforming adoption, limited number of RF chains are utilized, and equal number of RF chains are assigned to each group, then $D_g = D/G$. In beam acquisition mode, the angular search sector of inter-

¹ Here, we assume that users come in groups, either by nature or by the use of proper user-grouping algorithms.

est Ω_ϕ is determined to be $(-45^\circ, 45^\circ)$. While constructing the JADPP and sparsity map of all active users, the angular resolution in ϕ is taken as 0.25° ($M = \frac{90^\circ}{0.25^\circ} = 360$) to construct fine digital beams, number of RF chains D is set to 8, and the length of the slow-time training data T in (3.1) is taken to be equal to the channel memory $L = 32$ unless otherwise stated. For AMF in (3.10) and MF in (3.12), the number of digital beams D_{search} is set to 5, look spread σ in (3.8) is taken as 3° , and J is taken as 5 unless specified differently. In CFAR thresholding, where the sparsity map of all active users are obtained, the desired false alarm rate \bar{P}_{FA} is set to 10^{-3} in (4.4) and (4.6), and the length of guard interval Π_{ϕ_i} in (4.7) is taken as 4° . In the simulations, CFAR threshold for both spatial and temporal thresholding is calculated for the case when J is equal to 1, and $\hat{\beta}_l^{(k)}$'s in (4.5) are obtained after averaging power values of the spatio-temporal cells in the guard interval Π_{ϕ_i} . In our scenario, simultaneously active users use non-orthogonal training waveforms composed of $L = 32$ chips, and these are obtained by truncating length-63 *Kasami* codes without any optimization². In our simulation setup, at the BS, the average received signal strength of different UEs in the same group are assumed to be equal. Moreover, in order to observe the near-far effect³, at the BS, the case of unequal average received power of UEs in different groups is investigated. The average received group power is defined as $\bar{\beta}^{(g)} \triangleq \frac{1}{K_g} \sum_{k=1}^{K_g} \beta^{(g_k)}$. Two different cases are considered. In the first case $\bar{\beta}^{(g)}$'s are assumed to be equal, and in the second case, different average received power levels at BS are assumed for different groups, in which $10 \log \left(\frac{\bar{\beta}^{(4)}}{\bar{\beta}^{(3)}} \right) = 10 \log \left(\frac{\bar{\beta}^{(3)}}{\bar{\beta}^{(2)}} \right) = 10 \log \left(\frac{\bar{\beta}^{(2)}}{\bar{\beta}^{(1)}} \right) = 5$ dB or $10 \log \left(\frac{\bar{\beta}^{(4)}}{\bar{\beta}^{(3)}} \right) = 10 \log \left(\frac{\bar{\beta}^{(3)}}{\bar{\beta}^{(2)}} \right) = 10 \log \left(\frac{\bar{\beta}^{(2)}}{\bar{\beta}^{(1)}} \right) = 10$ dB are taken. While constructing the P_D in (4.9), and nMSE in (6.14), MC based averaging technique is utilized by taking sufficiently high number of realizations.

² There are more efficient approaches (other than the truncation of Kasami codes) yielding waveforms with better cross- and auto correlation properties, but training optimization is beyond the scope of this work.

³ The near-far effect occurs since average received signal strength of different UEs may differ significantly depending on their distance to the BS.

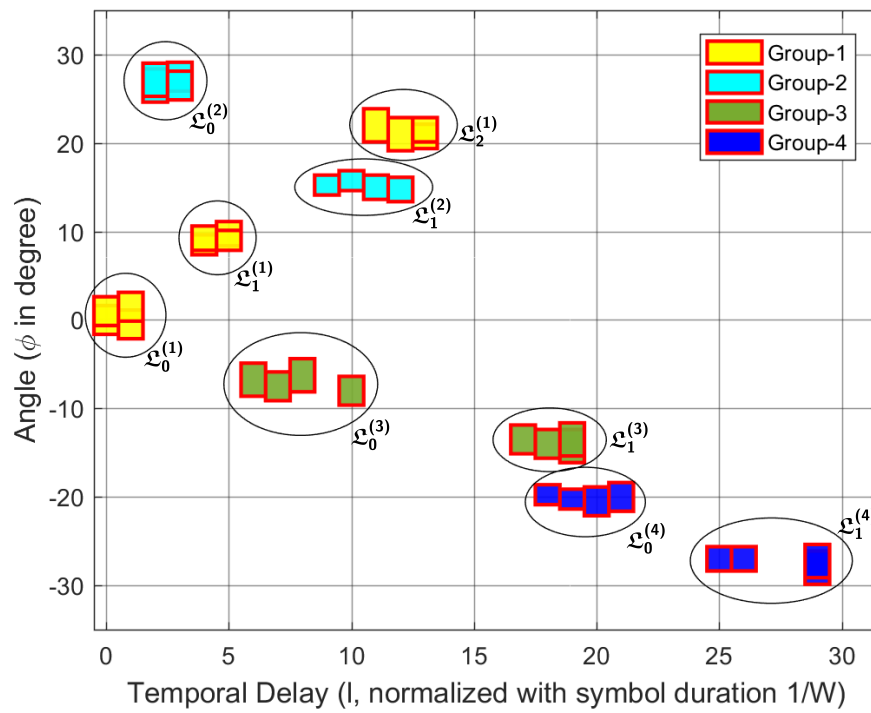


Figure 7.1: Joint angle-delay map of all users

k	g	Active MPC index	Mean AoA	Angular Spread
1	1	{0, 5, 11}	{0, 9.75, 22}	{3, 2.5, 3.5}
2		{1, 4, 13}	{-0.5, 8.5, 20.75}	{3, 2, 2.5}
3		{0, 4, 12}	{1, 9.25, 21}	{3, 2.5, 3.5}
4		{1, 5, 13}	{1.5, 9, 21.5}	{3, 2, 2.5}
5	2	{3, 9}	{27.5 15.25}	{3, 2}
6		{2, 12}	{26.5 14.75}	{3.5, 2.5}
7		{3, 10}	{26.5 15.75}	{3, 2}
8		{2, 11}	{27.15 15}	{3.5, 2.5}
9	3	{8, 17}	{-6.25 -13.5}	{3.5, 3}
10		{10, 19}	{-8 -14.25}	{3.5, 3}
11		{6, 18}	{-6.75 -14}	{3.5, 3}
12		{7, 19}	{-7.5 -13.5}	{3, 3.5}
13	4	{20, 29}	{-20.5 -28}	{3, 3.5}
14		{18, 25}	{-19.75 -27}	{2 2.5}
15		{21, 29}	{-20 -27.25}	{3, 3.5}
16		{19, 26}	{-20.25 -27}	{2, 2.5}

Table 7.1: True Angle-Delay profile of all users

7.2 Performance vs. SNR

In Fig. 7.2, performance of AMF and MF type JADPP estimators based CFAR thresholding in terms of average P_D with respect to average group SNR, namely $\text{SNR}^{(g)} = \frac{\bar{\beta}^{(g)}}{N_0}$ is given. In Fig. 7.2, when $\text{SNR}^{(g)}$ s are equal, AMF outperforms MF for both 8 and 16 users cases. The difference between two methods is more apparent when the number of simultaneously active users is 16 where the inter-group interference is more effective for weakest group users. When there are closely spaced users, the interfering signal needs to be learned and suppressed adaptively (by using the secondary temporal cells) as in the case of AMF, in order to detect MPCs of intended users with high probability. Contrary to AMF, MF does not take the effect of interfering signals to desired MPC, which results in considerable performance degradation.

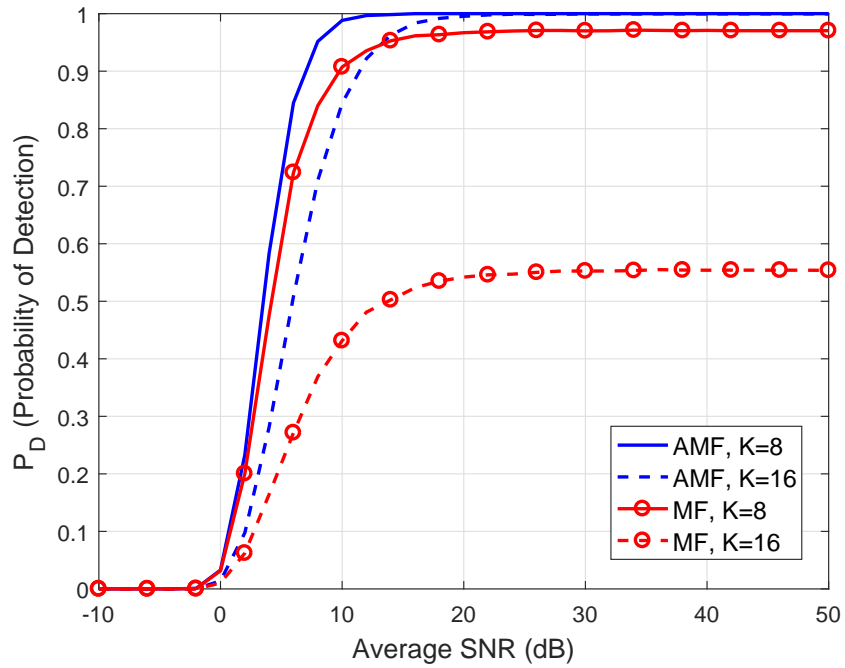


Figure 7.2: Average P_D vs SNR curves for equal averaged received power levels ($T = 32$, $D_{search} = 5$)

In Fig. 7.3 and Fig. 7.4, nMSE performances of different instantaneous CSI estimators, namely RR-MMSE in (6.6) and BA-LS in (6.10), for the effective channel are depicted for $K = 8$ and $K = 16$ cases where $\text{SNR}^{(g)}$ s are assumed to be equal. It is observed that when AMF based CFAR thresholding is used to obtain the sparsity map and JADPP, the performances of RR-MMSE and BA-LS estimators are very close to each other, and the gap between their performances and that of the RR-MMSE estimator with true CCM is very small. We can conclude that AMF based CFAR thresholding is very effective to construct the sparsity map and CCMs even with use of small amount of slow-time training data. It is seen that the BA-LS with AMF, utilizing the estimated sparsity map only, appears to be so effective such that the benchmark performance is attained (without necessitating the true knowledge of CCMs) at significantly reduced dimensions. On the other hand, MF based thresholding seems to yield performance losses especially for the case of large number of active users. Since MF type JADPP estimation does not take the interfering users into account, it is not possible to locate MPCs on joint angle-delay map accurately enough especially when the slow-time training amount is limited. In this case, since the CCMs are inaccurately constructed, the updated analog beamformer ($\mathbf{S}^{(g)}$) is not effective anymore for suppressing the inter-group interference. This results in significant performance degradation for RR-MMSE and BA-LS estimators based on MF when compared to AMF based thresholding. Here, the superiority of AMF against MF shown by average P_D vs SNR curves in Fig. 7.2, is also validated in terms of channel estimation accuracy.

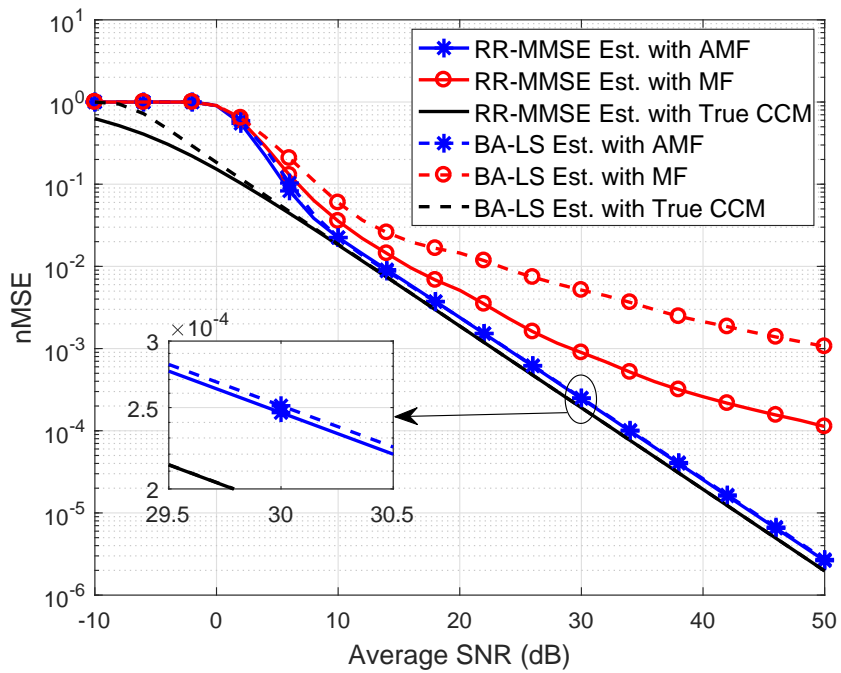


Figure 7.3: Performance of different channel estimators for equal averaged received power levels ($K = 8, T = T_{fast} = 32, D_{search} = 5$)

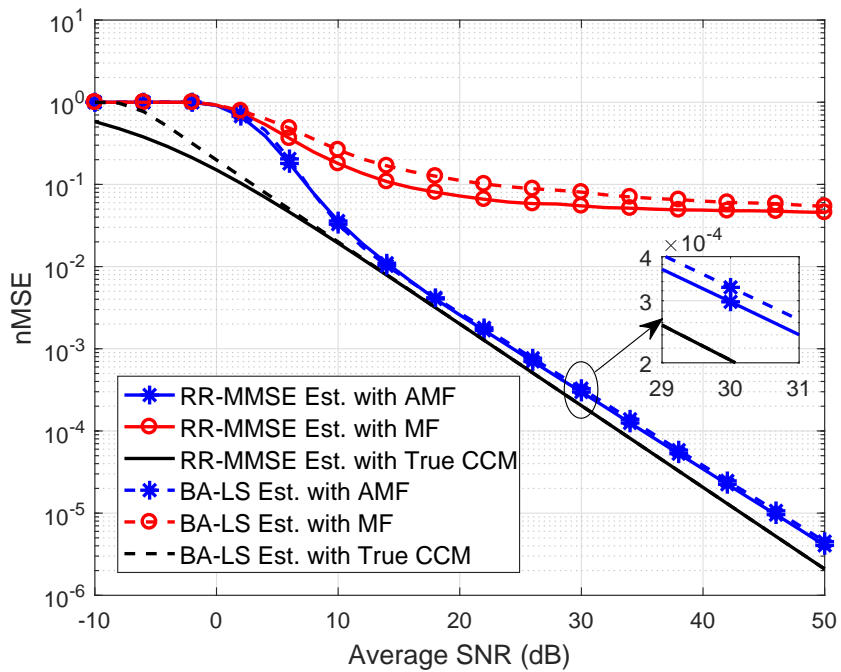


Figure 7.4: Performance of different channel estimators for equal averaged received power levels ($K = 16, T = T_{fast} = 32, D_{search} = 5$)

In Fig. 7.5, when $\bar{\beta}^{(g)}$'s are different among different groups (there is 15 dB difference between the average received power of the users in the weakest and strongest group, i.e., $10 \log \left(\frac{\bar{\beta}^{(4)}}{\bar{\beta}^{(1)}} \right) = 15 \text{ dB}$) and $K = 8$, it can be seen that the AMF based CFAR thresholding is very robust against the near-far effect. That is to say, when compared to Fig. 7.2, average P_D of the weakest users in Group-1 seems to be not affected with the strong interfering signals of other users. However, in MF case, the average P_D of weakest users is significantly reduced such that it cannot exceed 0.1 even for large values of SNR. This means that the activity of users in Group-1 is missed by MF based thresholding with high probability in most of the time when strong interfering user groups are present.

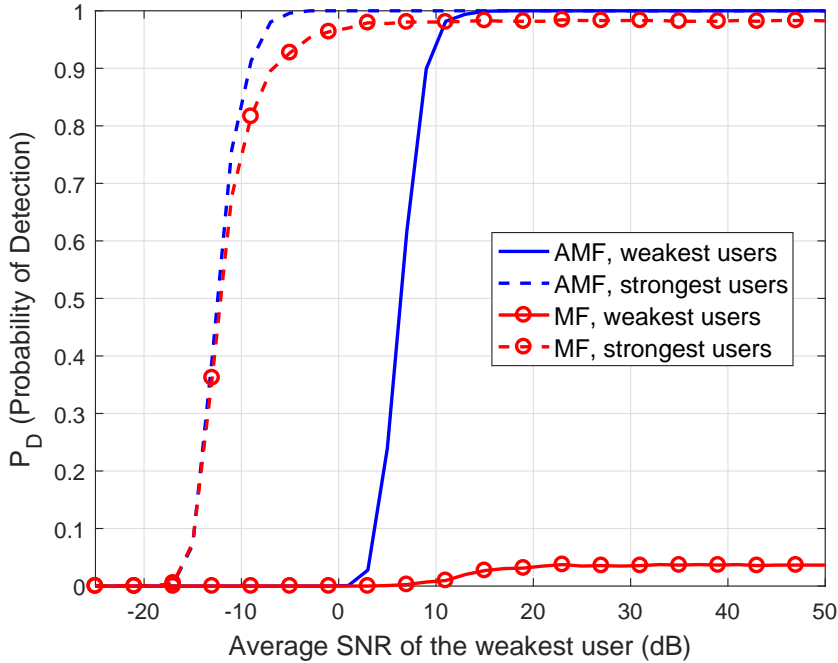


Figure 7.5: Average P_D vs SNR curves for different averaged received power levels ($K = 8, T = 32, D_{search} = 5, 10 \log \left(\frac{\bar{\beta}^{(4)}}{\bar{\beta}^{(1)}} \right) = 15 \text{ dB}$)

In Fig. 7.6 and Fig. 7.7, nMSE performances of different instantaneous CSI estimators are investigated when there are unequal average received power among different groups, i.e., $10 \log \left(\frac{\bar{\beta}^{(4)}}{\bar{\beta}^{(1)}} \right) = 15$ dB is taken for $K = 8$ users. In this case, the performance of reduced rank estimators based on AMF still attains that of the true CCM case. The figure confirms the robustness of AMF type thresholding against increased level of inter-group interference. It is still possible to construct CCMs accurately enough irrespective of differences between the received power levels of different groups. However, the performance of MF based estimators seems to be highly sensitive to the unequal power levels among different groups, i.e., the near-far effect is more apparently observed. In this case, MF fails to locate the MPCs for weak users accurately on joint angle-delay map, which leads to poor channel estimation accuracy for them as shown in Fig. 7.6. For strong user group, the CCMs can be constructed accurately enough so that the performance of MF based channel estimators is close to that of AMF based ones. It can be noted that the findings in Fig. 7.6 and Fig. 7.7 are highly consistent with the ones given by average P_D curves in Fig. 7.5.

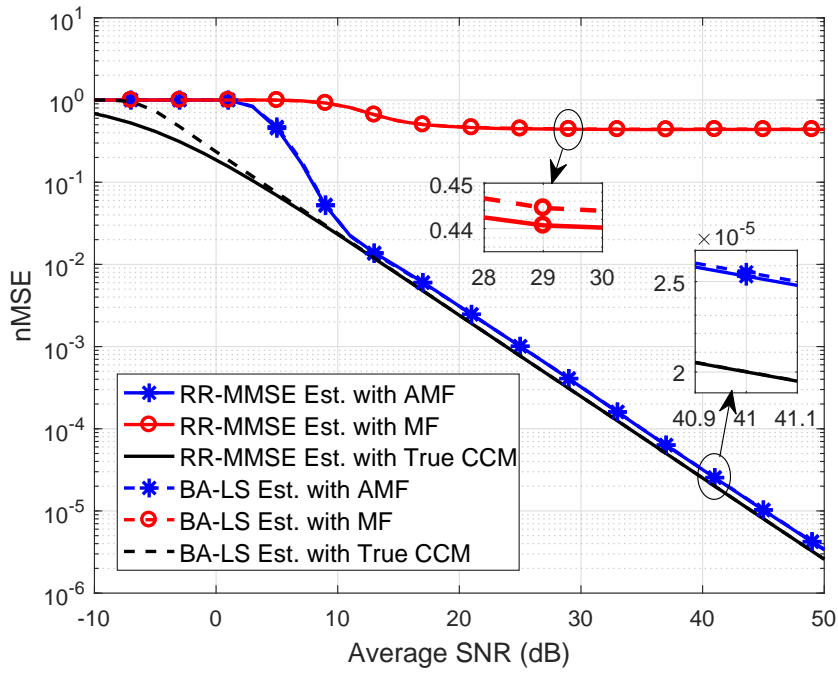


Figure 7.6: Performance of different channel estimators for weakest user group ($K = 8, T = T_{fast} = 32, D_{search} = 5, 10 \log (\bar{\beta}^{(4)} / \bar{\beta}^{(1)}) = 15 \text{ dB}$)

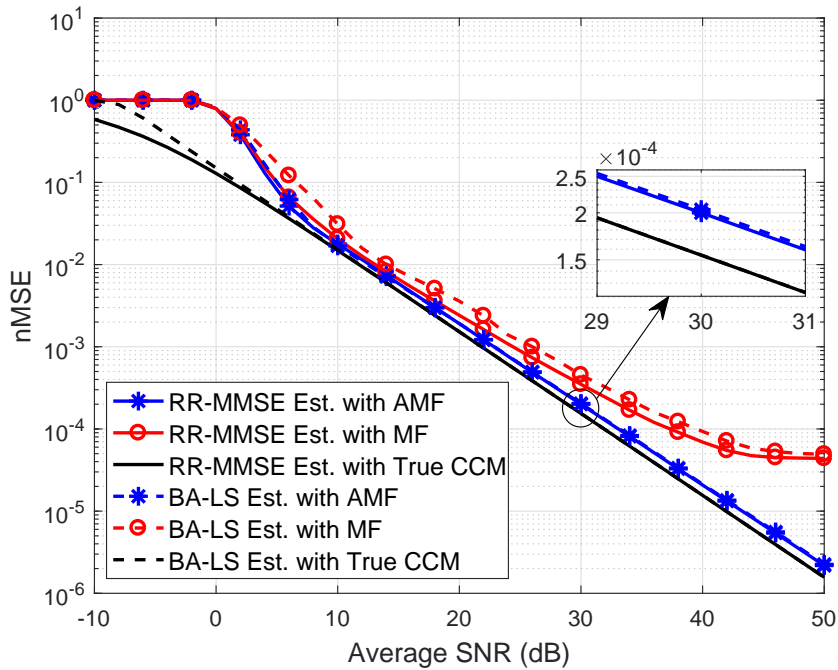


Figure 7.7: Performance of different channel estimators for strongest user group ($K = 8, T = T_{fast} = 32, D_{search} = 5, 10 \log (\bar{\beta}^{(4)} / \bar{\beta}^{(1)}) = 15 \text{ dB}$)

In Fig. 7.8, P_D performance of AMF and MF based CFAR thresholding algorithms for $K = 16$ users and unequal average received power among different groups case, where $10 \log \left(\frac{\bar{\beta}^{(4)}}{\bar{\beta}^{(1)}} \right) = 15$ dB is taken, is investigated. When compared to the results given in Fig. 7.5, it is seen that the performance of AMF for weakest group users and the performance of MF for all users decrease due the increase in the total number of users which leads to increase in the inter-user interference.

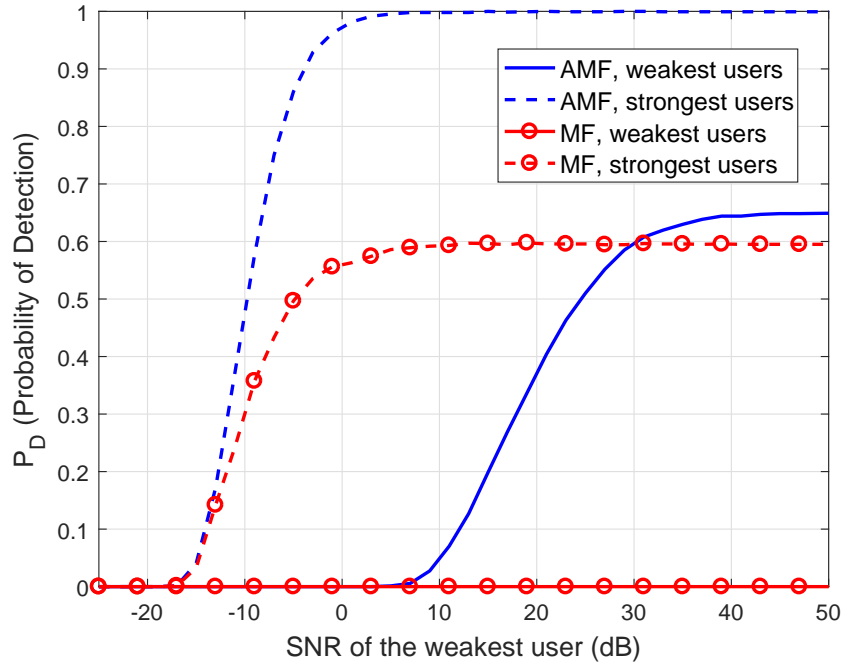


Figure 7.8: Average P_D vs SNR curves for different averaged received power levels ($K = 16, T = 32, D_{search} = 5, 10 \log \left(\frac{\bar{\beta}^{(4)}}{\bar{\beta}^{(1)}} \right) = 15$ dB)

In Fig. 7.9 and Fig. 7.10, nMSE performances are provided for the case of unequal average received power among different groups, where $10 \log \left(\frac{\bar{\beta}^{(4)}}{\bar{\beta}^{(1)}} \right) = 15$ dB is taken for $K = 16$ users. In accordance with the results demonstrated in Fig. 7.8, for the strongest user group, AMF based MMSE and BA-LS estimators attains the performance of MMSE estimator with true CCM knowledge for strongest user group, while the performance of weakest user group deviates from the benchmark results which is different than the results obtained in Fig. 7.6 where there are 8 active users and less inter-group interference. Since MF based thresholding does not detect the MPCs of weakest users, in Fig. 7.9, performance of the MF based channel estimators gets the worst possible value, $\text{nMSE} = 1$. Moreover, for the strongest user group, the performance of MF based channel estimators is decreased with respect to the results given in Fig. 7.7 due to the increased number of users.

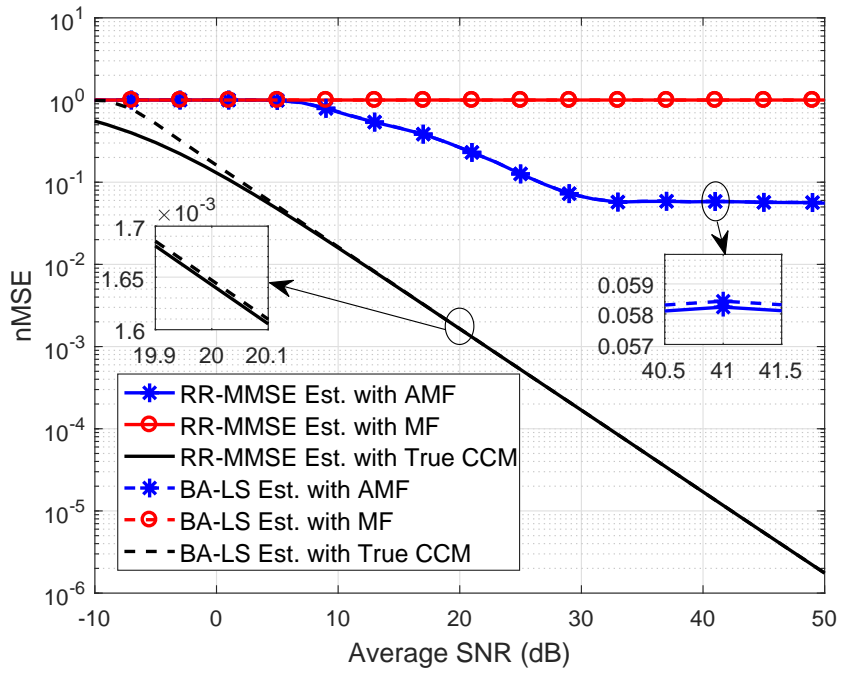


Figure 7.9: Performance of different channel estimators for weakest user group ($K = 16, T = T_{fast} = 32, D_{search} = 5, 10 \log (\bar{\beta}^{(4)} / \bar{\beta}^{(1)}) = 15 \text{ dB}$)

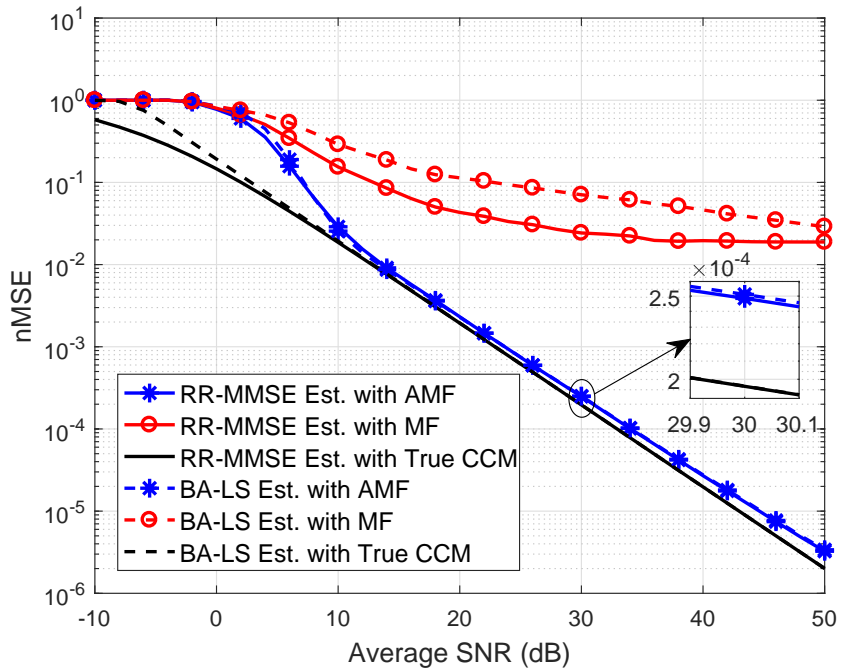


Figure 7.10: Performance of different channel estimators for strongest user group ($K = 16, T = T_{fast} = 32, D_{search} = 5, 10 \log (\bar{\beta}^{(4)} / \bar{\beta}^{(1)}) = 15 \text{ dB}$)

In Fig. 7.11, the case of unequal average received power among different groups is investigated, where $10 \log \left(\frac{\bar{\beta}^{(4)}}{\bar{\beta}^{(1)}} \right) = 30$ dB is taken this time for $K = 16$ users. In this case, the P_D values of strongest group users are similar to the results shown in Fig. 7.6 for both AMF and MF techniques, while for weakest group users P_D is 0 for both algorithms. This means that, since inter-user interference is increased, weakest group users are not detected by AMF and MF based thresholding algorithms anymore when T is taken as 32, and other parameters influencing JADPP and sparsity map construction are chosen as stated in the beginning of this chapter.

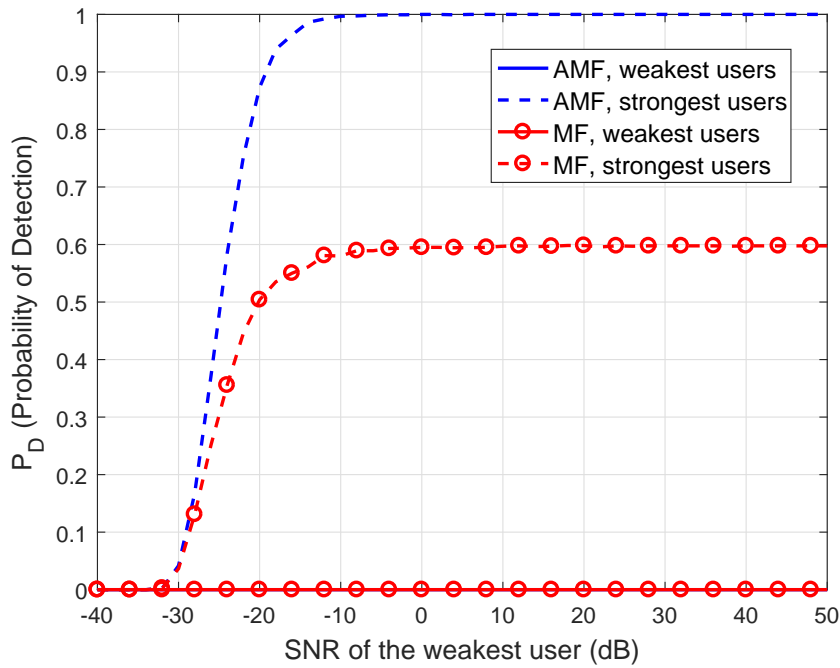


Figure 7.11: Average P_D vs SNR curves for different averaged received power levels ($K = 16$, $T = 32$, $D_{search} = 5$, $10 \log \left(\frac{\bar{\beta}^{(4)}}{\bar{\beta}^{(1)}} \right) = 30$ dB)

In Fig. 7.12 and Fig. 7.13, the corresponding nMSE curves are given for weakest and strongest group users respectively. Since there is no detection for weakest group users, for both AMF and MF based channel estimators, nMSE is always 1 for all SNR values. For strongest group users, the performance is almost same as in Fig. 7.10 where there are 15 dB power difference between weakest and strongest user groups. Note that, although there is less inter-group interference, nMSE performance of MF based channel estimators are not improved for strongest user group.

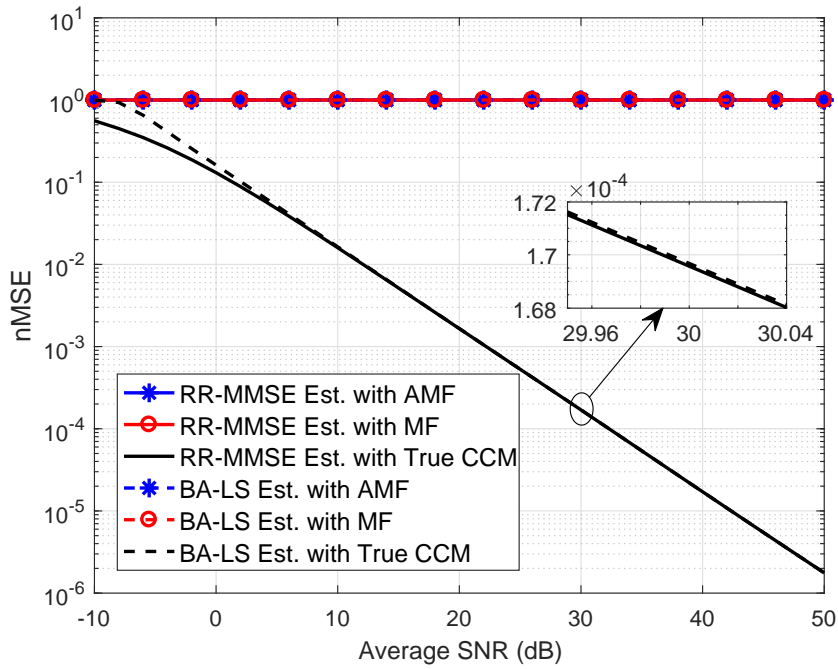


Figure 7.12: Performance of different channel estimators for weakest user group ($K = 16, T = T_{fast} = 32, D_{search} = 5, 10 \log (\bar{\beta}^{(4)} / \bar{\beta}^{(1)}) = 30 \text{ dB}$)

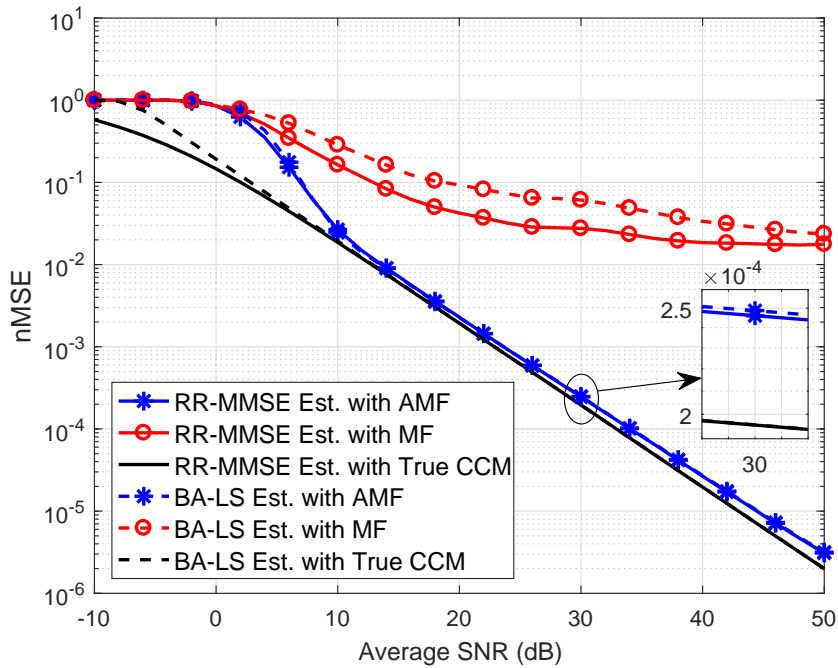


Figure 7.13: Performance of different channel estimators for strongest user group ($K = 16, T = T_{fast} = 32, D_{search} = 5, 10 \log (\bar{\beta}^{(4)} / \bar{\beta}^{(1)}) = 30 \text{ dB}$)

In Fig. 7.14, the case of 30 dB difference between weakest and the strongest user groups, i.e., $10 \log \left(\frac{\bar{\beta}^{(4)}}{\bar{\beta}^{(1)}} \right) = 30$ dB, is investigated for $K = 16$ users when T is set to 128 which is different than Fig. 7.11. Note that, the performance of MF based thresholding algorithm for strongest group users is significantly increased, reaches to 1, while there is still no change for the weakest group users. For AMF based thresholding algorithm, there is no change for the performance of strongest group users because it already reaches to 1 when T is taken as 32. For the weakest group users, P_D still mostly equals to 0 for AMF based thresholding, however, the small performance improvement when SNR is above 16 dB can be noticed.

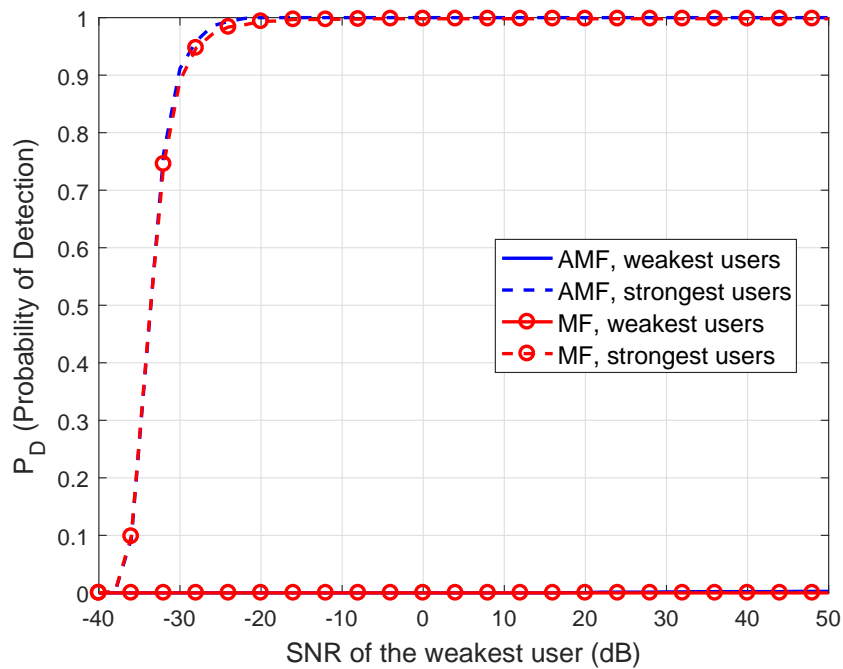


Figure 7.14: Average P_D vs SNR curve for different averaged received power levels ($K = 16$, $T = 128$, $D_{search} = 5$, $10 \log \left(\frac{\bar{\beta}^{(4)}}{\bar{\beta}^{(1)}} \right) = 30$ dB)

In parallel with the results given in Fig. 7.14, it can be seen from Fig. 7.15 that nMSE of the AMF based channel estimators is not equal to 1 anymore since some MPCs of the weakest group users are now started to be detected in some realizations for $\text{SNR} > 16$ dB. In Fig. 7.16, due to the increase of the length of slow-time training sequence, now, it is seen that in addition to the performance of AMF based channel estimators, the performance MF based channel estimators almost attains the performance of MMSE estimator with true CCM knowledge, i.e., benchmark.

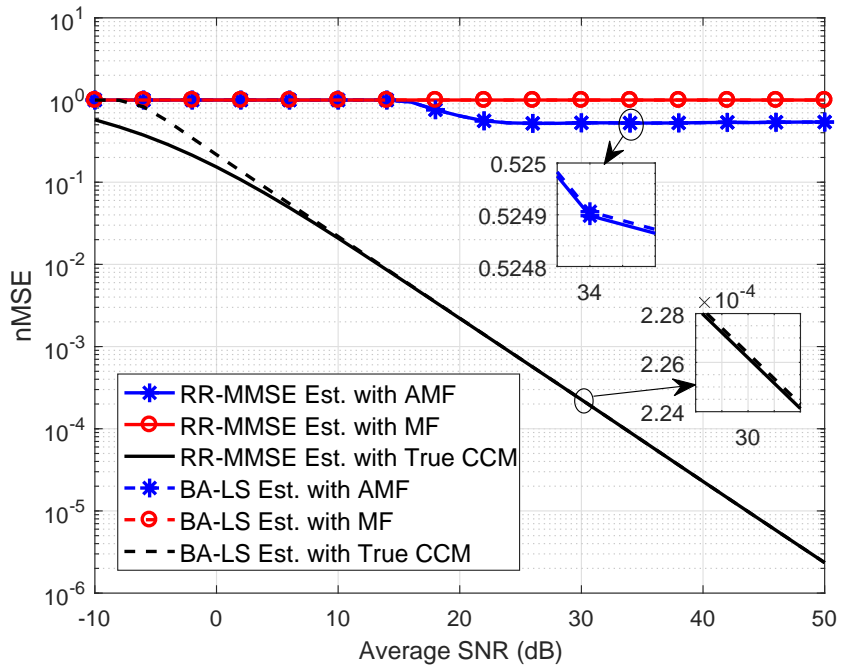


Figure 7.15: Performance of different channel estimators for weakest user group ($K = 16$, $T = 128$, $D_{search} = 5$, $T_{fast} = 32$, $10 \log (\bar{\beta}^{(4)} / \bar{\beta}^{(1)}) = 30$ dB)

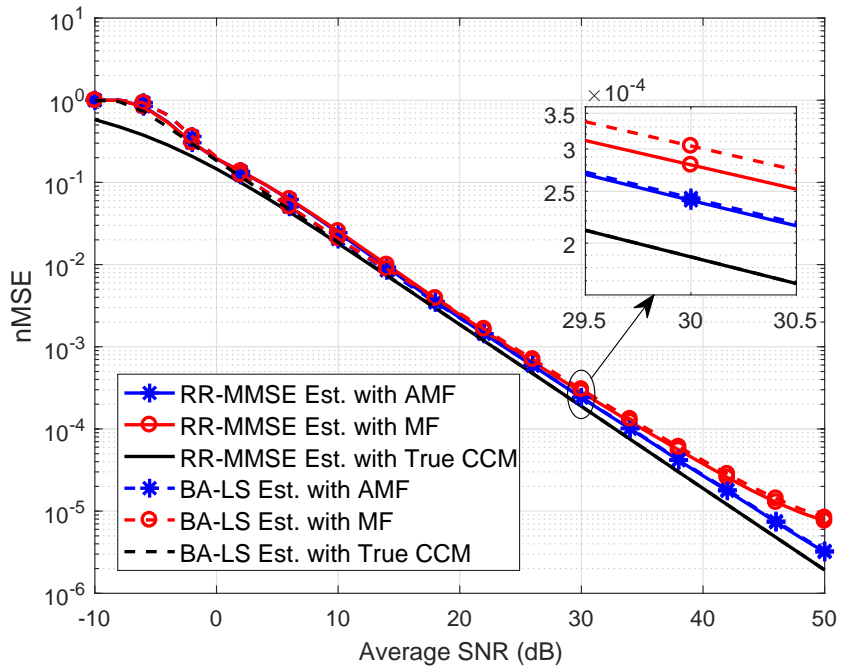


Figure 7.16: Performance of different channel estimators for strongest user group ($K = 16$, $T = 128$, $D_{search} = 5$, $T_{fast} = 32$, $10 \log (\bar{\beta}^{(4)} / \bar{\beta}^{(1)}) = 30$ dB)

In Fig. 7.17, P_D performances of AMF and MF based thresholding algorithms are depicted for the case when there are 16 active users and the power difference between the weakest group users and strongest group users is 30 dB. The difference between Fig. 7.11 and Fig. 7.17 is D_{search} . In this case, D_{search} is set to 10 instead of 5, and the change of performances are observed. It is seen From Fig. 7.17 that while the performance of strongest group user does not change much, P_D performance of AMF based thresholding algorithm starts to improve for weakest group users as SNR increases above 16 dB. However, increasing D_{search} from 5 to 10 does not affect the performance of MF based thresholding since increasing D_{search} helps estimating the interference matrix, $\mathbf{P}\mathbf{s}\mathbf{i}_t^{(k)}$, better and MF does not use this matrix. T

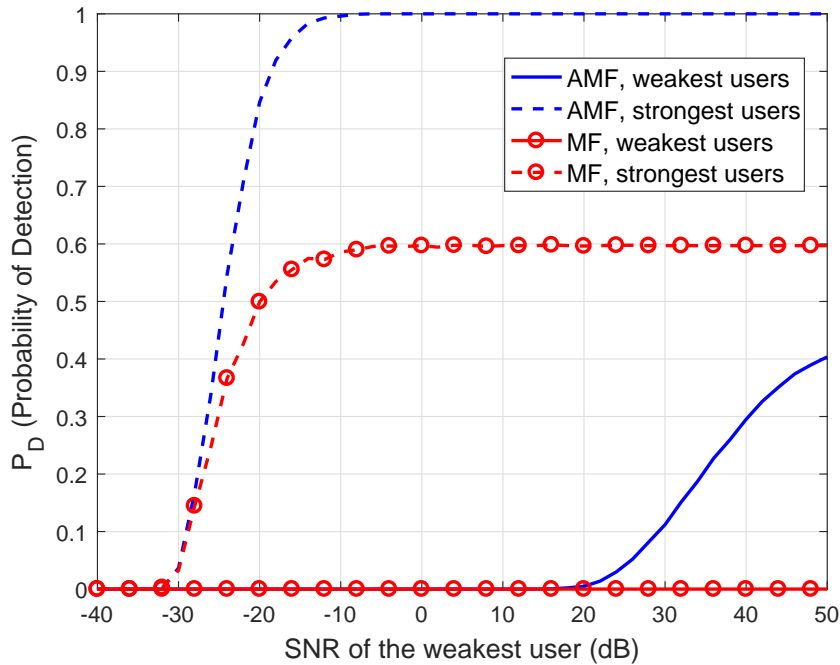


Figure 7.17: Average P_D vs SNR curves for different averaged received power levels ($K = 16, T = 32, D_{search} = 10, 10 \log (\bar{\beta}^{(4)} / \bar{\beta}^{(1)}) = 30$ dB)

In Fig. 7.18 and Fig. 7.19, nMSE performances of different channel estimators are demonstrated for the case when there are 16 active users and $10 \log (\bar{\beta}^{(4)} / \bar{\beta}^{(1)}) = 30$ dB. Here, D_{search} is taken as 10. In accordance with the P_D performances given in Fig. 7.17, the performance of MF based channel estimators are same as the ones which take D_{search} as 5. For the AMF based channel estimators, nMSE curves start to deviate from 1 when SNR is above 16 dB since the MPCs are started to be detected by the AMF based CFAR thresholding algorithm.

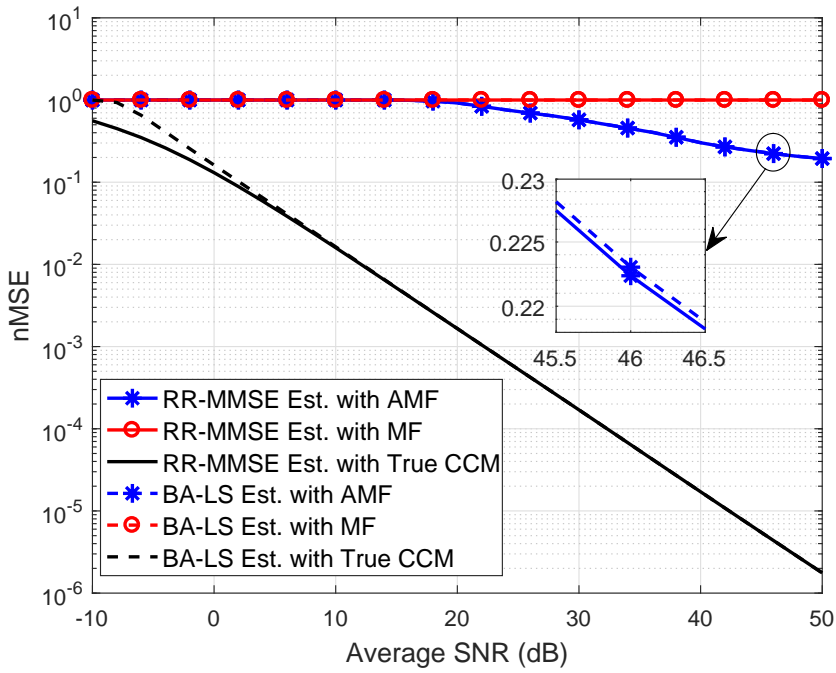


Figure 7.18: Performance of different channel estimators for weakest user group ($K = 16$, $T = 32$, $D_{search} = 10$, $T_{fast} = 32$, $10 \log (\bar{\beta}^{(4)} / \bar{\beta}^{(1)}) = 30$ dB)

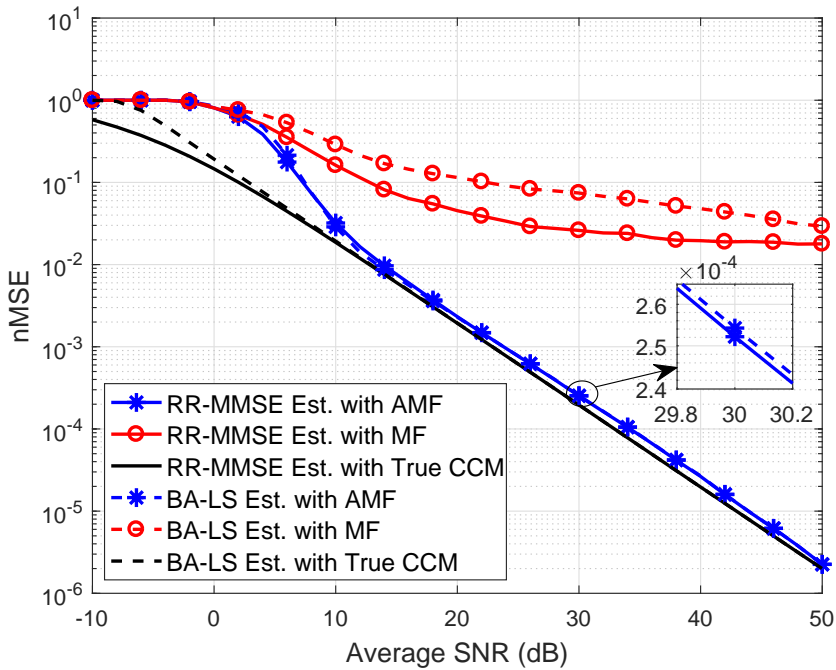


Figure 7.19: Performance of different channel estimators for strongest user group ($K = 16$, $T = 32$, $D_{search} = 10$, $T_{fast} = 32$, $10 \log (\bar{\beta}^{(4)} / \bar{\beta}^{(1)}) = 30$ dB)

7.3 Performance vs. Number of Slow-Time Training Snapshots

In Fig. 7.20 and Fig. 7.21, the P_D performance curves of AMF and MF based thresholding algorithms are demonstrated against different values of J , which is used to construct the JADPP before two-stage CFAR thresholding in (4.2), for 8 and 16 users cases respectively. Equal SNR case, in which $\text{SNR}^{(g)}$ s set to 10 and 30 dB for all user groups, is investigated. Note that, P_D of AMF based thresholding algorithm is almost equal to 1 in both 8 and 16 users case when SNR is 30 dB even for $J = 1$. However, MF based thresholding requires 20 snapshots to detect all active MPCs of 8 users while it cannot attain the same performance for $K = 16$ case even for 30 slow-time training snapshots. When SNR is 10 dB, P_D of AMF based thresholding algorithm reaches to 1 after 10 snapshots, requires more slow-time training snapshots to reach the same performance in 30 dB case, while MF based thresholding requires 30 snapshots when there are 8 active users. When there are 16 active users, P_D of MF based thresholding algorithm never reaches to 1. It can be seen that increasing J is not enough for MF to attain the performance it has when there are 8 users.

In Fig. 7.22 and 7.23, nMSE performances of different estimators are shown against different values of J when there are 8 and 16 active users with equal average received power respectively. Here, $T = T_{fast} = 32$ are taken. As it can be seen, a very small amount of training snapshots is sufficient for AMF based channel estimators to sustain nearly optimal performance (given by RR-MMSE with true CCM). In contrast, MF based estimators require much larger amount of slow-time training snapshots to guarantee accurate enough CCM construction. In accordance with the results given in Fig. 7.21, increasing J does not help MF based channel estimators to attain the benchmark performance for 16 active users. In other words, nMSE performance of MF based channel estimators given in Fig. 7.4 cannot be improved by increasing J only.

Therefore, the considerable advantage of the proposed AMF based reduced rank estimators in terms of training overhead over the MF based ones is highlighted for slow-time training mode.

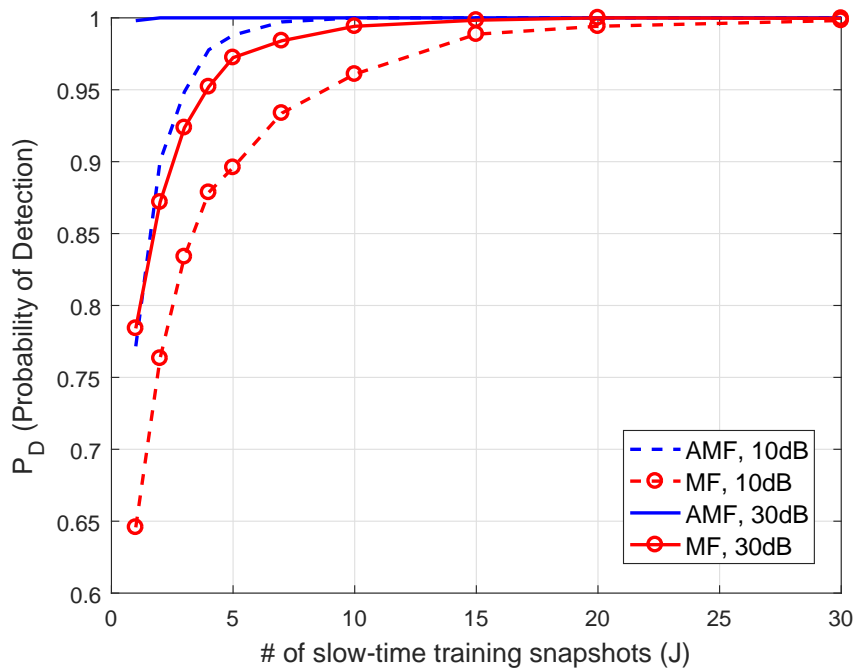


Figure 7.20: Average P_D vs J curves for equal averaged received power levels ($K = 8$, $D_{search} = 5$, $T = 32$, $\text{SNR}^{(g)} = 30$ dB for $g = 1, \dots, G$)

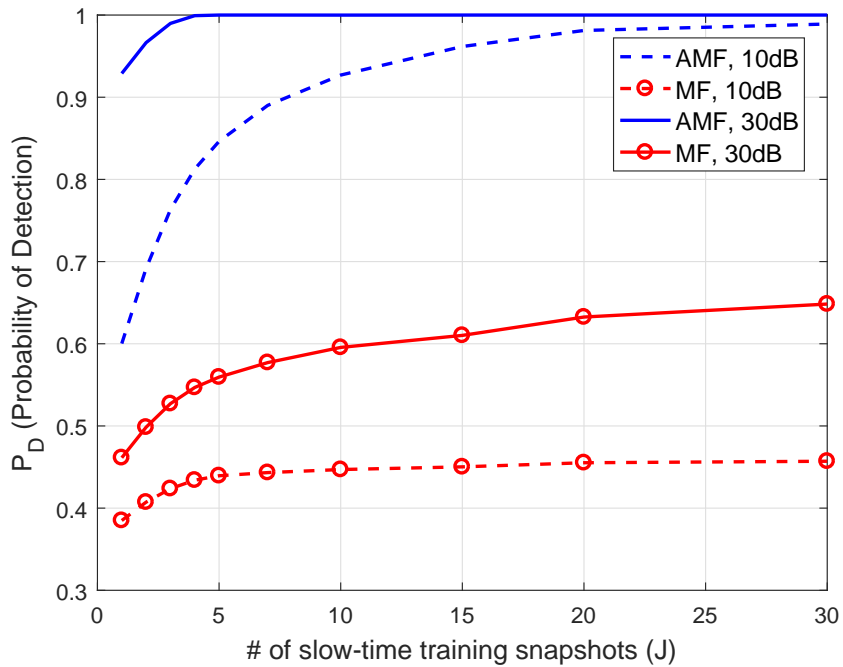


Figure 7.21: Average P_D vs J curves for equal averaged received power levels ($K = 16$, $D_{search} = 5$, $T = 32$, $\text{SNR}^{(g)} = 30$ dB for $g = 1, \dots, G$)

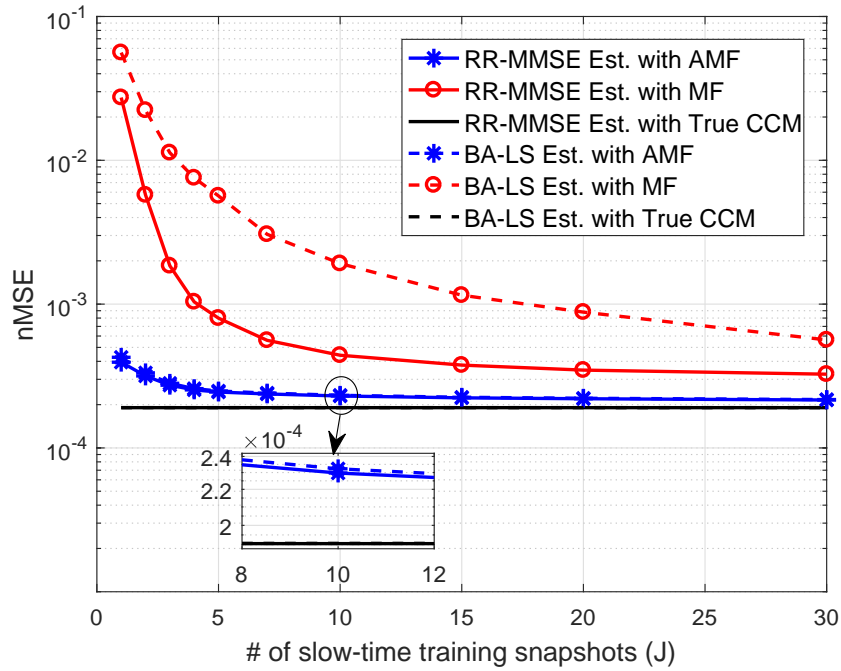


Figure 7.22: Performance of different channel estimators averaged over all groups for different J ($K = 8$, $D_{search} = 5$, $T = T_{fast} = 32$, $\text{SNR}^{(g)} = 30$ dB for $g = 1, \dots, G$)

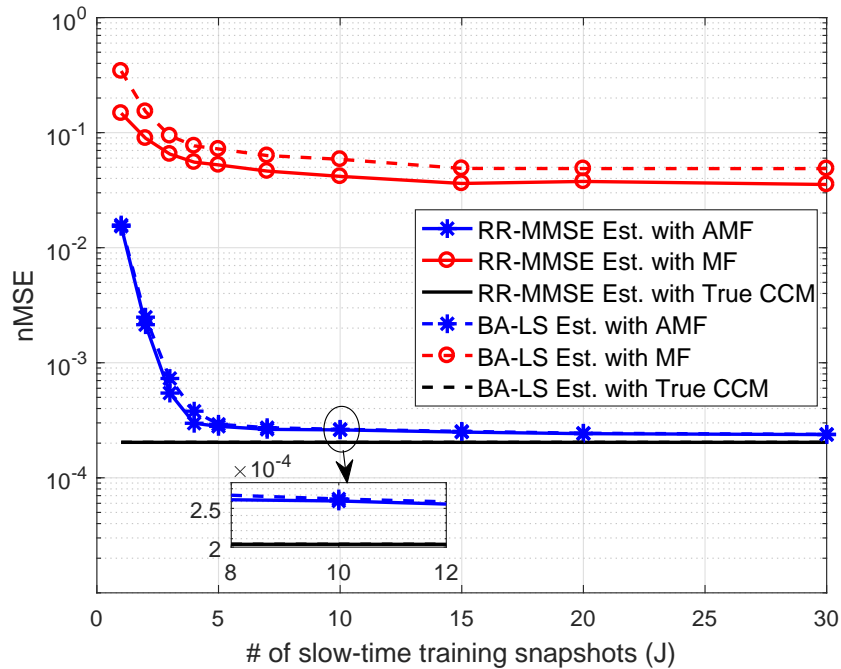


Figure 7.23: Performance of different channel estimators averaged over all groups for different J ($K = 16$, $D_{search} = 5$, $T = T_{fast} = 32$, $\text{SNR}^{(g)} = 30$ dB for $g = 1, \dots, G$)

In Fig. 7.24 and Fig. 7.25, P_D curves as a function of J are demonstrated for 8 and 16 users case respectively, when there are 15 dB power difference between weakest and strongest group users, i.e., $10 \log \left(\frac{\bar{\beta}^{(4)}}{\bar{\beta}^{(1)}} \right) = 15$ dB is taken. It is assumed that $\text{SNR}^{(1)}$ is 30 dB, and $\text{SNR}^{(4)}$ is 45 dB. Note that the performance of AMF for strongest group users is similar to the performance of AMF when $\text{SNR}^{(g)}$ s are taken as equal. However, when 16 active users are present, it is seen that the AMF does not reach 1 for weakest group users even for large values of J , and the performance of MF is very low irrespective of J . For strongest group users, increasing J helps MF to increase its performance up to a certain value only.

In Fig. 7.26 and Fig. 7.27 nMSE curves are provided for the weakest and strongest user groups respectively when $K = 8$. When there are 16 active users, nMSE curves in Fig. 7.28 and Fig. 7.29 are obtained for weakest and strongest user groups respectively. All results are obtained when $\text{SNR}^{(1)}$ is 30 dB, and $\text{SNR}^{(4)}$ is 45 dB. In parallel with the results deduced from the P_D curves, for 8 users case, the performance of AMF based channel estimators increases for both weakest and strongest user groups. However, the performance of MF based channel estimators does not increase steadily for strongest user groups as J increases when $K = 8$. It can be seen from Fig. 7.24 that P_D of MF based thresholding reaches to 1 for strongest user groups while nMSE curves of MF based channel estimators do not attain the benchmark performance for large values of J . This is not a surprising finding since P_D results indicates whether the center of an active MPC is detected or not while nMSE performance is affected from the width of the angular spread determined and false alarms. In Fig. 7.28 nMSE performance of AMF based estimators and in Fig. 7.29 nMSE performance of MF based estimators increases as J becomes larger which is highly consistent with the results given in Fig. 7.25.

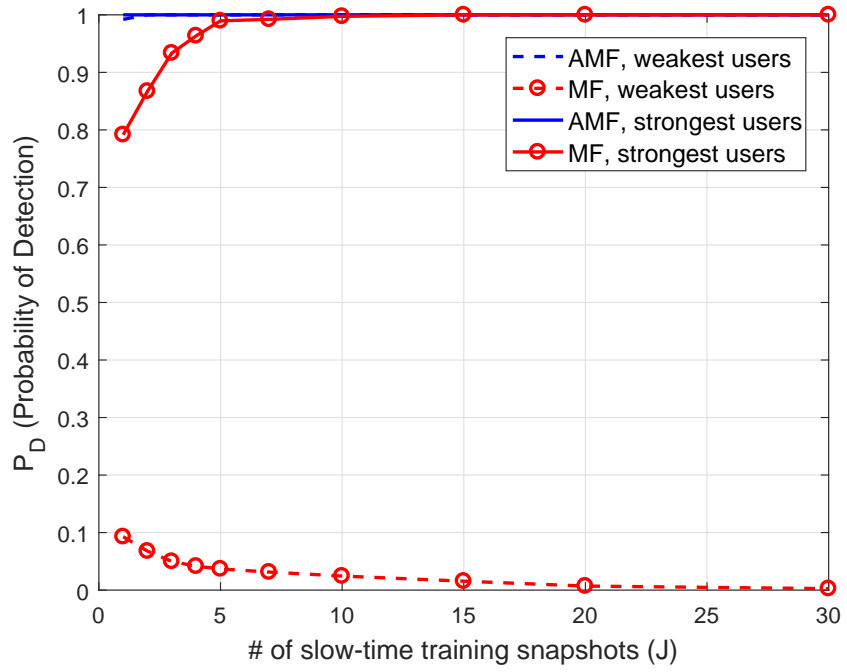


Figure 7.24: Average P_D vs J curves for different averaged received power levels ($K = 8$, $D_{search} = 5$, $T = 32$, $10 \log (\bar{\beta}^{(4)} / \bar{\beta}^{(1)}) = 15$ dB)

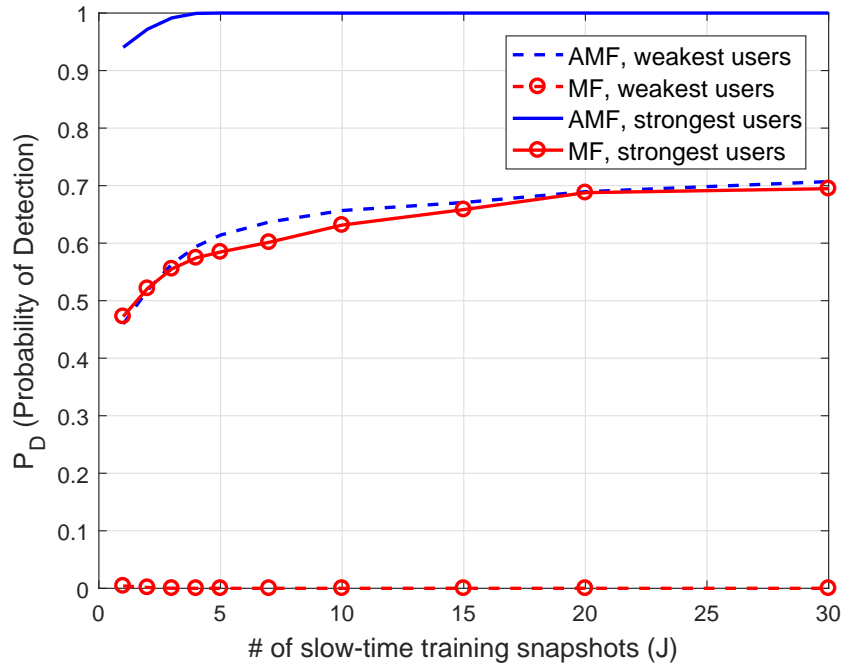


Figure 7.25: Average P_D vs J curves for different averaged received power levels ($K = 16$, $D_{search} = 5$, $T = 32$, $10 \log (\bar{\beta}^{(4)} / \bar{\beta}^{(1)}) = 15$ dB)

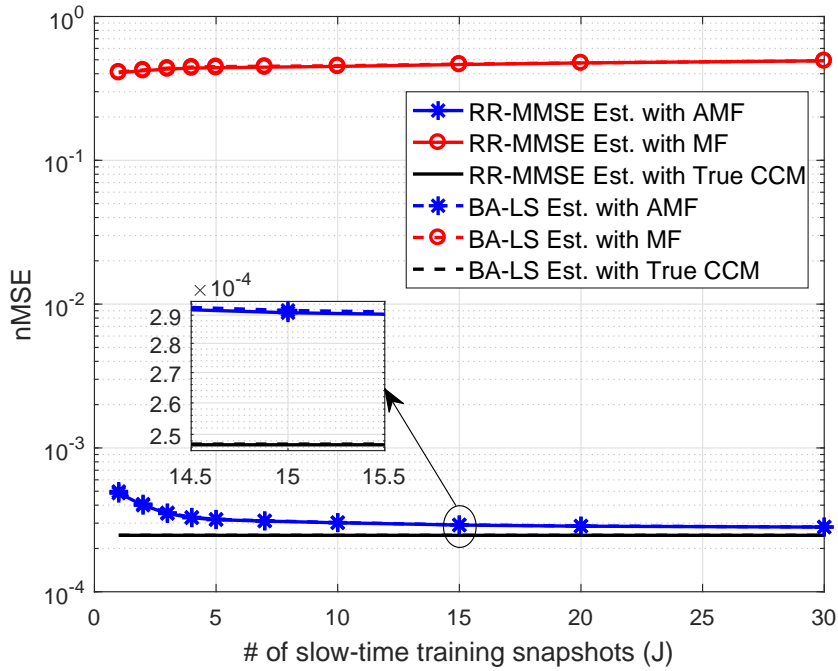


Figure 7.26: Performance of different channel estimators in terms of nMSE vs J for weakest user group ($K = 8$, $D_{search} = 5$, $T = T_{fast} = 32$, $10 \log (\bar{\beta}^{(4)} / \bar{\beta}^{(1)}) = 15$ dB)

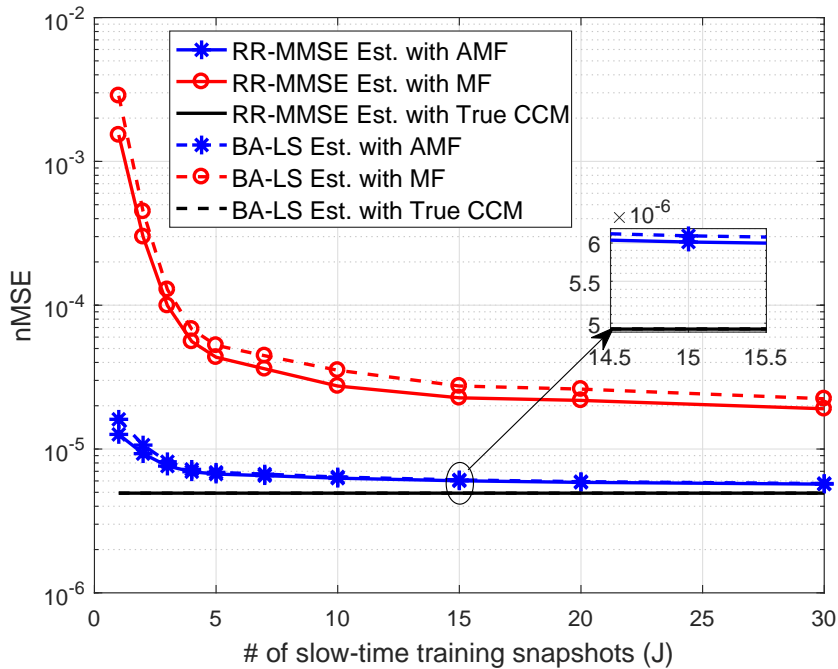


Figure 7.27: Performance of different channel estimators in terms of nMSE vs J for strongest user group ($K = 8$, $D_{search} = 5$, $T = T_{fast} = 32$, $10 \log (\bar{\beta}^{(4)} / \bar{\beta}^{(1)}) = 15$ dB)

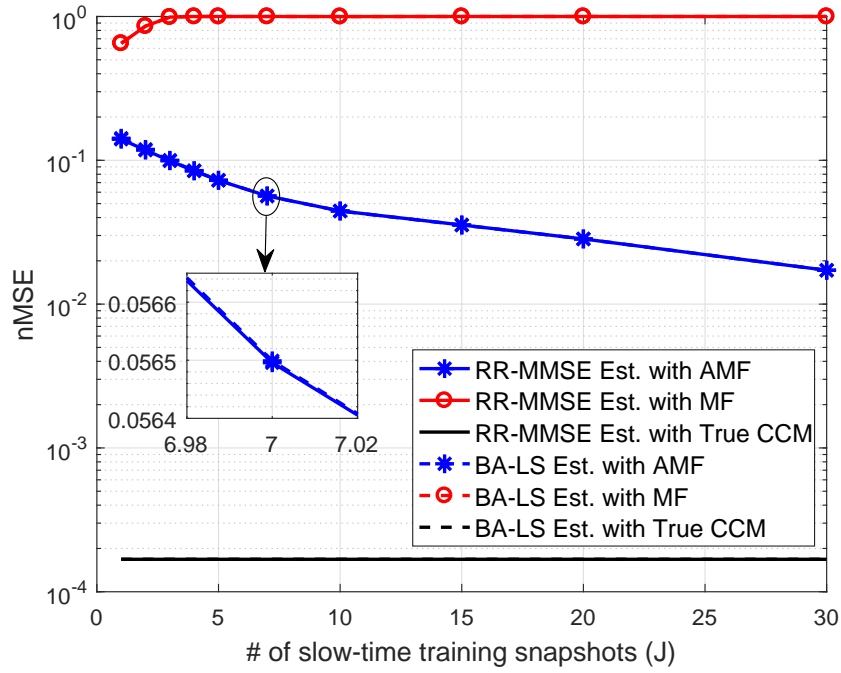


Figure 7.28: Performance of different channel estimators in terms of nMSE vs J for weakest user group ($K = 16$, $D_{search} = 5$, $T = T_{fast} = 32$, $10 \log(\bar{\beta}^{(4)} / \bar{\beta}^{(1)}) = 15$ dB)

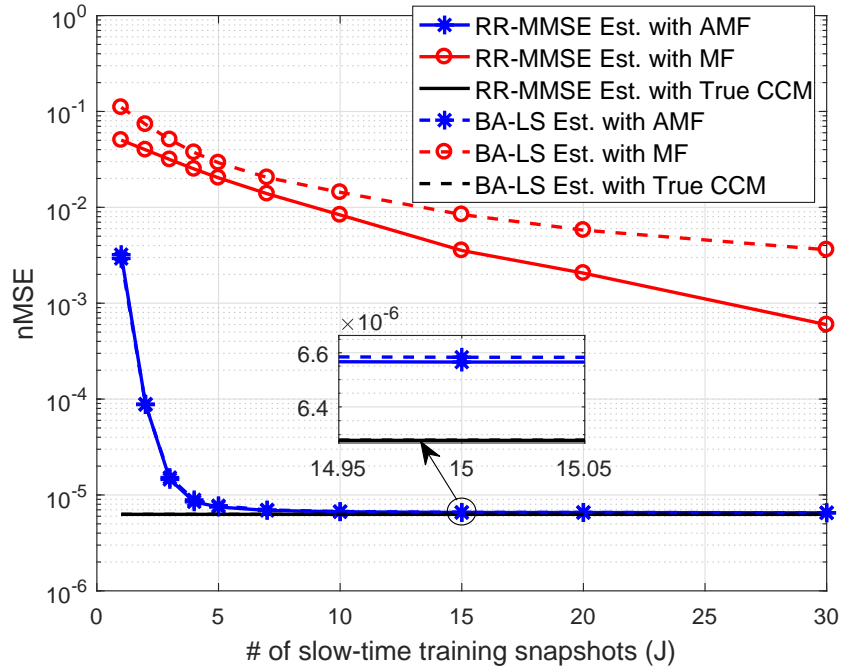


Figure 7.29: Performance of different channel estimators in terms of nMSE vs J for strongest user group ($K = 16$, $D_{search} = 5$, $T = T_{fast} = 32$, $10 \log(\bar{\beta}^{(4)} / \bar{\beta}^{(1)}) = 15$ dB)

7.4 Performance vs. Fast-Time Training Length

In Fig. 7.30 and Fig. 7.31, nMSE performances of different channel estimators are given as a function of T_{fast} when the length of slow-time training data, T , used for the acquisition of CCMs and sparsity map is fixed to 32, for 8 and 16 users respectively. In fast-time channel acquisition mode, small amount of training data is sufficient to estimate effective instantaneous CSI by exploiting previously acquired slowly varying parameters. When the sparsity map is obtained accurately enough with the use of AMF based CFAR thresholding, RR-MMSE and BA-LS, which are aware of the spatial signatures of the channels, necessitates significantly reduced amount of fast-time training when compared to the conventional LS type estimator, which is unaware of the jointly sparse structure of the MIMO channel. On the other hand, conventional LS type estimator shows superior performance to BA-LS type estimator for larger fast-time training data when MF based thresholding is adopted. That is because of the inaccurate construction of the sparsity map, which degrades the performance of BA-LS type estimator significantly in case of MF based thresholding. It is important to note that the results of conventional LS channel estimator with AMF or MF corresponds to the performance of full dimensional LS channel estimator after projection onto the beamspace formed by AMF or MF based thresholding algorithms.

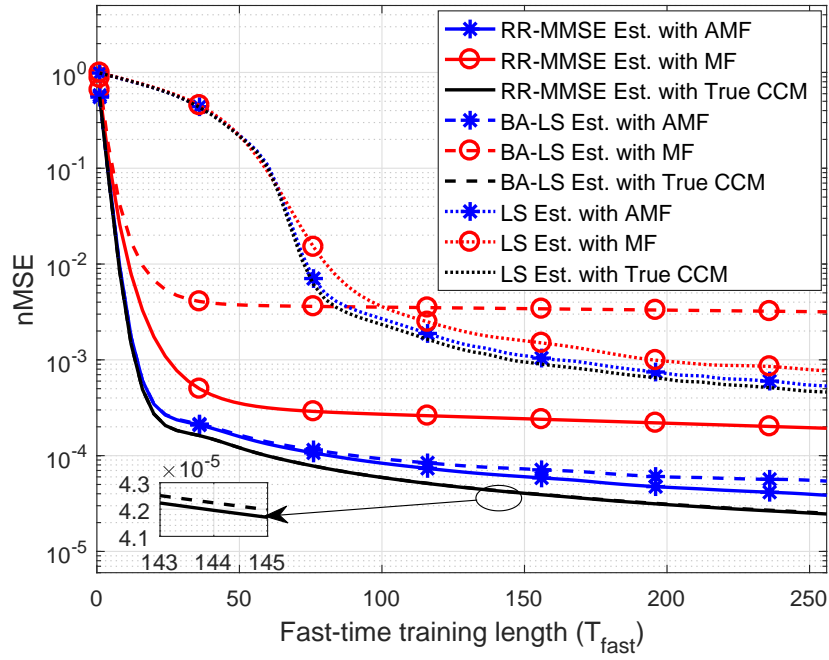


Figure 7.30: Performance of different channel estimators averaged over all groups for different T_{fast} ($K = 8$, $D_{search} = 5$, $T = 32$, $\text{SNR}^{(g)} = 30$ dB for $g = 1, \dots, G$)

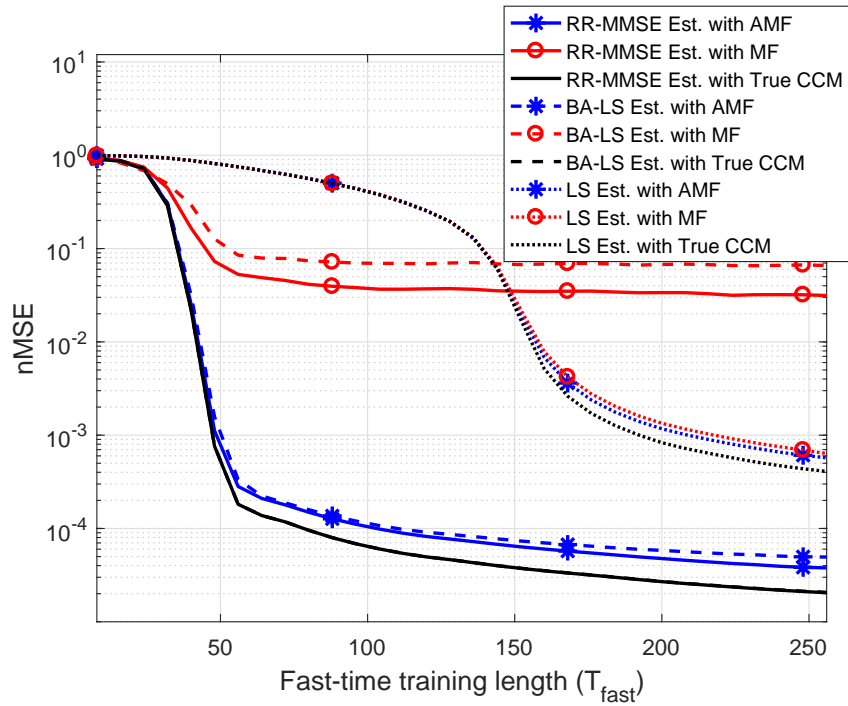


Figure 7.31: Performance of different channel estimators averaged over all groups for different T_{fast} ($K = 16$, $D_{search} = 5$, $T = 32$, $\text{SNR}^{(g)} = 30$ dB for $g = 1, \dots, G$)

7.5 Performance vs. Slow-Time Training Length

In Fig. 7.32, the average P_D curves of different SNR values are demonstrated as a function of slow-time training data, T , when 16 users exist with equal SNR. As T increases, the performances of both AMF and MF based thresholding algorithms rise considerably. It is important to note that P_D of both AMF and MF approaches to 1 even when SNR is taken as -5 dB which is not seen in the previous results since T is always set to 32 there. There is also a small increase in the P_D for even -10 dB SNR case when $T > 140$.

In Fig. 7.33, nMSE curves of different channel estimators are given for the scenario stated above when SNR is taken as 20 dB for all user groups. It is noticeable that, MF based channel estimators attain the benchmark performance for $T > 80$ while AMF based channel estimators need $T > 40$ to achieve the benchmark. This behaviour is consistent with the P_D performance of AMF and MF based thresholding algorithms given in Fig. 7.32.

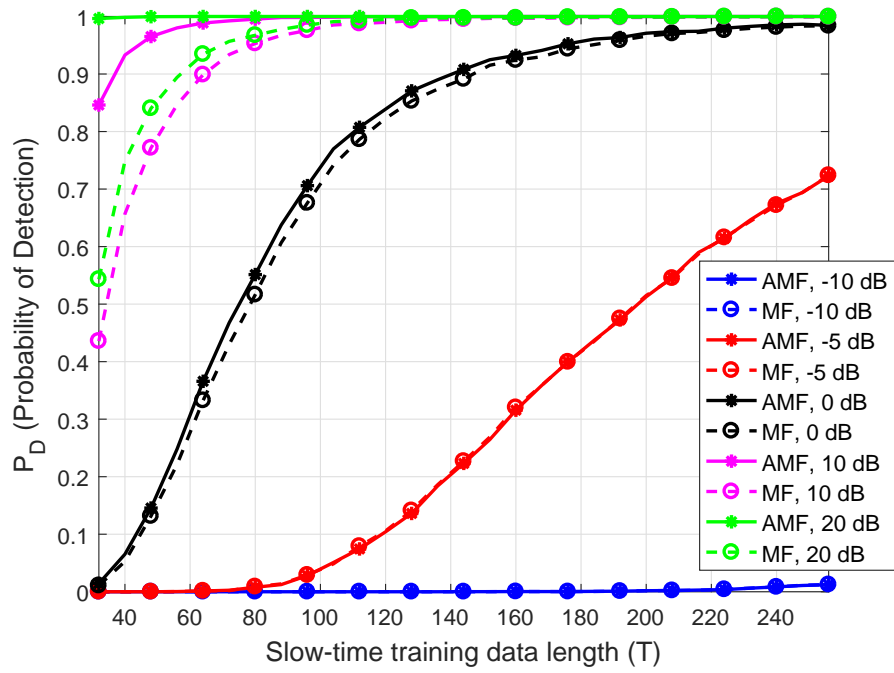


Figure 7.32: Average P_D vs T curves for equal averaged received power levels ($K = 16$, $D_{search} = 5$)

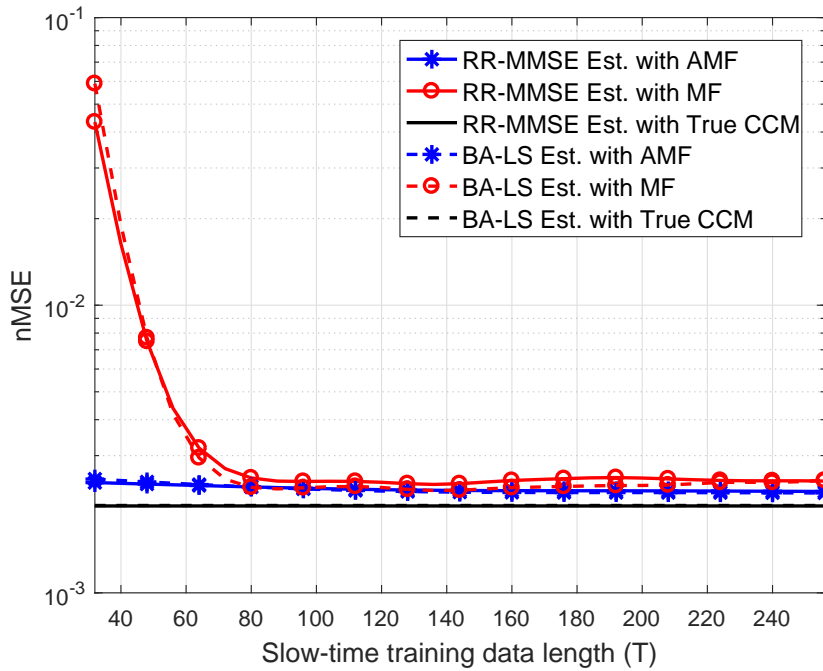


Figure 7.33: Performance of different channel estimators averaged over all groups for different T ($K = 16$, $D_{search} = 5$, $T_{fast} = 32$, $\text{SNR}^{(g)} = 20$ dB for $g = 1, \dots, G$)

In Fig. 7.34 the average P_D curves of weakest and strongest group users are demonstrated as a function of slow-time training data, T , when 16 active users exist. Here, $\text{SNR}^{(1)} = 20$ dB and $\text{SNR}^{(4)} = 35$ dB are taken. Note that increasing T remarkably increases the performances of both AMF and MF based thresholding algorithms. P_D is equal to zero for weakest group users when T is taken as 32 which is consistent with the findings given in Fig. 7.8.

In Fig. 7.35 and Fig. 7.36 the corresponding nMSE curves are given for weakest and strongest user groups respectively. The positive correlation between nMSE performances and T also exists in the given results. nMSE performances of AMF based channel estimators for weakest user group and MF based channel estimators for strongest group user attain the benchmark performance as T increases. Note that this behaviour is not seen in Fig. 7.9 and Fig. 7.10 where T is taken as 32.

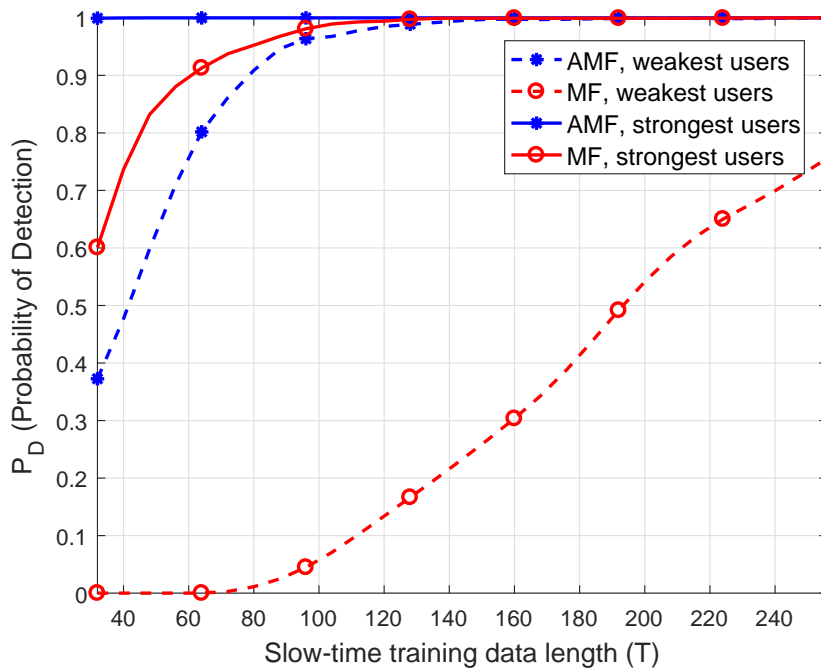


Figure 7.34: Average P_D vs T curves for different averaged received power levels ($K = 16$, $D_{search} = 5$, $10 \log (\bar{\beta}^{(4)} / \bar{\beta}^{(1)}) = 15$ dB)

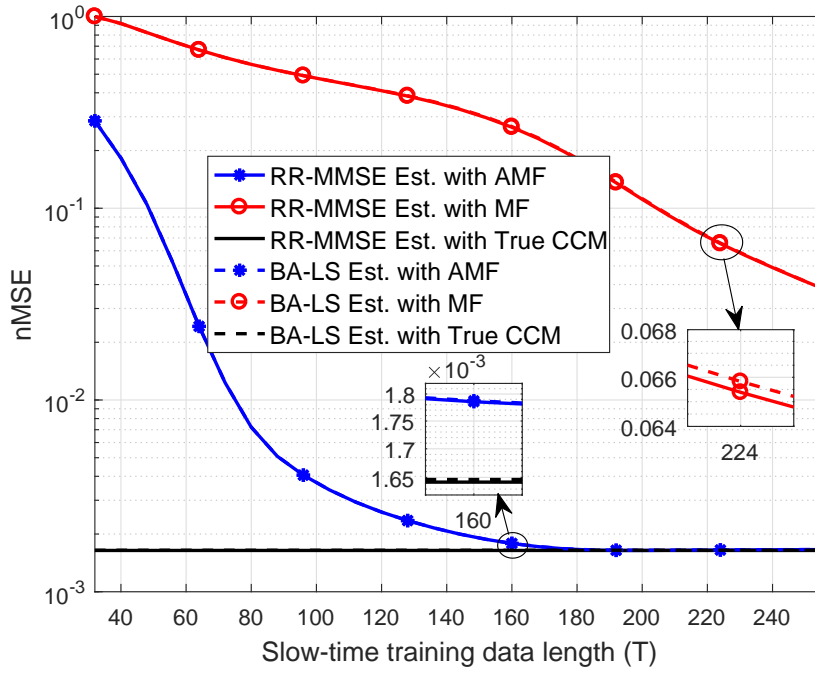


Figure 7.35: Performance of different channel estimators in terms of nMSE vs T for weakest user group ($K = 16$, $D_{search} = 5$, $T_{fast} = 32$, $10 \log (\bar{\beta}^{(4)} / \bar{\beta}^{(1)}) = 15$ dB)

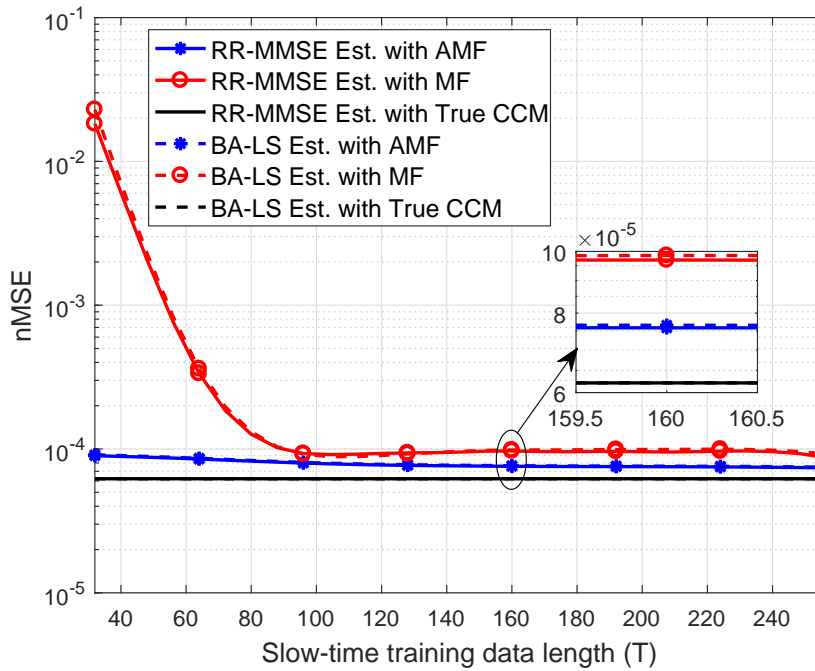


Figure 7.36: Performance of different channel estimators in terms of nMSE vs T for strongest user group ($K = 16$, $D_{search} = 5$, $T_{fast} = 32$, $10 \log (\bar{\beta}^{(4)} / \bar{\beta}^{(1)}) = 15$ dB)

In Fig. 7.37 the average P_D curves of weakest and strongest group users are demonstrated as a function of slow-time training data, T , when 16 active users exist. Here, $\text{SNR}^{(1)} = 20$ dB and $\text{SNR}^{(4)} = 50$ dB are taken.

In Fig. 7.38 and Fig. 7.39 the corresponding nMSE curves are given for weakest and strongest user groups respectively.

For the strongest user group, P_D of MF based thresholding algorithm in Fig. 7.37 increases as T increases and corresponding nMSE performances of MF based channel estimators in Fig. 7.39 approach to nMSE performance of the benchmark. In Fig. 7.38, nMSE curves of AMF based channel estimators deviates from 1 which implies that there are some detected MPCs belonging to weakest user group and it can be confirmed from the results demonstrated in Fig. 7.37 where it is seen that P_D performance of AMF based thresholding algorithm for weakest users slowly improves.

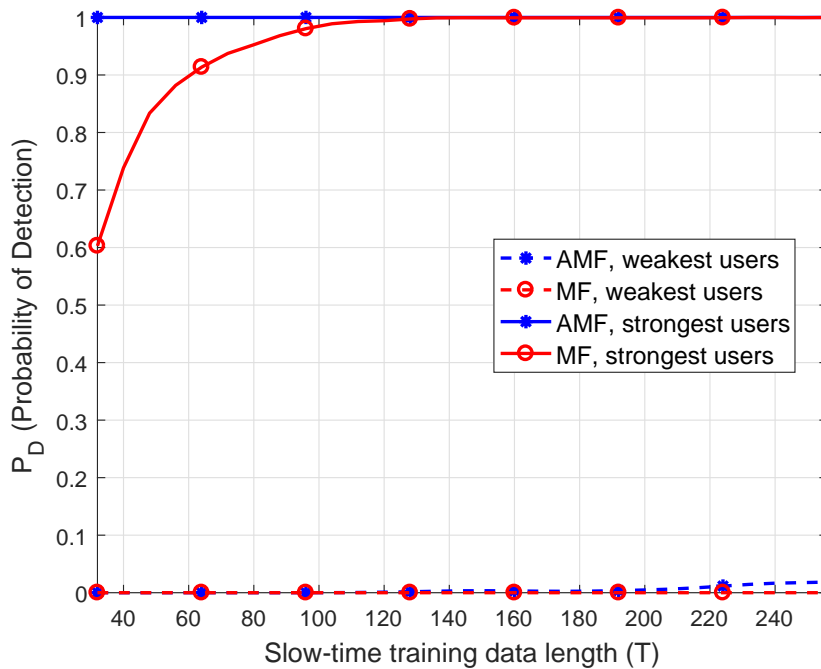


Figure 7.37: Average P_D vs T curves for different averaged received power levels ($K = 16$, $D_{search} = 5$, $10 \log (\bar{\beta}^{(4)} / \bar{\beta}^{(1)}) = 30$ dB)

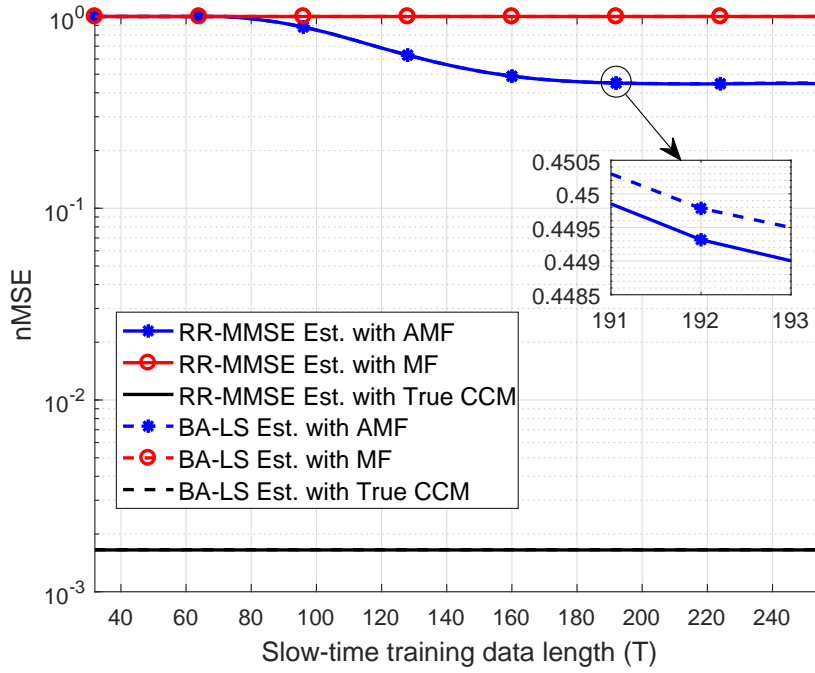


Figure 7.38: Performance of different channel estimators in terms of nMSE vs T for weakest user group ($K = 16$, $D_{search} = 5$, $T_{fast} = 32$, $10 \log (\bar{\beta}^{(4)} / \bar{\beta}^{(1)}) = 30$ dB)

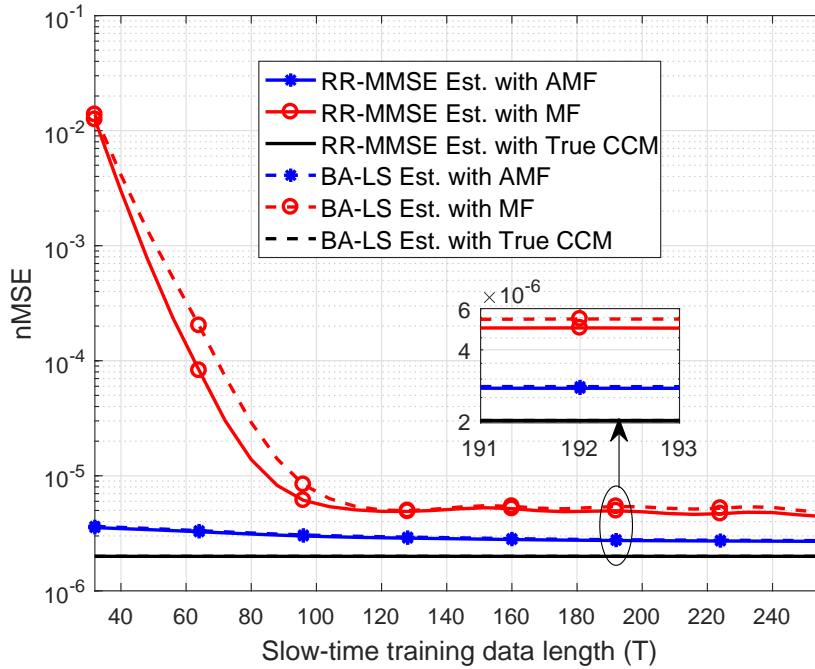


Figure 7.39: Performance of different channel estimators in terms of nMSE vs T for strongest user group ($K = 16$, $D_{search} = 5$, $T_{fast} = 32$, $10 \log (\bar{\beta}^{(4)} / \bar{\beta}^{(1)}) = 30$ dB)

7.6 Performance vs. Number of RF Chains

In Fig. 7.40 and Fig. 7.41, nMSE performances of different channel estimators based on AMF and MF type JADPP estimators are demonstrated for $K = 8$ and $K = 16$ users cases respectively. It is seen from both figures that, increasing the number of RF chains utilized in the hybrid beamformer architecture deteriorates the performance of channel estimators. As the total number of RF chains increases, the effective channel dimension increases leading to increase in the leakage from the noise and interference subspace. Also, since there are large amount of RF chains available now, RF chain distribution algorithm is likely to assign RF chains to MPCs which are declared as active by the thresholding algorithms although they are not. This assignment results in illuminating spatial regions where intended users are not actually present, and thus capturing leakage from there.

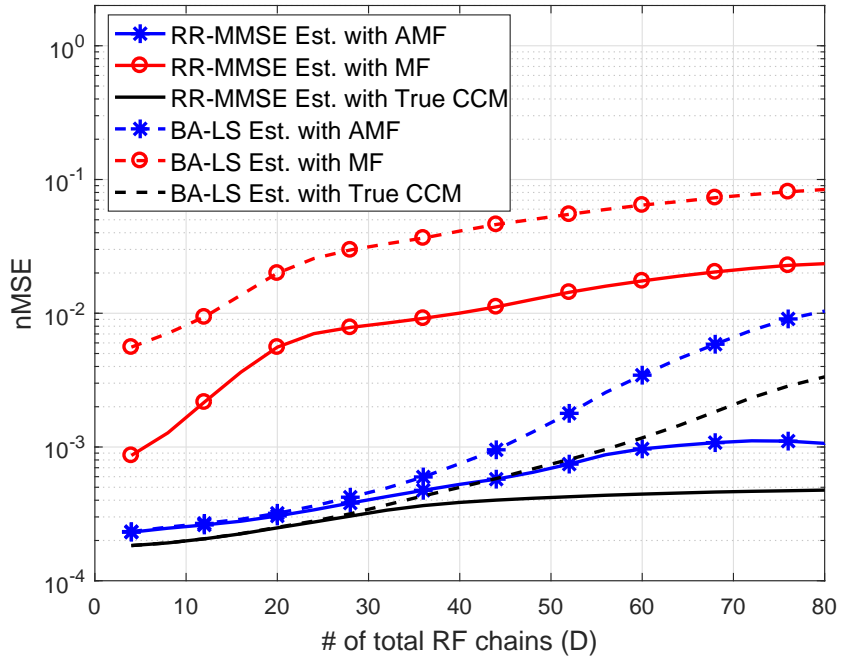


Figure 7.40: Performance of different channel estimators averaged over all groups for different D ($K = 8$, $D_{search} = 5$, $T = T_{fast} = 32$, $\text{SNR}^{(g)} = 30$ dB for $g = 1, \dots, G$)

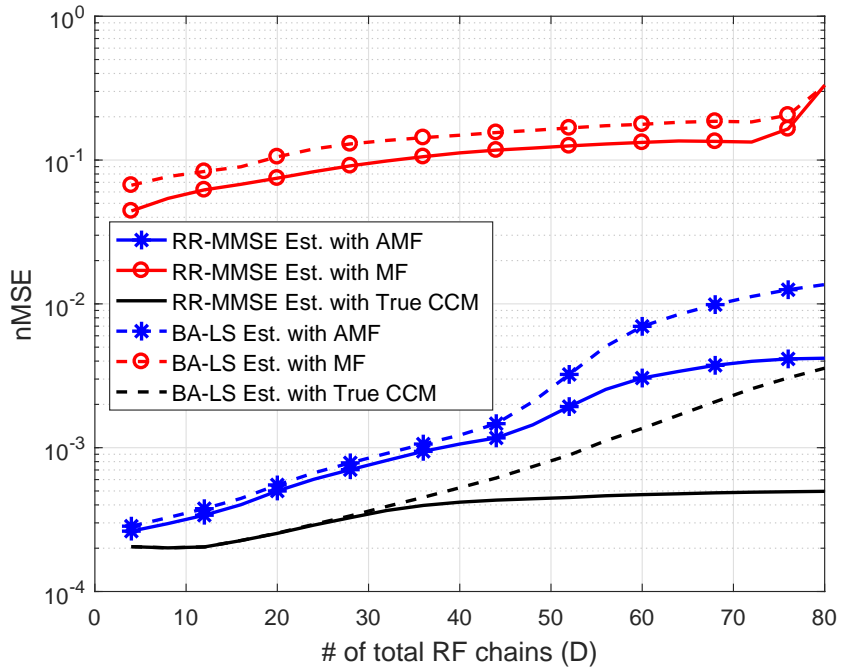


Figure 7.41: Performance of different channel estimators averaged over all groups for different D ($K = 16$, $D_{search} = 5$, $T = T_{fast} = 32$, $\text{SNR}^{(g)} = 30$ dB for $g = 1, \dots, G$)

7.7 Performance vs. Look Spread

In Fig. 7.42, the P_D curves of AMF and MF type JADPP estimators against the look spread σ is given for $\text{SNR}^{(g)} = 10$ dB and $\text{SNR}^{(g)} = 30$ dB cases. In Fig. 7.43 and Fig. 7.44, nMSE curves of channel estimators are demonstrated for $\text{SNR}^{(g)} = 10$ dB and $\text{SNR}^{(g)} = 30$ dB cases respectively. The given results indicate that increasing σ beyond a certain value decreases the performance of JADPP and channel estimators. Note that σ determines the width of the digital search beams. When σ is continuously increased and the number of digital search beams, D_{search} , is kept constant, the intended region of interest can not be illuminated effectively anymore. To avoid the performance losses after $\sigma = 10^\circ$ in the given results, one must increase D_{search} as well.

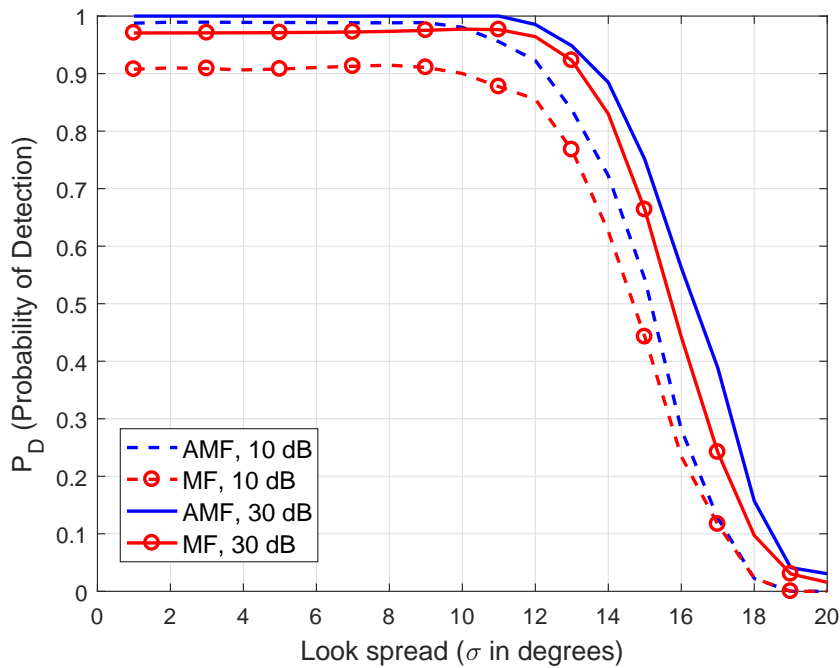


Figure 7.42: Average P_D vs σ curves for equal averaged received power levels ($K = 8$, $D_{search} = 5$, $T = 32$)

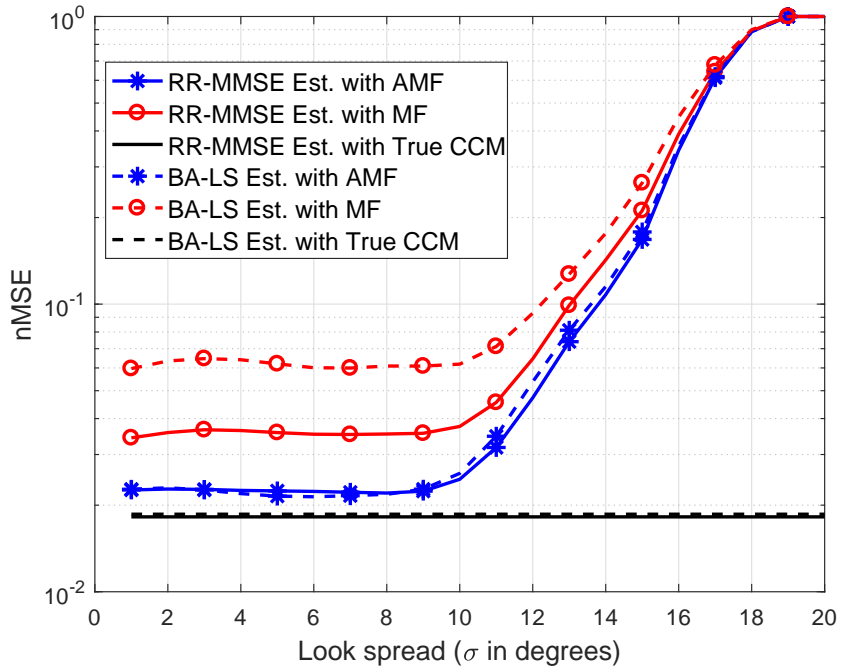


Figure 7.43: Performance of different channel estimators averaged over all groups for different values of σ ($K = 8$, $D_{search} = 5$, $T = T_{fast} = 32$, $\text{SNR}^{(g)} = 10$ dB for $g = 1, \dots, G$)

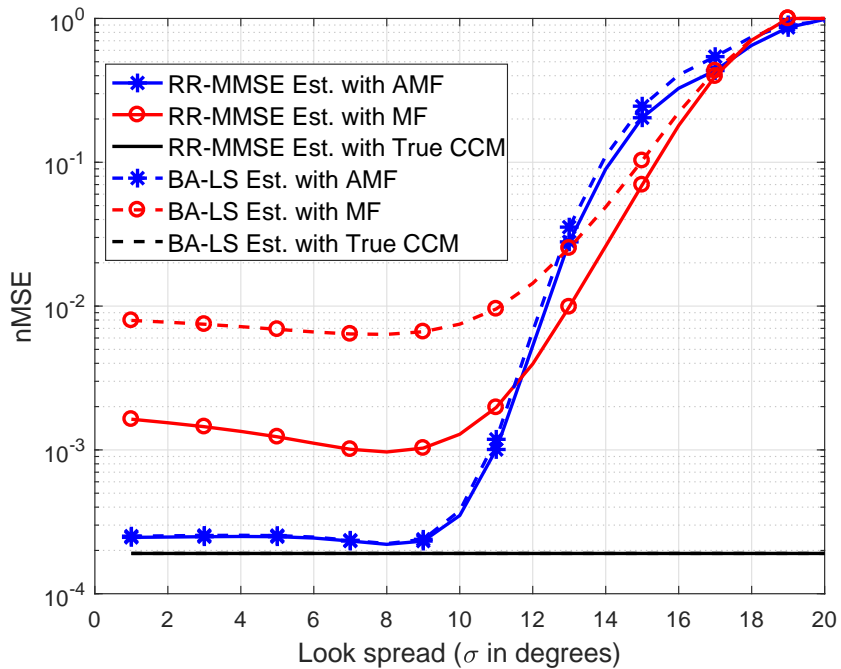


Figure 7.44: Performance of different channel estimators averaged over all groups for different values of σ ($K = 8$, $D_{search} = 5$, $T = T_{fast} = 32$, $\text{SNR}^{(g)} = 30$ dB for $g = 1, \dots, G$)

7.8 Performance vs. Search Dimension

In Fig. 7.45 P_D curves of AMF and MF based thresholding algorithms are given for both $\text{SNR}^{(g)} = 10$ dB and $\text{SNR}^{(g)} = 30$ dB cases when 8 users are active with equal power. Also, nMSE curves for AMF and MF based channel estimators are given for $\text{SNR}^{(g)} = 10$ dB case in Fig. 7.47 and $\text{SNR}^{(g)} = 30$ dB case in Fig. 7.48.

In Fig. 7.46 P_D curves of AMF and MF based thresholding algorithms are given for $K = 16$ case as well. Also, corresponding nMSE curves are provided in Fig. 7.49 and in Fig. 7.50.

Note that the performance of MF based estimators do not change much as D_{search} increases. However, the performance of AMF based estimators are increased as D_{search} becomes larger. Increasing D_{search} helps the BS to illuminate the intended angular sector providing AMF to eliminate the effect of interferers better. It is noticeable that AMF based thresholding algorithm and channel estimators requires D_{search} to be equal to at least 3 for $K = 8$ case, and 5 for $K = 16$ case, for maximum performance.

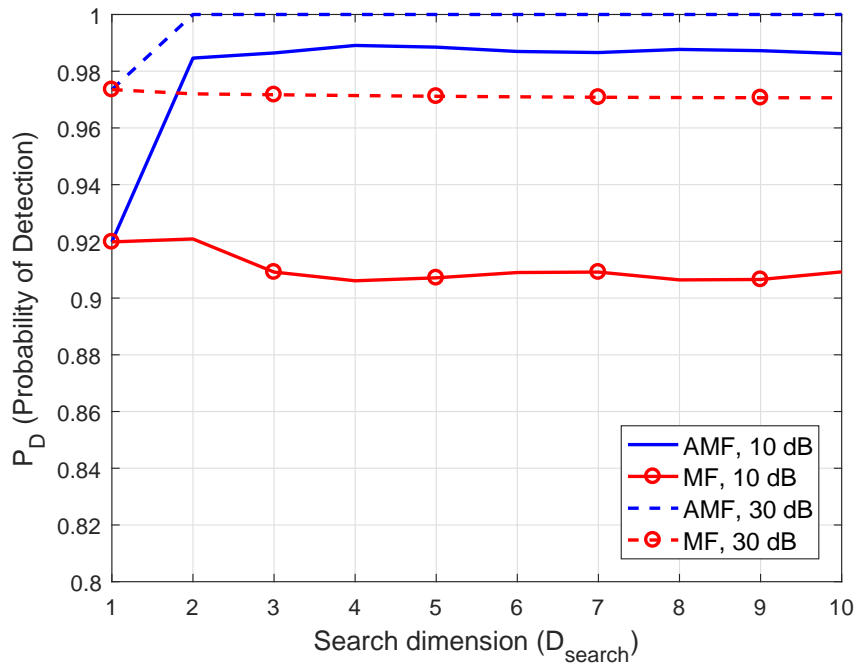


Figure 7.45: Average P_D vs D_{search} curves for equal averaged received power levels ($K = 8, T = 32$)

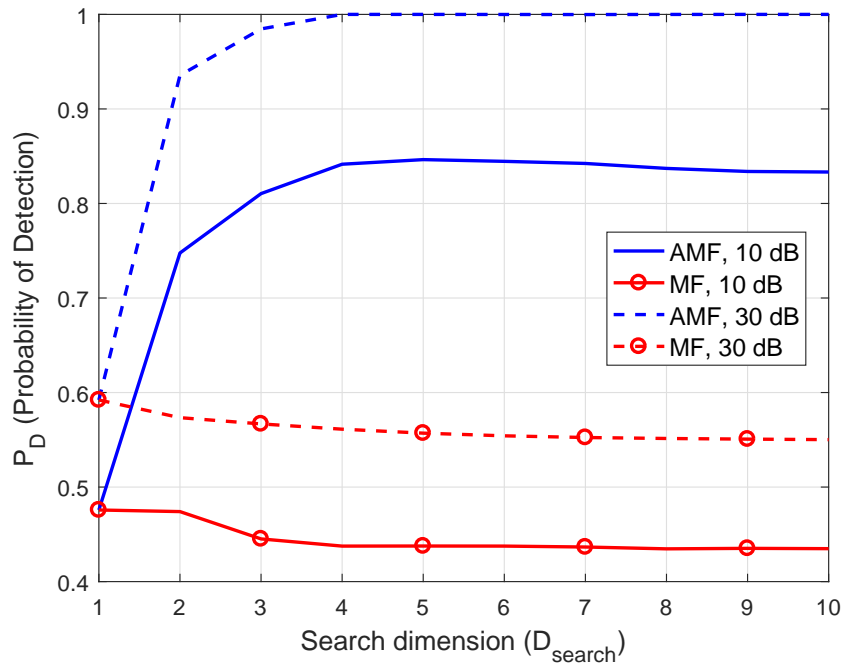


Figure 7.46: Average P_D vs D_{search} curves for equal averaged received power levels ($K = 16, T = 32$)

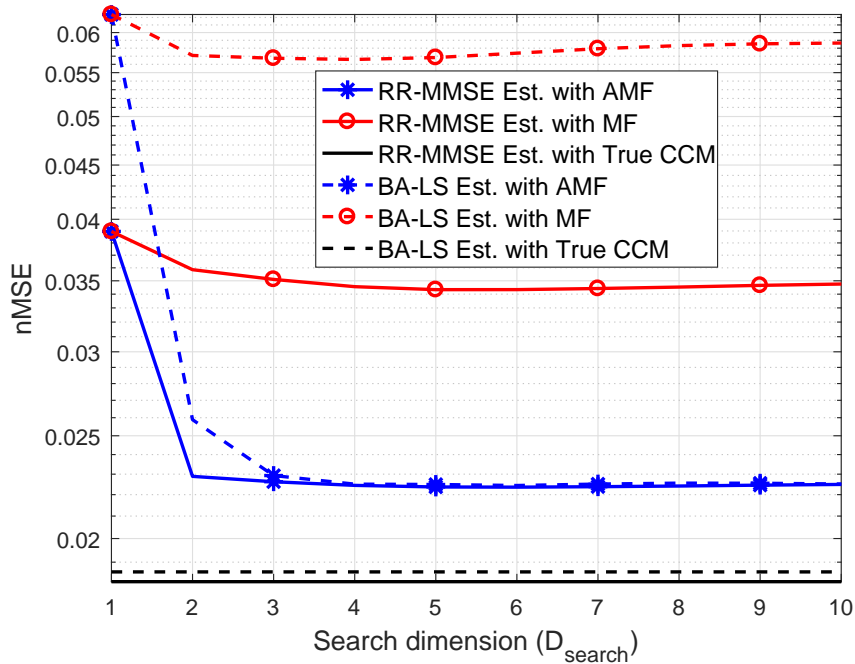


Figure 7.47: Performance of different channel estimators averaged over all groups for different values of D_{search} ($K = 8$, $T = T_{fast} = 32$, $\text{SNR}^{(g)} = 10$ dB for $g = 1, \dots, G$)

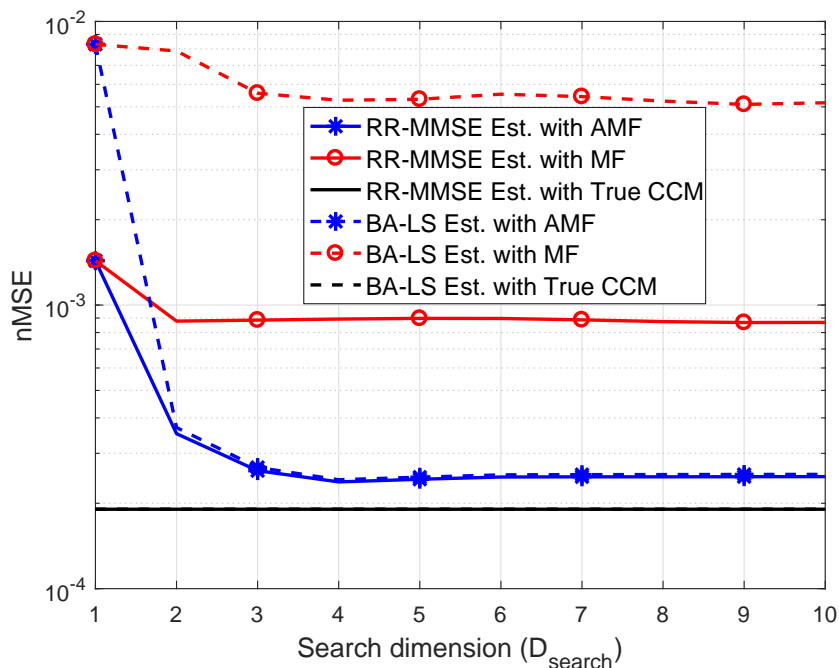


Figure 7.48: Performance of different channel estimators averaged over all groups for different values of D_{search} ($K = 8$, $T = T_{fast} = 32$, $\text{SNR}^{(g)} = 30$ dB for $g = 1, \dots, G$)

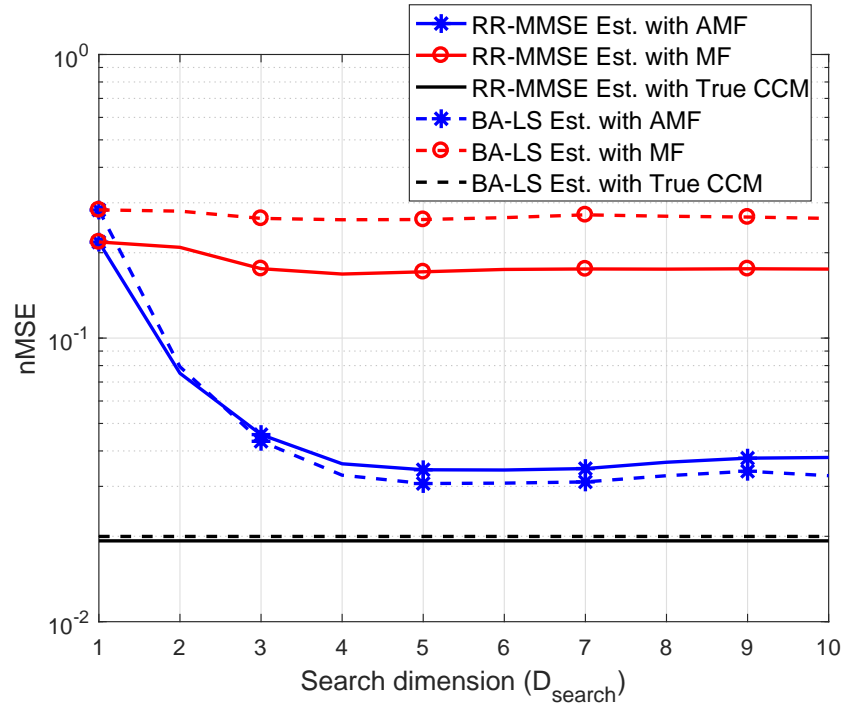


Figure 7.49: Performance of different channel estimators averaged over all groups for different values of D_{search} ($K = 16$, $T = T_{fast} = 32$, $SNR^{(g)} = 10$ dB for $g = 1, \dots, G$)

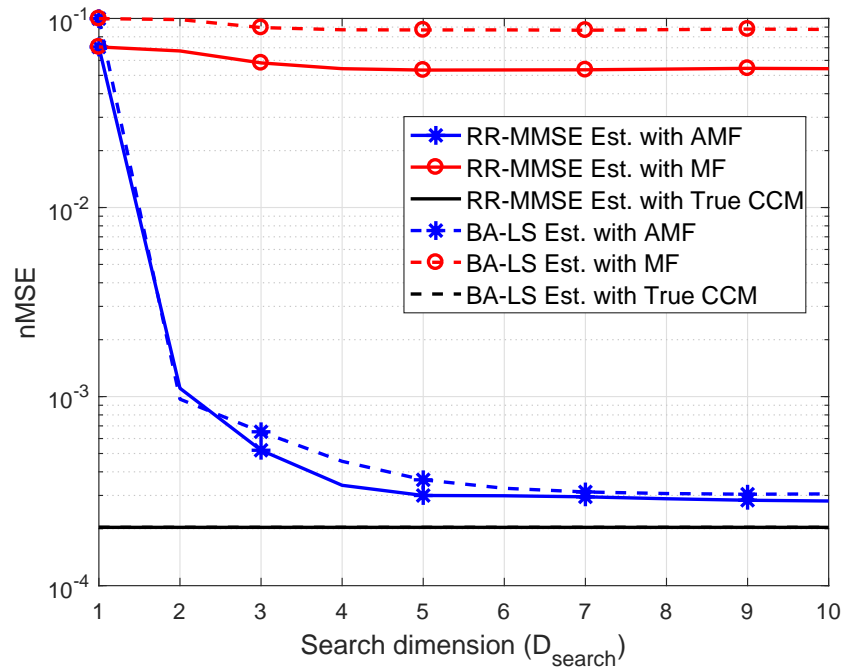


Figure 7.50: Performance of different channel estimators averaged over all groups for different values of D_{search} ($K = 16$, $T = T_{fast} = 32$, $SNR^{(g)} = 30$ dB for $g = 1, \dots, G$)

In Fig. 7.51 and Fig. 7.52, P_D curves are given with respect to D_{search} for 8 and 16 users cases. It is assumed that there is 15 dB power difference between weakest and strongest user groups, i.e., $10 \log \left(\frac{\bar{\beta}^{(4)}}{\bar{\beta}^{(1)}} \right) = 15$ dB is taken. It is assumed that $\text{SNR}^{(1)}$ is 30 dB, and $\text{SNR}^{(4)}$ is 45 dB. Note that, when there are 16 active users, weakest users requires D_{search} to be equal to 10 at least.

In Fig. 7.53 and Fig. 7.54, nMSE curves of different channel estimators are given for weakest and strongest user groups respectively when $K = 8$. In Fig. 7.55 and Fig. 7.56, nMSE curves of different channel estimators are given for weakest and strongest user groups respectively when $K = 16$. It is noticeable that as the total number of users increases, larger values of D_{search} are needed by the weakest user group to attain benchmark performance.

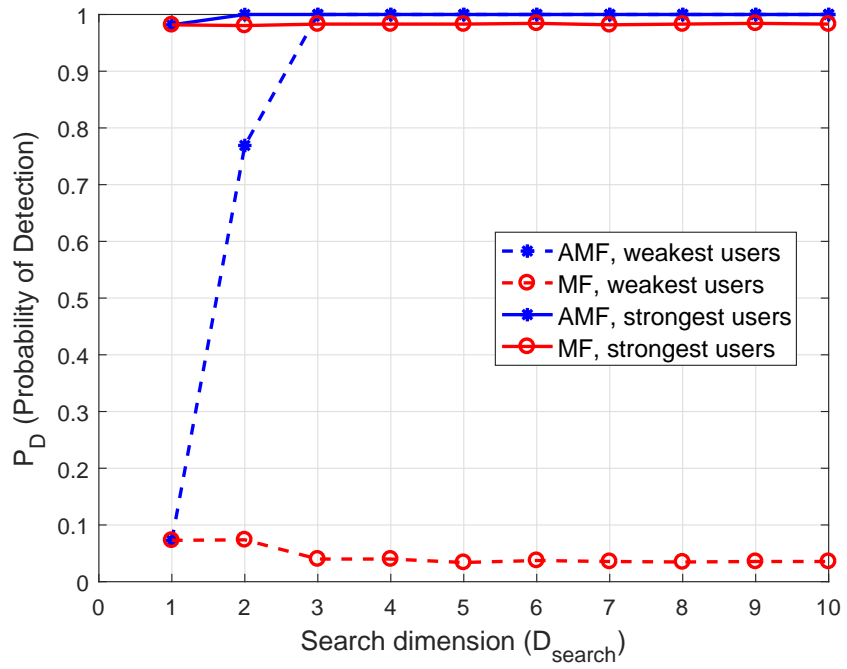


Figure 7.51: Average P_D vs D_{search} curves for different averaged received power levels ($K = 8$, $T = 32$, $10 \log(\bar{\beta}^{(4)}/\bar{\beta}^{(1)}) = 15$ dB)

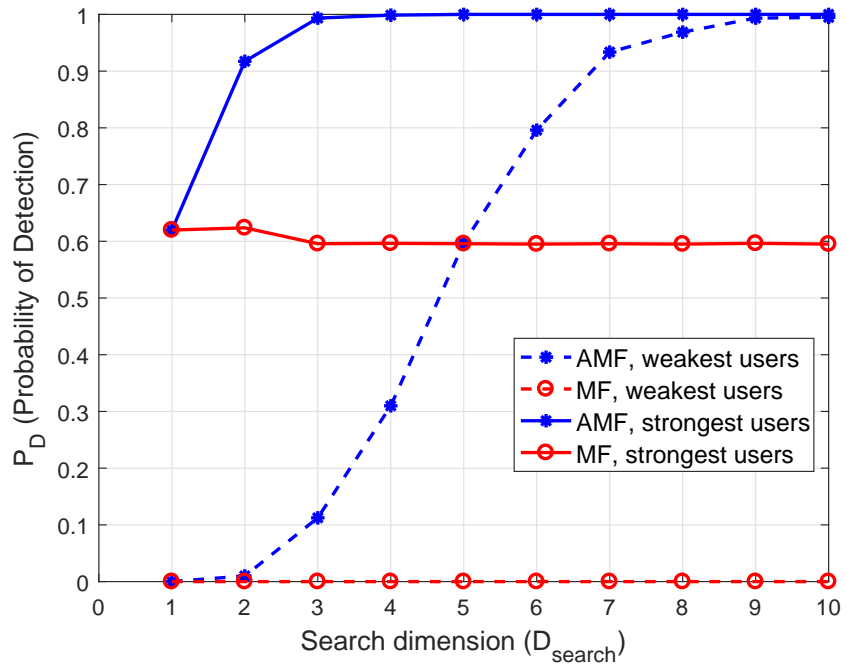


Figure 7.52: Average P_D vs D_{search} curves for different averaged received power levels ($K = 16$, $T = 32$, $10 \log(\bar{\beta}^{(4)}/\bar{\beta}^{(1)}) = 15$ dB)

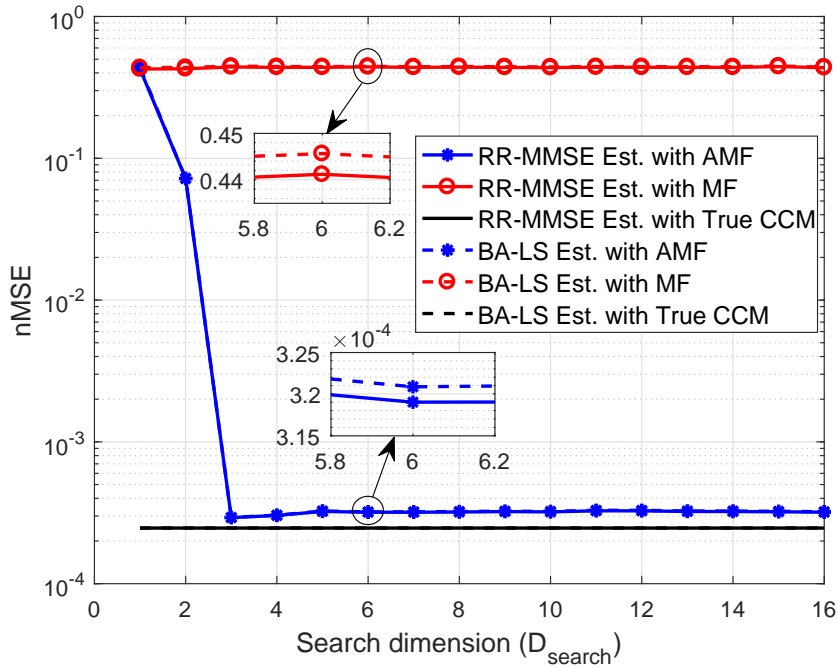


Figure 7.53: Performance of different channel estimators in terms of nMSE vs D_{search} for weakest user group ($10 \log (\bar{\beta}^{(4)} / \bar{\beta}^{(1)}) = 15$ dB, $K = 8$, $T = T_{fast} = 32$)

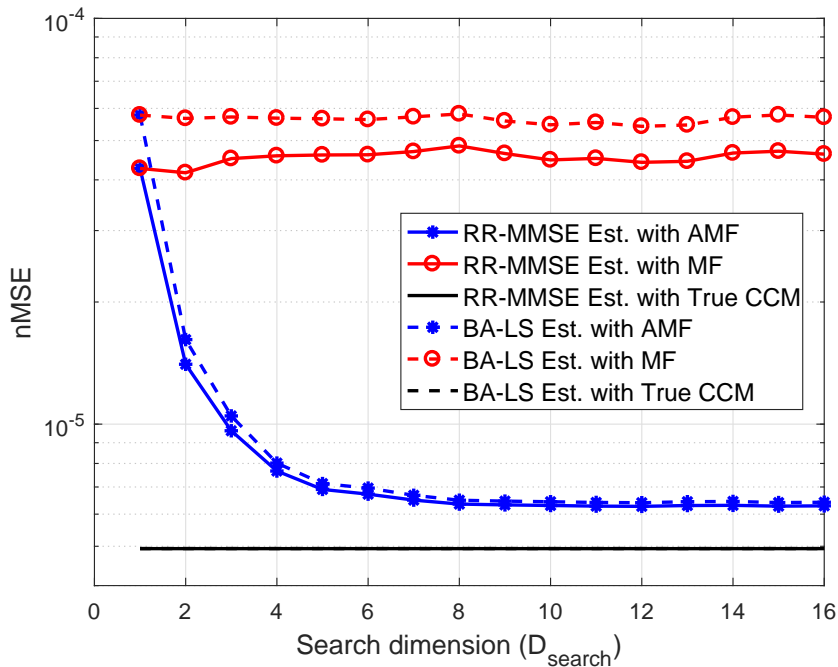


Figure 7.54: Performance of different channel estimators in terms of nMSE vs D_{search} for strongest user group ($10 \log (\bar{\beta}^{(4)} / \bar{\beta}^{(1)}) = 15$ dB, $K = 8$, $T = T_{fast} = 32$)

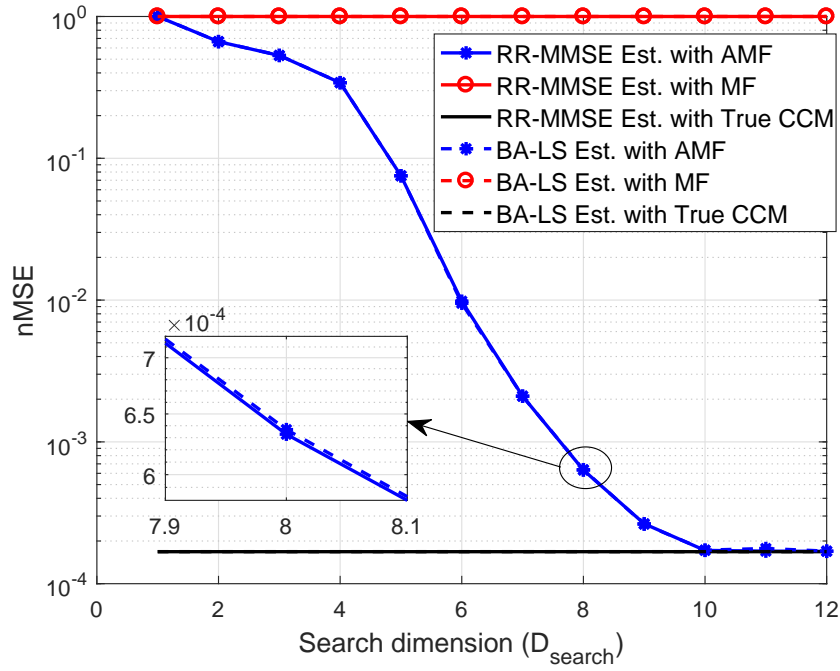


Figure 7.55: Performance of different channel estimators in terms of nMSE vs D_{search} for weakest user group ($10 \log (\bar{\beta}^{(4)} / \bar{\beta}^{(1)}) = 15$ dB, $K = 16$, $T = T_{fast} = 32$)

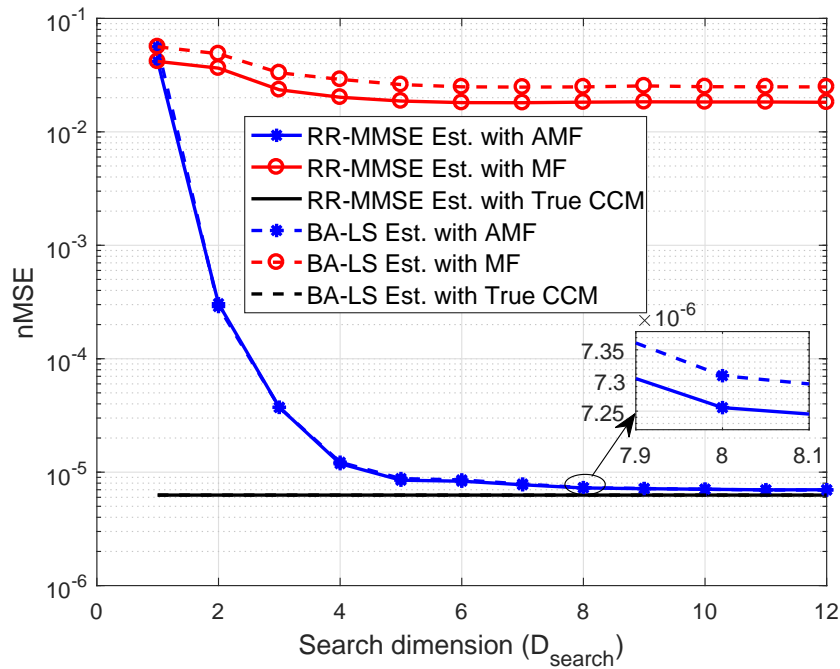


Figure 7.56: Performance of different channel estimators in terms of nMSE vs D_{search} for strongest user group ($10 \log (\bar{\beta}^{(4)} / \bar{\beta}^{(1)}) = 15$ dB, $K = 16$, $T = T_{fast} = 32$)

In Fig. 7.57 and Fig. 7.58, P_D curves are given with respect to D_{search} for $T = 32$ and $T = 128$ cases when there are 16 active users and 30 dB power difference between weakest and strongest user groups, i.e., $10 \log \left(\frac{\bar{\beta}^{(4)}}{\bar{\beta}^{(1)}} \right) = 30$ dB. It is assumed that $\text{SNR}^{(1)}$ is 20 dB, and $\text{SNR}^{(4)}$ is 50 dB. It is seen that when T is taken as 128, $D_{search} = 1$ is sufficient for strongest users to achieve maximum performance. Also, when $T = 128$, increasing D_{search} improves P_D performance rapidly.

In Fig. 7.59 and Fig. 7.60 nMSE curves of AMF and MF based channel estimators are given for $T = 32$ case. Similarly, for $T = 128$ case, nMSE curves in Fig. 7.61 and Fig. 7.62 are given for weakest and strongest user groups respectively.

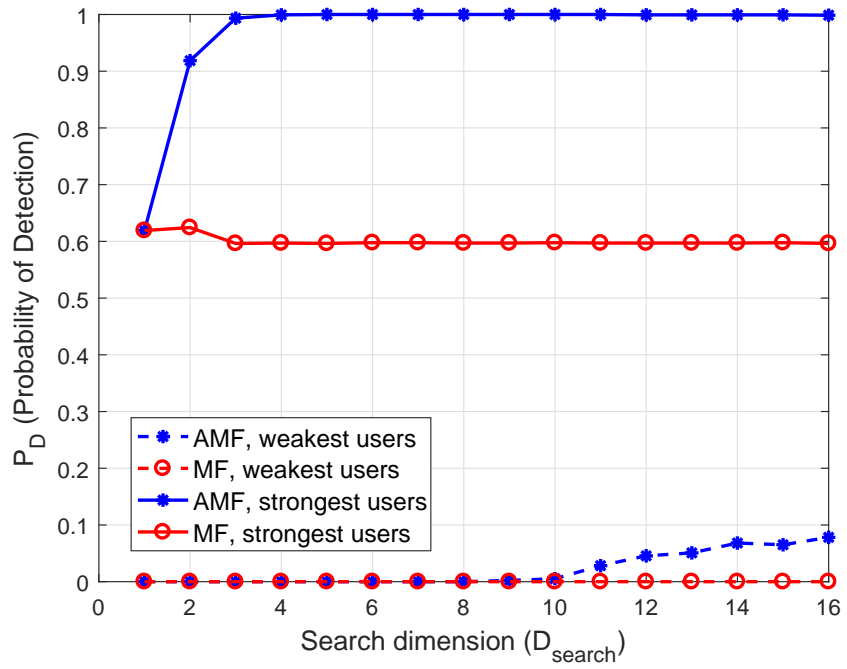


Figure 7.57: Average P_D vs D_{search} curves for different averaged received power levels ($K = 16$, $T = 32$, $10 \log (\bar{\beta}^{(4)} / \bar{\beta}^{(1)}) = 30$ dB)

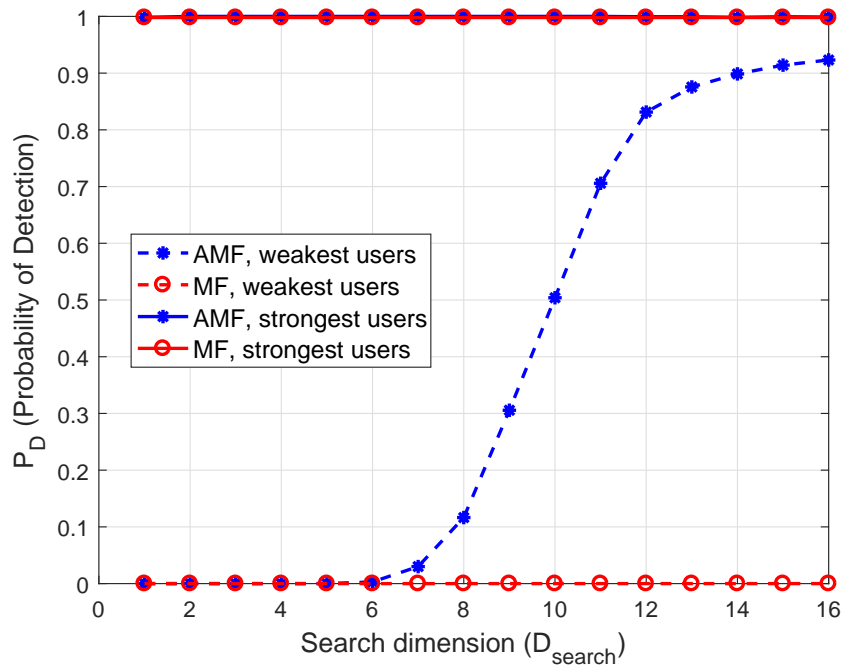


Figure 7.58: Average P_D vs D_{search} curves for different averaged received power levels ($K = 16$, $T = 128$, $10 \log (\bar{\beta}^{(4)} / \bar{\beta}^{(1)}) = 30$ dB)

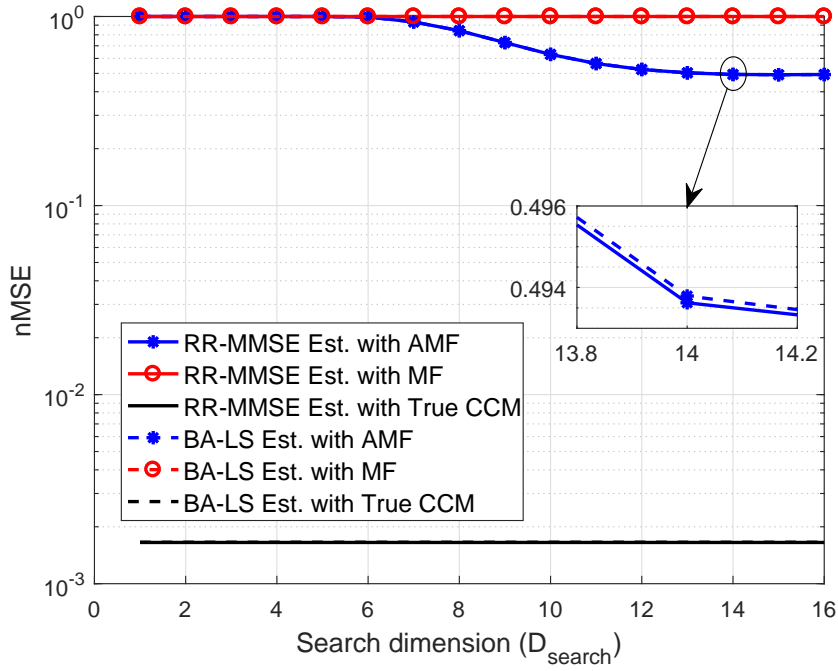


Figure 7.59: Performance of different channel estimators in terms of nMSE vs D_{search} for weakest user group ($10 \log (\bar{\beta}^{(4)} / \bar{\beta}^{(1)}) = 30$ dB, $K = 16$, $T = T_{fast} = 32$)

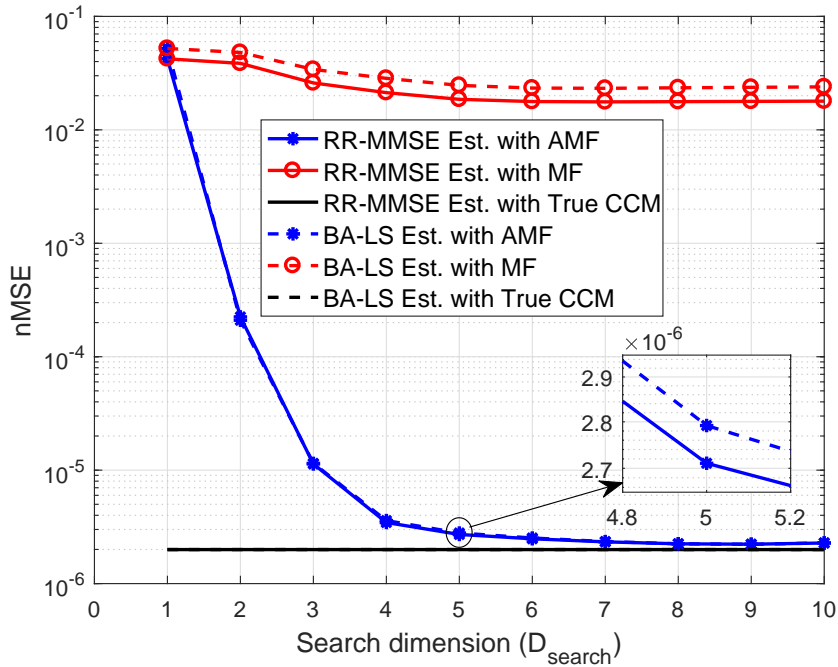


Figure 7.60: Performance of different channel estimators in terms of nMSE vs D_{search} for strongest user group ($10 \log (\bar{\beta}^{(4)} / \bar{\beta}^{(1)}) = 30$ dB, $K = 16$, $T = T_{fast} = 32$)

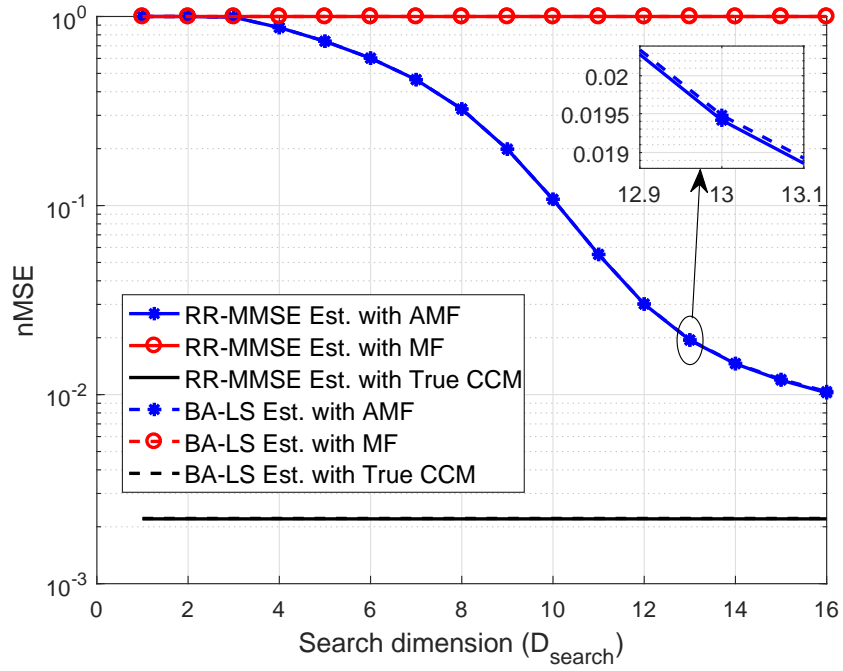


Figure 7.61: Performance of different channel estimators in terms of nMSE vs D_{search} for weakest user group ($K = 16, T = 128, T_{fast} = 32, 10 \log(\bar{\beta}^{(4)}/\bar{\beta}^{(1)}) = 30$ dB)

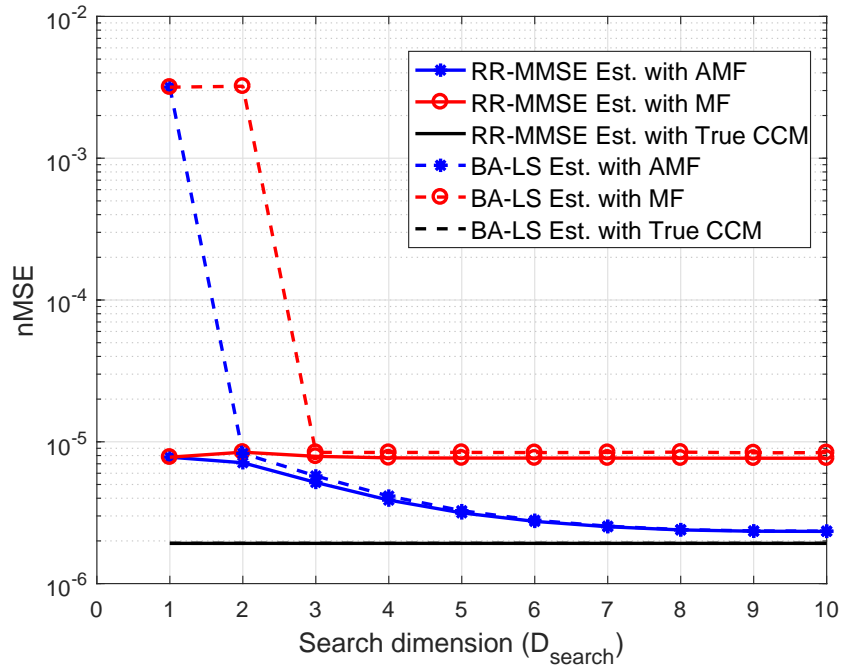


Figure 7.62: Performance of different channel estimators in terms of nMSE vs D_{search} for strongest user group ($K = 16, T = 128, T_{fast} = 32, 10 \log(\bar{\beta}^{(4)}/\bar{\beta}^{(1)}) = 30$ dB)

7.9 Performance vs. Number of Angular Resolution Cells

In Fig. 7.63 and Fig. 7.64 P_D and nMSE performance curves are given in terms of the number of angular resolution cells which is expressed in degrees (angular resolution is 0.25°), M , which is used to calculate spatial CFAR threshold in (4.6). It is seen that some amount secondary cells are required for P_D and nMSE performances to be improved since CFAR threshold is calculated more correctly as the number of secondary cells increases. The results are consistent with the fact that as M increases CFAR loss decreases [50].

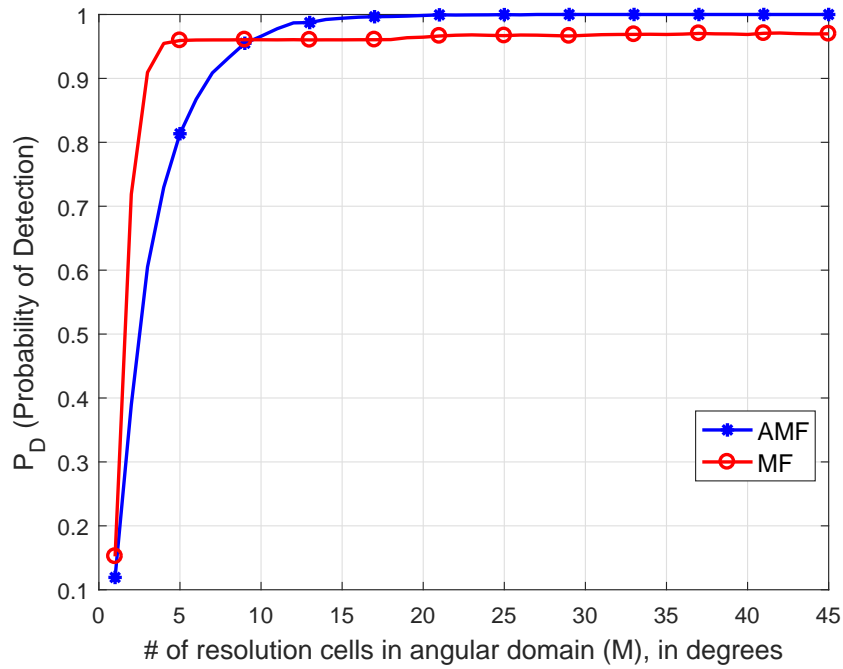


Figure 7.63: Average P_D vs M curve for equal averaged received power levels ($K = 8$, $D_{search} = 5$, $T = T_{fast} = 32$, $\text{SNR}^{(g)} = 30$ dB for $g = 1, \dots, G$)

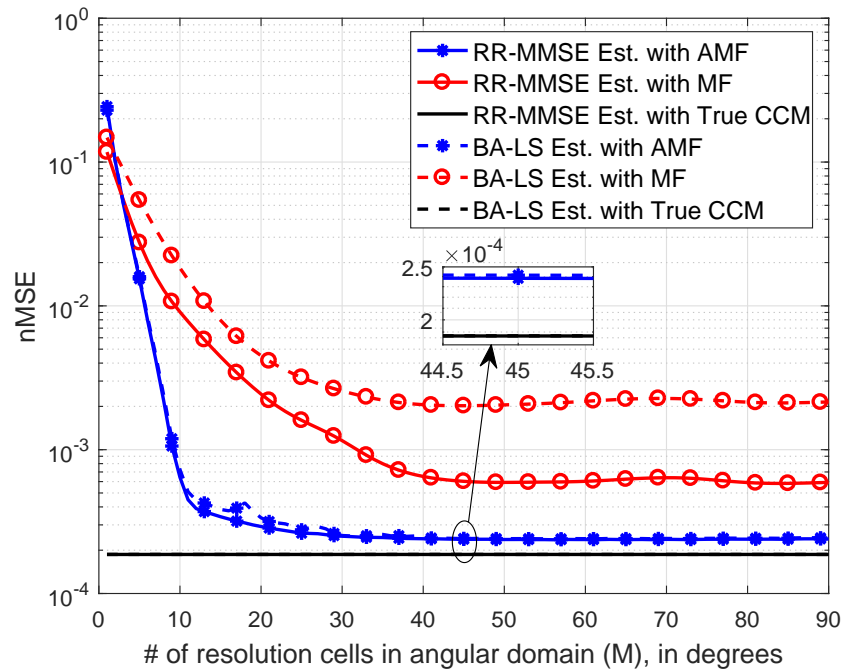


Figure 7.64: Performance of different channel estimators averaged over all groups for different values of M ($K = 8$, $D_{search} = 5$, $T = T_{fast} = 32$, $\text{SNR}^{(g)} = 30$ dB for $g = 1, \dots, G$)

7.10 Performance vs. Angular Spread of MPCs

In Fig. 7.65 and Fig. 7.66 average P_D curves of AMF and MF based CFAR thresholding algorithms are depicted for different AS values of MPCs. Here, it is assumed all MPCs demonstrated in Fig. 7.1 have same amount of AS. It can be seen from the results that as the AS of the MPCs increase, the performance of both AMF and MF based thresholding algorithms decreases, while MF deteriorates faster. The performance loss is an expected result since we assume narrow AS in the proposed channel model given in (3.3). As the AS of MPCs increases, channel power spreads over the AS, and therefore our channel model starts to become invalid.

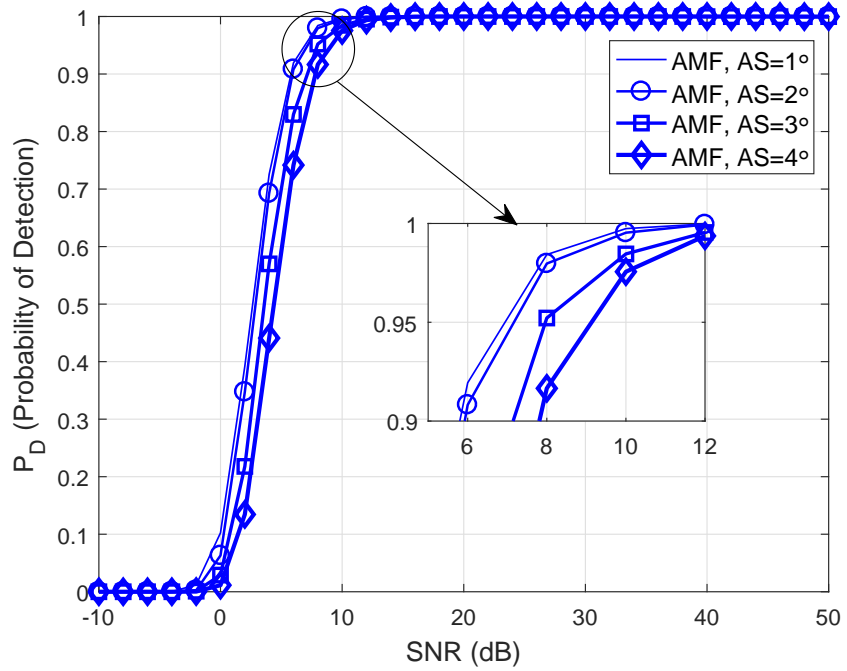


Figure 7.65: Average P_D curves of AMF for equal averaged received power levels ($K = 8, D_{search} = 5, T = 32$)

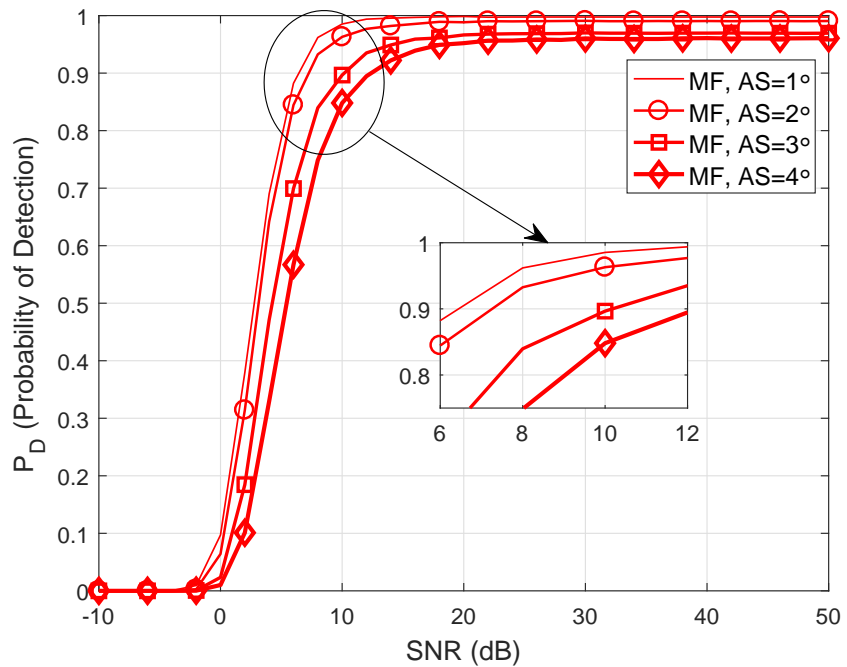


Figure 7.66: Average P_D curves of MF for equal averaged received power levels ($K = 8, D_{search} = 5, T = 32$)

CHAPTER 8

CONCLUSIONS

In this thesis, we proposed a novel joint angle-delay domain power profile and sparsity map estimator based on which CCMs of each users are constructed in full dimension, and then effective beam and channel acquisition are carried out. The work done in this thesis contributes the literature in many aspects. Firstly, we provide a novel adaptive algorithm to construct JADPP and sparsity map of a user channel inspiring from radar literature. Secondly, we propose a fully parametric CCM construction method based on the estimated long term parameters. It is proved that the estimated CCMs are asymptotically convergent to the true counterparts. Third, we proposed a nearly optimal beamformer design which uses estimated CCMs and also sparsity map of the users. Lastly, based on the estimated CCMs and reconstructed beamformers two different channel estimators are proposed. It is shown that the proposed estimators attain the performance of the MMSE channel estimator with true covariance knowledge. This performance is achieved by using reduced amount of slow-and-fast time training data when compared to the conventional channel estimators. The work presented here is open to be developed further and can be examined in terms of different aspects such as training codes, user mobility, user-grouping, RF chain distribution, MPC grouping and beamformer design. How to obtain power profile and sparsity map for OFDM transmission scheme might also be a future study worth to investigate.

To summarize the work presented in this thesis, in Chapter 2, we expressed the statistical signal and MPC models that the proposed methods are based on. An equivalent multi-ray channel model is also provided.

In Chapter 3, the signal models given in Chapter 2 are transformed into a model from

which the interested channel strengths at each spatio-temporal cell is acquired. Then, the hybrid beamformer structure adopted in this thesis is presented, and how the initial beams are formed and the sector of interest is scanned by these beams are detailed. Finally, two different JADPP estimators are derived.

In Chapter 4, sparsity map of each user on angle-delay plane is obtained by applying proposed two-stage CFAR thresholding algorithm onto the JADPPs constructed in the previous chapter. Then, the CCMs of each MPCs are acquired by means of JADPPs and sparsity map. Later, an exemplary scenario is given to illustrate the obtained power profiles and sparsity maps of active users. Also, two performance metrics (P_D and P_{FA}) are defined to be able to evaluate the performance of the proposed AMF or MF based two-stage CFAR thresholding algorithms.

In Chapter 5, a covariance based reduced-rank analog beamformer design is proposed. First, the common covariance matrices are constructed for user groups based on the JSMD framework. Then, an MPC grouping algorithm is proposed for significantly overlapping nonresolvable MPCs in angular domain. Finally, the construction of a nearly optimal analog beamformer along with optimal RF chain distribution is given.

In Chapter 6, based on the sparsity map and CCMs obtained in Chapter 4, and analog beamformer matrices updated in Chapter 5, two different reduced-rank channel estimators are proposed.

In Chapter 7, P_D and nMSE curves obtained from MC based simulation results are demonstrated in terms of different parameters used in slow-time beam acquisition and fast-time instantaneous channel estimation modes.

REFERENCES

- [1] T. L. Marzetta, “Noncooperative cellular wireless with unlimited numbers of base station antennas,” *IEEE Trans. Wireless Commun.*, vol. 9, pp. 3590–3600, November 2010.
- [2] J. G. Andrews, S. Buzzi, W. Choi, S. V. Hanly, A. Lozano, A. C. K. Soong, and J. C. Zhang, “What will 5G be?,” *IEEE J. Sel. Areas Commun.*, vol. 32, pp. 1065–1082, June 2014.
- [3] E. G. Larsson, O. Edfors, F. Tufvesson, and T. L. Marzetta, “Massive MIMO for next generation wireless systems,” *IEEE Commun. Mag.*, vol. 52, pp. 186–195, February 2014.
- [4] F. Rusek, D. Persson, B. K. Lau, E. G. Larsson, T. L. Marzetta, O. Edfors, and F. Tufvesson, “Scaling up MIMO: Opportunities and challenges with very large arrays,” *IEEE Signal Processing Mag.*, vol. 30, pp. 40–60, Jan 2013.
- [5] A. Ghosh, T. A. Thomas, M. C. Cudak, R. Ratasuk, P. Moorut, F. W. Vook, T. S. Rappaport, G. R. MacCartney, S. Sun, and S. Nie, “Millimeter-wave enhanced local area systems: A high-data-rate approach for future wireless networks,” *IEEE J. Sel. Areas Commun.*, vol. 32, pp. 1152–1163, June 2014.
- [6] A. L. Swindlehurst, E. Ayanoglu, P. Heydari, and F. Capolino, “Millimeter-wave massive MIMO: the next wireless revolution?,” *IEEE Commun. Mag.*, vol. 52, pp. 56–62, Sep. 2014.
- [7] X. Rao and V. K. N. Lau, “Distributed compressive csit estimation and feedback for FDD multi-user massive MIMO systems,” *IEEE Trans. Signal Process.*, vol. 62, pp. 3261–3271, June 2014.
- [8] Z. Gao, L. Dai, Z. Wang, and S. Chen, “Spatially common sparsity based adaptive channel estimation and feedback for FDD massive MIMO,” *IEEE Trans. Signal Process.*, vol. 63, pp. 6169–6183, Dec 2015.

- [9] H. Xie, F. Gao, and S. Jin, "An overview of low-rank channel estimation for massive MIMO systems," *IEEE Access*, vol. 4, pp. 7313–7321, 2016.
- [10] H. Xie, F. Gao, S. Zhang, and S. Jin, "A unified transmission strategy for TD-D/FDD massive MIMO systems with spatial basis expansion model," *IEEE Trans. Veh. Technol.*, vol. 66, pp. 3170–3184, April 2017.
- [11] S. Haghghatshoar and G. Caire, "Massive MIMO channel subspace estimation from low-dimensional projections," *IEEE Trans. Signal Process.*, vol. 65, pp. 303–318, Jan 2017.
- [12] I. S. Reed, J. D. Mallett, and L. E. Brennan, "Rapid convergence rate in adaptive arrays," *IEEE Trans. Aerospace and Electronic Systems*, vol. AES-10, pp. 853–863, Nov 1974.
- [13] Jian Li, P. Stoica, and Zhisong Wang, "On robust Capon beamforming and diagonal loading," *IEEE Transactions on Signal Processing*, vol. 51, pp. 1702–1715, July 2003.
- [14] D. Romero, D. D. Ariananda, Z. Tian, and G. Leus, "Compressive covariance sensing: Structure-based compressive sensing beyond sparsity," *IEEE Signal Processing Mag.*, vol. 33, pp. 78–93, Jan 2016.
- [15] S. Park and R. W. Heath, "Spatial channel covariance estimation for the hybrid mimo architecture: A compressive sensing-based approach," *IEEE Trans. Wireless Commun.*, vol. 17, pp. 8047–8062, Dec 2018.
- [16] S. Haghghatshoar and G. Caire, "Low-complexity massive mimo subspace estimation and tracking from low-dimensional projections," *IEEE Trans. Signal Process.*, vol. 66, pp. 1832–1844, April 2018.
- [17] H. Xie, F. Gao, S. Jin, J. Fang, and Y. Liang, "Channel estimation for TD-D/FDD massive MIMO systems with channel covariance computing," *IEEE Trans. Wireless Commun.*, vol. 17, pp. 4206–4218, June 2018.
- [18] M. R. Akdeniz, Y. Liu, M. K. Samimi, S. Sun, S. Rangan, T. S. Rappaport, and E. Erkip, "Millimeter wave channel modeling and cellular capacity evaluation," *IEEE J. Sel. Areas Commun.*, vol. 32, pp. 1164–1179, June 2014.

- [19] L. Lu, G. Y. Li, A. L. Swindlehurst, A. Ashikhmin, and R. Zhang, “An overview of massive MIMO: Benefits and challenges,” *IEEE J. Sel. Topics Signal Process.*, vol. 8, pp. 742–758, Oct 2014.
- [20] A. Pitarokoilis, S. K. Mohammed, and E. G. Larsson, “On the optimality of single-carrier transmission in large-scale antenna systems,” *IEEE Wireless Commun. Lett.*, vol. 1, pp. 276–279, August 2012.
- [21] G. M. Guvensen and E. Ayanoglu, “A generalized framework on beamformer design and csi acquisition for single-carrier massive MIMO systems in millimeter wave channels,” in *2016 IEEE Globecom Workshops (GC Wkshps)*, pp. 1–7, Dec 2016.
- [22] A. Kurt and G. M. Guvensen, “An efficient hybrid beamforming and channel acquisition for wideband mm-wave massive mimo channels,” in *ICC 2019 - 2019 IEEE International Conference on Communications (ICC)*, pp. 1–7, May 2019.
- [23] X. Song, S. Haghghatshoar, and G. Caire, “Efficient beam alignment for millimeter wave single-carrier systems with hybrid mimo transceivers,” *IEEE Trans. Wireless Commun.*, vol. 18, pp. 1518–1533, March 2019.
- [24] G. M. Guvensen and E. Ayanoglu, “A Generalized Framework on Beamformer Design and CSI Acquisition for Single-Carrier Massive MIMO Systems in Millimeter Wave Channels,” *arXiv e-prints*, p. arXiv:1607.01436, Jul 2016.
- [25] S. Noh, M. D. Zoltowski, Y. Sung, and D. J. Love, “Pilot beam pattern design for channel estimation in massive mimo systems,” *IEEE J. Sel. Topics Signal Process.*, vol. 8, pp. 787–801, Oct 2014.
- [26] J. Jose, A. Ashikhmin, T. L. Marzetta, and S. Vishwanath, “Pilot contamination and precoding in multi-cell TDD systems,” *IEEE Trans. Wireless Commun.*, vol. 10, pp. 2640–2651, August 2011.
- [27] A. Adhikary, J. Nam, J. Ahn, and G. Caire, “Joint spatial division and multiplexing—the large-scale array regime,” *IEEE Trans. Inf. Theory*, vol. 59, pp. 6441–6463, Oct 2013.

- [28] J. Nam, A. Adhikary, J. Ahn, and G. Caire, “Joint spatial division and multiplexing: Opportunistic beamforming, user grouping and simplified downlink scheduling,” *IEEE J. Sel. Topics Signal Process.*, vol. 8, pp. 876–890, Oct 2014.
- [29] A. F. Molisch, V. V. Ratnam, S. Han, Z. Li, S. L. H. Nguyen, L. Li, and K. Haneda, “Hybrid beamforming for massive mimo: A survey,” *IEEE Commun. Mag.*, vol. 55, pp. 134–141, Sep. 2017.
- [30] Z. Li, S. Han, S. Sangodoyin, R. Wang, and A. F. Molisch, “Joint optimization of hybrid beamforming for multi-user massive MIMO downlink,” *IEEE Trans. Wireless Commun.*, vol. 17, pp. 3600–3614, June 2018.
- [31] A. Goldsmith, *Wireless Communications*. Cambridge University Press, 2005.
- [32] T. S. Rappaport, S. Sun, R. Mayzus, H. Zhao, Y. Azar, K. Wang, G. N. Wong, J. K. Schulz, M. Samimi, and F. Gutierrez, “Millimeter wave mobile communications for 5G cellular: It will work!,” *IEEE Access*, vol. 1, pp. 335–349, 2013.
- [33] T. S. Rappaport, F. Gutierrez, E. Ben-Dor, J. N. Murdock, Y. Qiao, and J. I. Tamir, “Broadband millimeter-wave propagation measurements and models using adaptive-beam antennas for outdoor urban cellular communications,” *IEEE Trans. Antennas Propag.*, vol. 61, pp. 1850–1859, April 2013.
- [34] A. Alkhateeb, G. Leus, and R. W. Heath, “Limited feedback hybrid precoding for multi-user millimeter wave systems,” *IEEE Trans. Wireless Commun.*, vol. 14, pp. 6481–6494, Nov 2015.
- [35] A. Adhikary, E. Al Safadi, M. K. Samimi, R. Wang, G. Caire, T. S. Rappaport, and A. F. Molisch, “Joint spatial division and multiplexing for mm-wave channels,” *IEEE J. Sel. Areas Commun.*, vol. 32, pp. 1239–1255, June 2014.
- [36] L. You, X. Gao, A. L. Swindlehurst, and W. Zhong, “Channel acquisition for massive MIMO-OFDM with adjustable phase shift pilots,” *IEEE Trans. Signal Process.*, vol. 64, pp. 1461–1476, March 2016.
- [37] J. Ma, S. Zhang, H. Li, F. Gao, and S. Jin, “Sparse bayesian learning for the time-varying massive MIMO channels: Acquisition and tracking,” *IEEE Trans. Commun.*, vol. 67, pp. 1925–1938, March 2019.

- [38] J. Sykora, “Tapped delay line model of linear randomly time-variant WSSUS channel,” *Electronics Letters*, vol. 36, pp. 1656–1657, Sep. 2000.
- [39] P. Bello, “Characterization of randomly time-variant linear channels,” *IEEE Trans. Commun.*, vol. 11, pp. 360–393, December 1963.
- [40] L. You, X. Gao, X. Xia, N. Ma, and Y. Peng, “Pilot reuse for massive MIMO transmission over spatially correlated rayleigh fading channels,” *IEEE Trans. Wireless Commun.*, vol. 14, pp. 3352–3366, June 2015.
- [41] F. A. Dietrich and W. Utschick, “Pilot-assisted channel estimation based on second-order statistics,” *IEEE Trans. Signal Process.*, vol. 53, pp. 1178–1193, March 2005.
- [42] S. Haghghatshoar and G. Caire, “Enhancing the estimation of mm-wave large array channels by exploiting spatio-temporal correlation and sparse scattering,” *arXiv preprint arXiv:1602.03091*, 2016.
- [43] A. Hajimiri, H. Hashemi, A. Natarajan, Xiang Guan, and A. Komijani, “Integrated phased array systems in silicon,” *Proc. IEEE*, vol. 93, pp. 1637–1655, Sep. 2005.
- [44] H. Van Trees, *Optimum Array Processing: Part IV of Detection, Estimation, and Modulation Theory*. Detection, Estimation, and Modulation Theory, Wiley, 2004.
- [45] O. E. Ayach, S. Rajagopal, S. Abu-Surra, Z. Pi, and R. W. Heath, “Spatially sparse precoding in millimeter wave MIMO systems,” *IEEE Trans. Wireless Commun.*, vol. 13, pp. 1499–1513, March 2014.
- [46] S. Han, C. I, Z. Xu, and C. Rowell, “Large-scale antenna systems with hybrid analog and digital beamforming for millimeter wave 5G,” *IEEE Commun. Mag.*, vol. 53, pp. 186–194, January 2015.
- [47] H. Chiang, W. Rave, T. Kadur, and G. Fettweis, “Hybrid beamforming based on implicit channel state information for millimeter wave links,” *IEEE J. Sel. Topics Signal Process.*, vol. 12, pp. 326–339, May 2018.

- [48] F. C. Robey, D. R. Fuhrmann, E. J. Kelly, and R. Nitzberg, "A CFAR adaptive matched filter detector," *IEEE Trans. Aerospace and Electronic Systems*, vol. 28, pp. 208–216, Jan 1992.
- [49] E. J. Kelly, "An adaptive detection algorithm," *IEEE Trans. Aerospace and Electronic Systems*, vol. AES-22, pp. 115–127, March 1986.
- [50] M. Richards, *Fundamentals Of Radar Signal Processing*. McGraw-Hill Education (India) Pvt Limited, 2005.
- [51] J. Chen and D. Gesbert, "Joint user grouping and beamforming for low complexity massive MIMO systems," in *2016 IEEE 17th International Workshop on Signal Processing Advances in Wireless Communications (SPAWC)*, pp. 1–6, July 2016.
- [52] D. Kim, G. Lee, and Y. Sung, "Two-stage beamformer design for massive MIMO downlink by trace quotient formulation," *IEEE Trans. Commun.*, vol. 63, pp. 2200–2211, June 2015.
- [53] K. B. Petersen and M. S. Pedersen, "The matrix cookbook," nov 2012. Version 20121115.

APPENDIX A

DERIVATION OF AMF TYPE JADPP ESTIMATOR

Let the i^{th} column of $\tilde{\mathbf{N}}_l^{(k)}$ in (3.9) be $\boldsymbol{\eta}_{l,i}^{(k)} \triangleq \left[\tilde{\mathbf{N}}_l^{(k)} \right]_{(:,i)}$. By using (2.2) and assuming that random training sequences are used (pseudo-random code), i.e.,

$$\mathbb{E} \left\{ x_n^{(k)} \left(x_{n'}^{(k')} \right)^* \right\} = \delta_{kk'} \delta_{nn'}, \quad (\text{A.1})$$

we can write the correlation matrix of the received sequence after hybrid beamforming $\tilde{\mathbf{y}}_n = \mathbf{U}^H \mathbf{y}_n$ in (2.1) as

$$\mathbf{R}_{\tilde{\mathbf{y}}} \triangleq \mathbb{E} \left\{ \tilde{\mathbf{y}}_n \tilde{\mathbf{y}}_n^H \right\} = \sum_{k=1}^K \sum_{l=0}^{L-1} \mathbf{U}^H \mathbf{R}_l^{(k)} \mathbf{U} + N_o \mathbf{I}_D. \quad (\text{A.2})$$

Then, it can be shown that $\mathbb{E} \left\{ \boldsymbol{\eta}_{l,m}^{(k)} \left(\boldsymbol{\eta}_{l,n}^{(k)} \right)^H \right\} = \mathbf{R}_{\boldsymbol{\eta},l}^{(k)} \delta_{mn}$ where $\mathbf{R}_{\boldsymbol{\eta},l}^{(k)} = \mathbf{R}_{\tilde{\mathbf{y}}} - \mathbf{U}^H \mathbf{R}_l^{(k)} \mathbf{U}$. Here, $\mathbf{R}_{\boldsymbol{\eta},l}^{(k)}$ can be regarded as the spatial autocorrelation matrix of interfering MPCs other than the one located in CUT. By using (3.5) and $\mathbf{R}_{\boldsymbol{\eta},l}^{(k)}$, we can write the conditional pdf of $\tilde{\mathbf{Y}}$ in (3.9) as follows

$$p \left(\tilde{\mathbf{Y}} \mid \mathbf{R}_{\boldsymbol{\eta},l}^{(k)}, \alpha_l^{(k)} \right) = \frac{\exp \left(- \text{Tr} \left\{ \left[\mathbf{R}_{\boldsymbol{\eta},l}^{(k)} \right]^{-1} \left(\tilde{\mathbf{Y}} - \alpha_l^{(k)} \tilde{\mathbf{u}}(\phi_i) (\mathbf{x}_l^{(k)})^H \right) \left(\tilde{\mathbf{Y}} - \alpha_l^{(k)} \tilde{\mathbf{u}}(\phi_i) (\mathbf{x}_l^{(k)})^H \right)^H \right\} \right)}{\pi^{NT} \left[\det \left(\mathbf{R}_{\boldsymbol{\eta},l}^{(k)} \right) \right]^T}. \quad (\text{A.3})$$

The ML estimate of $\alpha_l^{(k)}$ can be obtained as a result of the minimization problem given below

$$\begin{aligned} \hat{\alpha}_l^{(k)} &= \arg \max_{\alpha_l^{(k)}} \max_{\mathbf{R}_{\boldsymbol{\eta},l}^{(k)}} \ln p \left(\tilde{\mathbf{Y}} \mid \mathbf{R}_{\boldsymbol{\eta},l}^{(k)}, \alpha_l^{(k)} \right) \\ &= \arg \min_{\alpha_l^{(k)}} \min_{\mathbf{R}_{\boldsymbol{\eta},l}^{(k)}} \left\{ T \ln \det \left[\mathbf{R}_{\boldsymbol{\eta},l}^{(k)} \right] + \right. \\ &\quad \left. \text{Tr} \left\{ \left[\mathbf{R}_{\boldsymbol{\eta},l}^{(k)} \right]^{-1} \left(\tilde{\mathbf{Y}} - \alpha_l^{(k)} \tilde{\mathbf{u}}(\phi_i) (\mathbf{x}_l^{(k)})^H \right) \left(\tilde{\mathbf{Y}} - \alpha_l^{(k)} \tilde{\mathbf{u}}(\phi_i) (\mathbf{x}_l^{(k)})^H \right)^H \right\} \right\}. \end{aligned} \quad (\text{A.4})$$

In order to solve (A.4), the following matrix identities can be used: for given arbitrary matrices \mathbf{A} and \mathbf{X} , we can write $\frac{\partial}{\partial \mathbf{X}} \ln(\det(\mathbf{X})) = \mathbf{X}^{-1}$ and $\frac{\partial}{\partial \mathbf{X}} \text{Tr}\{\mathbf{X}^{-1}\mathbf{A}\} = -(\mathbf{X}^{-1}\mathbf{A}\mathbf{X}^{-1})^T$ [53]. By taking the partial derivative of the cost function in (A.4) with respect to $\mathbf{R}_{\eta,l}^{(k)}$ and equating it to $\mathbf{0}$, one get

$$\hat{\mathbf{R}}_{\eta,l}^{(k)} = \frac{\left(\tilde{\mathbf{Y}} - \alpha_l^{(k)} \tilde{\mathbf{u}}(\phi_i)(\mathbf{x}_l^{(k)})^H\right) \left(\tilde{\mathbf{Y}} - \alpha_l^{(k)} \tilde{\mathbf{u}}(\phi_i)(\mathbf{x}_l^{(k)})^H\right)^H}{T} \quad (\text{A.5})$$

which is simply the ML estimate of the autocorrelation matrix by using T samples. Then, by replacing $\mathbf{R}_{\eta,l}^{(k)}$ in (A.4) with $\hat{\mathbf{R}}_{\eta,l}^{(k)}$ in (A.5), the minimization in (A.4) can be simplified as

$$\hat{\alpha}_l^{(k)} = \arg \min_{\alpha_l^{(k)}} \det \left[\left(\tilde{\mathbf{Y}} - \alpha_l^{(k)} \tilde{\mathbf{u}}(\phi_i)(\mathbf{x}_l^{(k)})^H\right) \left(\tilde{\mathbf{Y}} - \alpha_l^{(k)} \tilde{\mathbf{u}}(\phi_i)(\mathbf{x}_l^{(k)})^H\right)^H \right]. \quad (\text{A.6})$$

To simplify the above minimization, the inner term can be expressed in the following quadratic form

$$\hat{\alpha}_l^{(k)} = \arg \min_{\alpha_l^{(k)}} \det \left[\left(\mathbf{z} - \mathbf{b}\alpha_l^{(k)}\right) \left(\mathbf{z} - \mathbf{b}\alpha_l^{(k)}\right)^H + \Psi \right] \quad (\text{A.7})$$

where $\mathbf{z} = \tilde{\mathbf{Y}}\mathbf{x}_l^{(k)} / \|\mathbf{x}_l^{(k)}\|^2$, $\mathbf{b} = \tilde{\mathbf{u}}(\phi_i) \|\mathbf{x}_l^{(k)}\|^2$ and Ψ is given in (3.11). Then, we can modify (A.7) as

$$\begin{aligned} \hat{\alpha}_l^{(k)} &= \arg \min_{\alpha_l^{(k)}} \det \left[\Psi^{1/2} \left[\Psi^{-1/2} \left(\mathbf{z} - \mathbf{b}\alpha_l^{(k)}\right) \left(\mathbf{z} - \mathbf{b}\alpha_l^{(k)}\right)^H \Psi^{-1/2} + \mathbf{I} \right] \Psi^{1/2} \right] \\ &= \arg \min_{\alpha_l^{(k)}} \det \left[\Psi^{-1/2} \left(\mathbf{z} - \mathbf{b}\alpha_l^{(k)}\right) \left(\mathbf{z} - \mathbf{b}\alpha_l^{(k)}\right)^H \Psi^{-1/2} + \mathbf{I} \right]. \end{aligned} \quad (\text{A.8})$$

By using the Sylvester's Theorem in [53], where $\det(\mathbf{I} + \mathbf{A}\mathbf{B}) = \det(\mathbf{I} + \mathbf{B}\mathbf{A})$, (A.8) can be rearranged as

$$\begin{aligned} \hat{\alpha}_l^{(k)} &= \arg \min_{\alpha_l^{(k)}} \det \left[1 + \left(\mathbf{z} - \mathbf{b}\alpha_l^{(k)}\right)^H \Psi^{-1} \left(\mathbf{z} - \mathbf{b}\alpha_l^{(k)}\right) \right] \\ &= \arg \min_{\alpha_l^{(k)}} \left(\mathbf{z} - \mathbf{b}\alpha_l^{(k)}\right)^H \Psi^{-1} \left(\mathbf{z} - \mathbf{b}\alpha_l^{(k)}\right) \\ &= \frac{\mathbf{b}^H \Psi^{-1} \mathbf{z}}{\mathbf{b}^H \Psi^{-1} \mathbf{b}}. \end{aligned} \quad (\text{A.9})$$

Finally, the ML estimate of the complex channel gain of l^{th} MPC of k^{th} user can be obtained as in the compact form given in (3.10).